(2)

UNCLASSIFIED
SECURITY CLASSIFICATION OF THIS PAGE

REPORT DOCUMENTATION PAGE

Form Approved
OMB No. 0704-0188

1a. REPORT SECURITY CLASSIFICATION UNCLASSIFIED	1b. RESTRICTIVE MARKINGS DTIC FILE COPY
2a. SECURITY CLASSIFICATION AUTHORITY	3. DISTRIBUTION / AVAILABILITY OF REPORT Approved for public release; Distribution is unlimited
2b. DECLASSIFICATION / DOWNGRADING SCHEDULE	
4. PERFORMING ORGANIZATION REPORT NUMBER(S)	5. MONITORING ORGANIZATION REPORT NUMBER(S) AFOSR-TR- 89-1227
6a. NAME OF PERFORMING ORGANIZATION Johns Hopkins University 6b. OFFICE SYMBOL (If applicable)	7a. NAME OF MONITORING ORGANIZATION AFOSR/NC
6c. ADDRESS (City, State, and ZIP Code) Laurel, MD 20707	7b. ADDRESS (City, State, and ZIP Code) Building 410 Bolling AFB DC 20332-6448
8a. NAME OF FUNDING / SPONSORING ORGANIZATION AFOSR 8b. OFFICE SYMBOL (If applicable) NC	9. PROCUREMENT INSTRUMENT IDENTIFICATION NUMBER AFOSR-86-0057
8c. ADDRESS (City, State, and ZIP Code) Building 410 Bolling AFB DC 20332-6448	10. SOURCE OF FUNDING NUMBERS PROGRAM ELEMENT NO. 61102F; PROJECT NO. 2310; TASK NO. A2; WORK UNIT ACCESSION NO.

11. TITLE (Include Security Classification)
(U) An Investigation of Atmospheric Emissions in Ultraviolet, Vacuum Ultraviolet and Extreme Ultraviolet Wavelengths

12. PERSONAL AUTHOR(S)
Dr Ching-I. Meng

13a. TYPE OF REPORT	13b. TIME COVERED	14. DATE OF REPORT (Year, Month, Day)	15. PAGE COUNT
Final	FROM _____ TO _____	July 1989	105

16. SUPPLEMENTARY NOTATION

17. COSATI CODES			18. SUBJECT TERMS (Continue on reverse if necessary and identify by block number)
FIELD	GROUP	SUB-GROUP	

19. ABSTRACT (Continue on reverse if necessary and identify by block number)

See Back

20. DISTRIBUTION / AVAILABILITY OF ABSTRACT ☐ UNCLASSIFIED/UNLIMITED ☐ SAME AS RPT ☐ DTIC USERS	21. ABSTRACT SECURITY CLASSIFICATION UNCLASSIFIED
22a NAME OF RESPONSIBLE INDIVIDUAL Lt Col James G. Stobie	22b TELEPHONE (Include Area Code) (202) 767-4963 22c. OFFICE SYMBOL AFOSR/NC

DD Form 1473, JUN 86 Previous editions are obsolete.

SECURITY CLASSIFICATION OF THIS PAGE
UNCLASSIFIED

19. The three and a half-year research supported by AFOSR under Grant 86-0057 had three objectives: (1) to understand the morphology of atmospheric optical UV emissions over the polar region associated with the solar and magnetospheric particle precipitations, (2) to understand the morphology of the middle and low latitude airglow, and (3) to investigate the UV background of the atmospheric emissions for possible application for remote sensing.

The focus of data analysis started on UV and FUV spectra taken from the polar-orbiting S3-4 satellite. To this date, the S304 has provided the only satellite measurement with the composite data set of the FUV (sometimes called Vacuum Ultraviolet) and UV wavelength regions. The S3-4 data set is suitable for the analyses of diffuse auroral emissions, and the study revealed the characteristic wavelength which can be used for remote-sensing and 2-D image in the auroral precipitating electron energetics.

Several significant results are obtained. The comparison of our observation to a transport model calculation, led to the contribution of defining some atmospheric constants currently in debate. The close examination of anomalous emission spectra led to the discovery of the UV spectra caused by energetic O+ precipitation. Finally, the Doppler shift of proton auroral La was observed for the first time. These results suggest a promising future for the use of UV emission analysts and the application of remote sensing to the global coverage of the energy deposition in both mid and high latitude regions.

Final Technical Report

Investigation of Atmospheric Emission in Ultraviolet, Vacuum Ultraviolet and Extreme Ultraviolet Wavelength.

(Grant AFOSR-86-0057)

by

Ching -I. Meng, Principal Investigator

The Johns Hopkins University

Applied Physics Laboratory

Laurel, Maryland 20707

July, 1989

Summary

The three and a half-year research supported by AFOSR under Grant 86-0057 had three objectives: (1) to understand the morphology of atmospheric optical UV emissions over the polar region associated with the solar and magnetospheric particle precipitations, (2) to understand the morphology of the middle and low latitude airglow, and (3) to investigate the UV background of the atmospheric emissions for possible application for remote sensing.

The focus of data analysis started on UV and FUV spectra taken from the polar-orbiting S3-4 satellite. To this date, the S3-4 has provided the only satellite measurement with the composite data set of the FUV (sometimes called Vacuum Ultraviolet) and UV wavelength regions. The S3-4 data set is suitable for the analyses of diffuse auroral emissions, and the study revealed the characteristic wavelength which can be used for remote-sensing and 2-D image in the auroral precipitating electron energetics.

Several significant results are obtained. The comparison of our observation to a transport model calculation, led to the contribution of defining some atmospheric constants currently in debate. The close examination of anomalous emission spectra led to the discovery of the UV spectra caused by energetic O^+ precipitation. Finally, the Doppler shift of proton auroral Lα was observed for the first time. These results suggest a promising future for the use of UV emission analysis and the application of remote sensing to the global coverage of the energy deposition in both mid and high latitude regions.

A. Introduction

The S3-4 satellite had two spectrometers and a photometer on board and provided data for a six-month period; more than 200 orbits of observation are used for this research. First, detailed analysis of the night-side auroral emission was performed to evaluate the data quality and their limitations. Most of the first year's effort was concentrated on the processing of auroral spectra: such as on the noise reduction, compensation for the temporal and spatial changes during a 21-second spectral scan for the rapid auroral emission changes (Ishimoto et al., 1988a). The low resolution (30Å) spectrometer data were analyzed first, because of high signals and more data available. The following sections describe data quality assessment, data products and results.

B. Data Quality Assessment

The spectral scan time of 21 seconds and the field of view of the spectrometers are quite large compared to the characteristic time and spatial scales of aurora display features. Spectra were normalized by using the photometer measurement with a small field of view and short integration time. This normalization procedure was very effective to produce auroral spectra in the diffuse auroral regions. The procedure was evaluated by using the observed intensity in the wavelength regions between 1600 and 1750Å, where the two spectrometer ranges overlap. The intensity match was quite good even though the two observations were made about 14 s apart. Furthermore, after the photometer normalization, the observed auroral spectral band systems that spread over the wide wavelength ranges (i.e. the Lyman-Birge-Hopfield (LBH) and the Vegard-Kaplan (VK) band systems) match the synthetic spectra very well. Figure 1 shows the comparison of the normalized auroral spectral observations from the

diffuse auroral region (Figure 1a) with synthetic VK band systems (Figure 1b) and with the synthetic LBH band systems (Figure 1c). The combined spectra from the FUV (broken line) and the UV (solid line) agree in the overlapping region with a deviation of less than 10% indicating a very reliable calibration. A good agreement between the observed and the synthetic spectra lends credibility to the photometer normalization technique as well if the atmospheric absorption between 1300 and 1900Å is taken into account.

C. Data products

Auroral emissions are results of intricate interactions between the atmosphere and incident particles. Studying observed intensities of these emissions and their relations enable us to understand the atmospheric phenomena. Conversely, the incident particles and the atmospheric conditions are investigated by using known emission mechanisms.

Auroral and airglow radiations consist of various molecular band systems such as the N_2 LBH, VK, and Herman-Kaplan, NO γ and δ, and O_2 Herzberg I bands, as well as atomic lines such as the NI (1200, 1493, and 1744Å), OI(1304 and 1356Å), NII(2143Å) and OII(2470Å) lines. Each line and band emission intensity is a clue to deduce the incident particle energy spectra and the atmospheric condition. The notable atomic features are separated from the two major band systems by using synthetic spectra (Figure 2). This procedure requires the estimation of O_2 Schumann-Runge (SR) absorption of the LBH emission. The absorption depends on the altitude distribution of the LBH emission and the atmospheric O_2 concentration. Assuming a Chapman layer type of LBH emission altitude distribution, we found a way to synthesize spectra by including the O_2 SR absorption from two emission intensities at any given wavelength. Figure 3

shows the LBH synthetic spectra using this method along with an observed spectrum. The detailed method is described in Ishimoto et al. (1989b) (See Appendix E). Applying this procedure provided the data products: OI(1356Å), NI(1493 and 1744Å), and NII(2143Å) lines as well as the LBH and VK band intensity.

D. Results

The investigation began with the selection of a number of orbits which satisfy the two criteria: 1) the observation made with the largest slit widths (30Å resolution) in order to detect rather weak auroral and airglow emissions, 2) the auxiliary photometer set to one of three (1340, 1550, and 1750Å) wavelengths for providing the continuous monitor of the auroral intensity variations within the spectrometer scan period. Seven orbits covering various levels of magnetic activity from K_p= 0 to 7+ were selected. Later, we selected the high resolution (8Å) spectral data taken during the periods of strong Lα emission from five auroral oval crossings to investigate the auroral Lα line Doppler shifting effect.

The individual orbits were analyzed in detail and the spectra were compared with atomic and molecular emissions of other observations. The emission mechanisms and cross sections were evaluated by using model calculations. The results of this effort confirmed that the quality of the S3-4 data set is suitable for the diffuse aurora investigation, and promises a future application of the UV for global coverage of the energy deposition in mid-high latitudes.

The analyses of these data with model calculations revealed several salient results:

1. The emission peaks at 1928Å and 2604Å in 30 Å resolution spectra consist of almost 100% LBH and VK band emission, and thus are representative of the intensities of the band systems. (See Ishimoto et al., 1988a in Appendix A for detail).

2. The observed emission intensities of the LBH(3-10) band, the VK(0-5) band and OI(1356Å) line in the diffuse aurora were consistent with what is inferred from a modified version of the model calculation by Strickland et al. (1983) and imply:

   - The average energy of incident electrons was 3keV, which agreed the value reported by auroral electrons measured by DMSP (Hardy et al., 1985).
   - The atmospheric oxygen density was 30% less than the model atmosphere used in the calculation by Strickland et al. (1983).
   - The atomic oxygen quenching coefficient for VK(0-5) band was deduced and agreed with the value given by Sharp (1971). (See Ishimoto et al., 1988a in Appendix A for detail).

3. The energy flux and average energy of the incident electrons can be inferred by the LBH(3-10) band intensity and the intensity ratio of the LBH(3-10) to VK(0-5) emission, respectively. (See Ishimoto et al., 1988a in Appendix A for detail).

4. Intensities of the NI (1744Å), NII(2143Å), and OI(1356Å) lines, and the LBH(3-10) band at 1928Å show a constant proportionality to each other. The correlations of these emission intensities were expected if the predominant emission mechanisms are direct electron impact on N_2 and O.

The inferred (2143Å) line emission cross section agreed with previously reported rocket results (Sharp, 1978 and Siskind and Barth, 1987) and were two orders of magnitude larger than the laboratory measurement by Erdman and Zipf (1986). (See Ishimoto et al., 1988c in Appendix C for detail).

5. Anomalous spectra taken from the equatorward section (-53 ~ -60^{o} geomagnetic latitude) of the expanded auroral oval during a very disturbed period were characterized as having : (1) very high line to band emission intensity ratio, (2) high rotational temperature (1000 K) of the VK band system, (3) very high vibrational temperature (3000 K) of the LBH band system on the basis and expectations from both laboratory measurement and model calculations. These emissions were attributed to keV oxygen precipitation. (See Ishimoto et al., 1989a in Appendix D for detail).
6. The Lyman alpha (Lα) emission intensity peak of a high resolution (8Å) spectrum were found to be Doppler-shifted up to 4Å when a geocoronal Lα emission profile was subtracted form the Lα emission profile observed over the auroral region. (See Ishimoto et al., 1989c in Appendix F for detail).

The results were published or to be published and they are attached as appendices.

References

Erdman, P. W. and Z. C. Zipf, Dissociation Excitation of the $N^+(^5S)$ State by Electron Impact on N_2: Excitation Function and Quenching, J. Geophys. Res., 91, A10, 11345-11351, 1986.

Hardy, D. A., M. S. Gussenhoven, and E. Holdman, A Statistical Model of Auroral Electron Precipitation, J. Geophys. Res., 90, A5, 4229-4248, 1985.

Ishimoto, M., G. R. Romick, C.-I. Meng, R. E. Huffman, Anomalous UV Auroral Spectra During a Large Magnetic Disturbance, J. Geophys. Res., 94, 6955-6960, 1989b.

Ishimoto, M., G. J. Romick, R. E. Huffman, and C.-I. Meng, Auroral Electron Energy and Flux From Molecular Nitrogen Ultraviolet Emissions Observed by the S3-4 Satellite, J. Geophys. Res., 93, 9854-9866, 1988a.

Ishimoto, M., G. J. Romick, C.-I. Meng, R. E. Huffman, V. Degen, Analysis of Atomic Ultraviolet Lines in the Diffuse Aurora, submitted to J. Geophys. Res., 1989b.

Ishimoto, M., G. J. Romick, and C.-I. Meng, Analytic Estimation of O_2 Schumann-Runge Absorption Simulation for Auroral LBH Band Emissions, submitted to J. Geophys. Res., 1989c.

Ishimoto, M., G. J. Romick, C.-I. Meng, R. E. Huffman, Doppler Shift of Auroral Lyman α observed from a satellite, Geophys. Res. Lett., 16, 143, 1989a.

Sharp, W. E., Rocket-Borne Spectroscopic Measurements in the Ultraviolet Aurora: Nitrogen Vegard-Kaplan Bands, J. Geophys. Res., 76, 987-1005, 1971.

Sharp, W. E., The Ultraviolet Aurora: the Spectrum Between 2100Å and 2300Å, Geophys. Res. Lett., 5, 703, 1978.

Siskind, D. E. and C. A. Barth, Rocket Observation of the NII 2143Å Emission in an Aurora, Geophys. Res. Letters, 14, 4, 479-482, 1987.

Strickland, D. J., J. R. Jasperse, and J. A. Whalen, Dependence of Auroral FUV Emissions on the Incident Electron Spectrum and Neutral Atmosphere, J. Geophys. Res., 88, A10, 8051-8062, 1983.

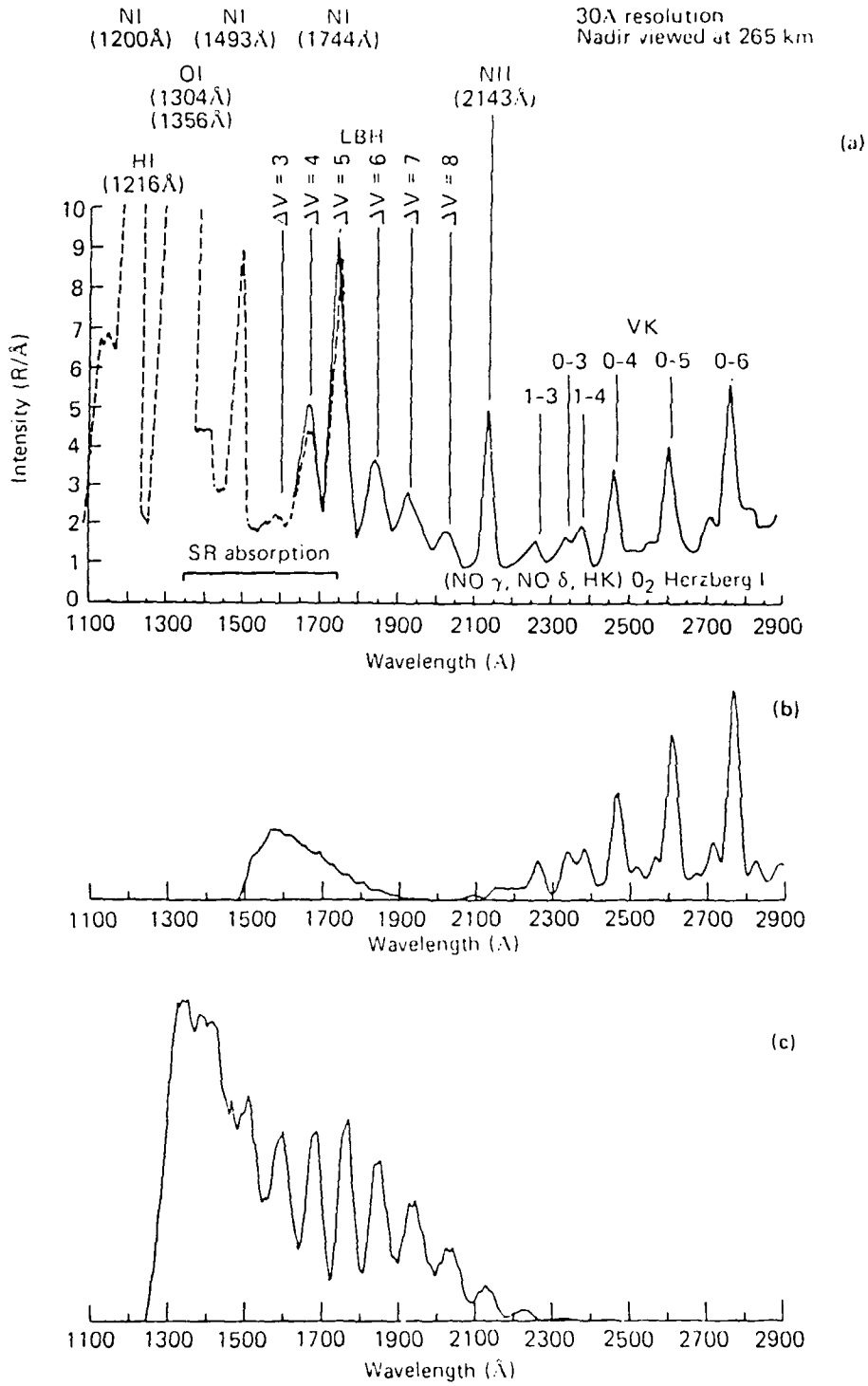

Figure 1. Comparison of the observed UV spectrum with LBH and VK synthetic spectra from Degen (1986). (a) Spectra obtained at about 1836 UT on June 2, 1978 by FUV (dotted line) and near-UV (solid line) spectrometers overlapping in the wavelength range 1600 to 1750 Å. (b) VK synthetic spectrum assuming T_r = 400 K. (Note uncertainty for high v for $\lambda < 2000$ Å; see text for details.) (c) LBH synthetic spectrum assuming T_r = 400 K and T_v = 400 K.

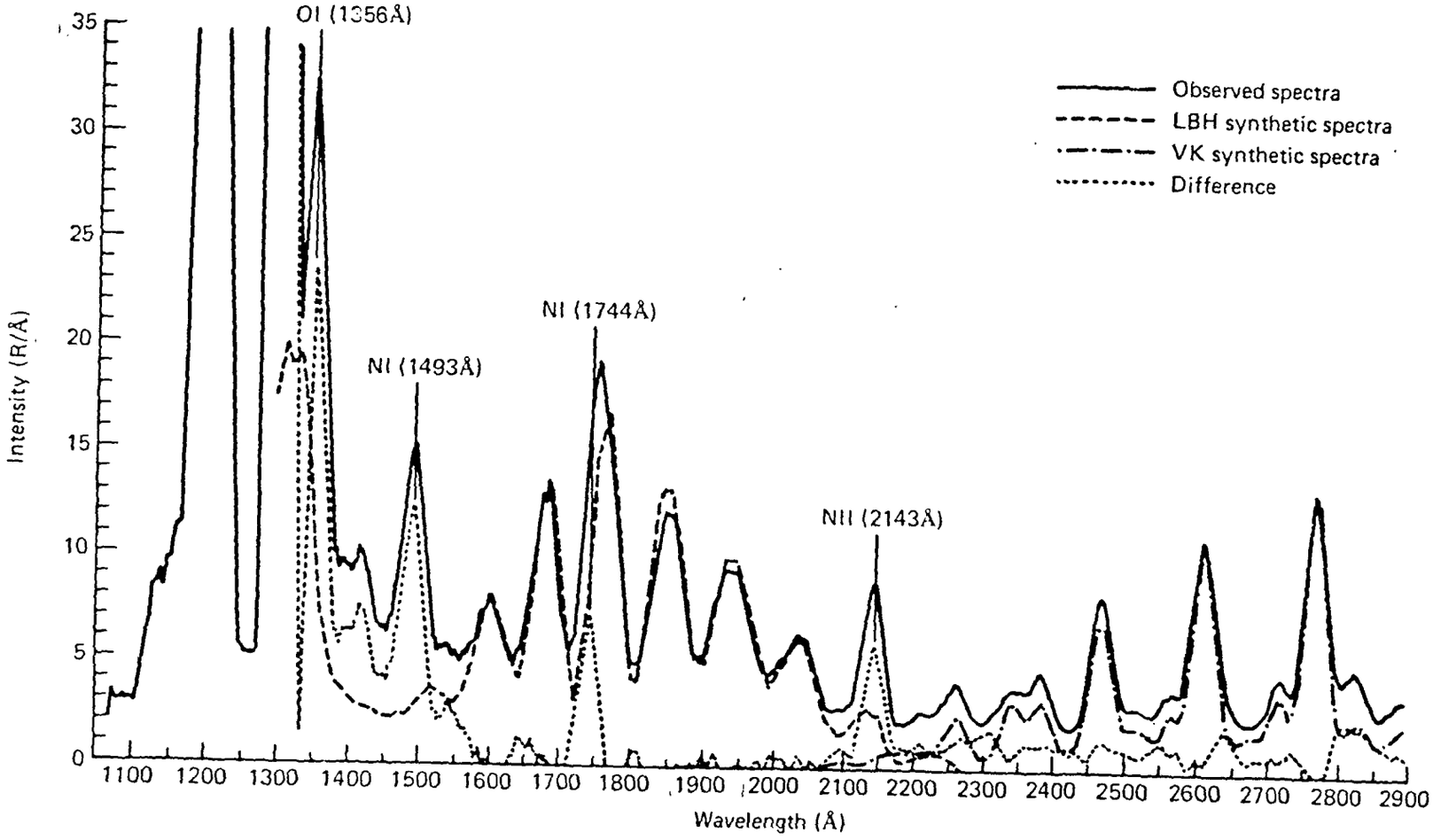

Figure 2. The effect of subtracting LBH and VK synthetic spectra from observed UV spectra between 1100 and 2900 Å. Intensities at the two peaks of 1928 and 2604 Å in the observed spectrum are used to normalize the LBH (3-10) and VK (0-5) synthetic bands. The normalized synthetic spectra are then subtracted from the observed spectrum. In the remaining spectrum, NI at 1493 Å and 1744 Å and NII at 2143 Å are clearly seen.

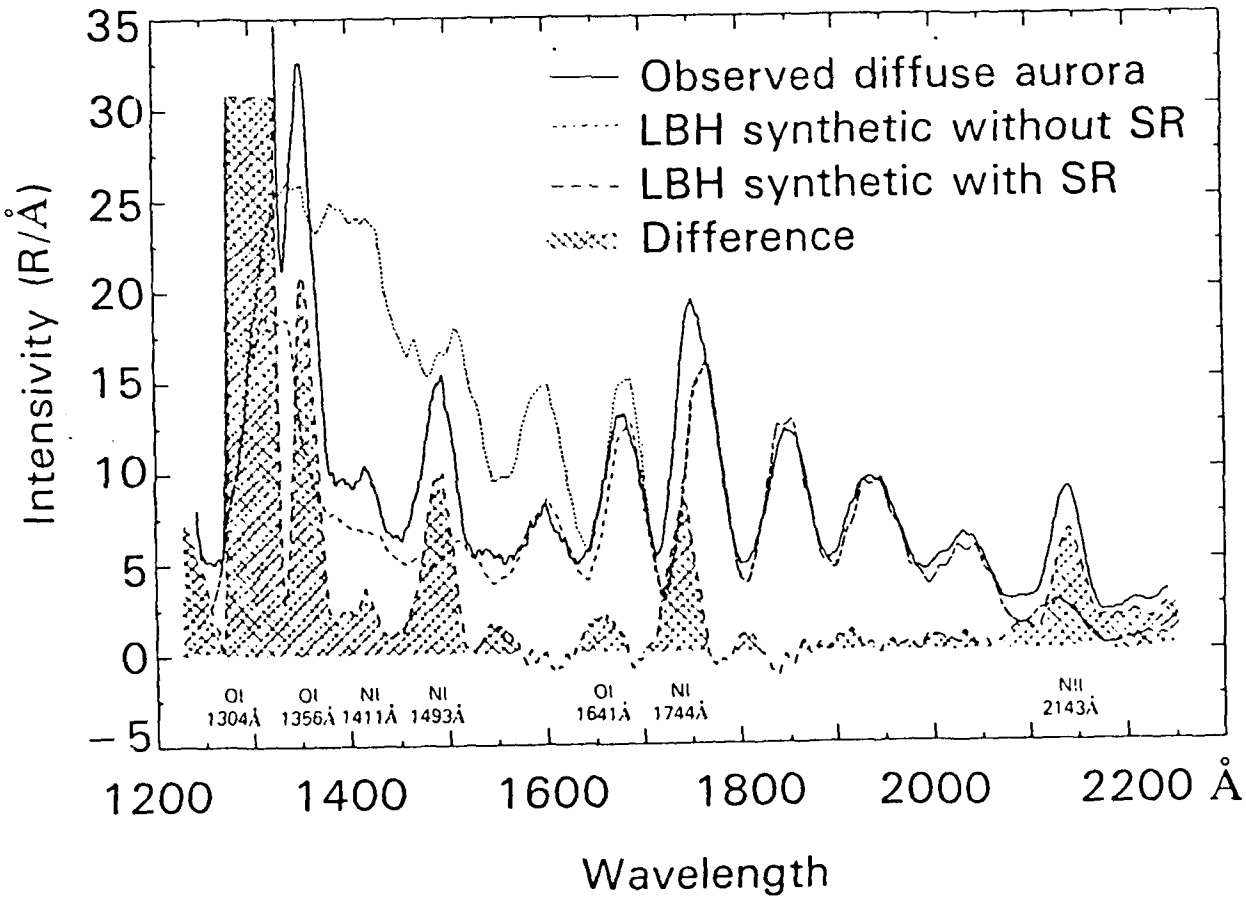

Figure 3. Application of the simplified SR absorption calculation on the LBH band system. A diffuse region auroral spectrum (solid line) is compared to the synthetic LBH spectrum (dotted line) normalized at 1928 Å. The synthetic LBH band system spectrum is modified by simple formula (Ishimoto et al., 1989b). The remainder spectrum (shaded area) resulting from the subtraction of the modified LBH from the observed spectrum, reveals the atomic lines.

Publications

Ishimoto, M., G. J. Romick, R. E. Huffman, and C. -I. Meng, Auroral electron energy and flux from molecular nitrogen ultraviolet emissions observed by the S3-4 satellite, J. Geophys. Res., 93, 9854-9866, 1988a

Ishimoto, M., G. J. Romick, R. E. Huffman, and C. -I. Meng, Ultraviolet spectra in the diffuse auroral region, Proceedings of SPIE- The International Society for Optical Engineering, 932, 179-189 1988b.

Ishimoto, M., G. J. Romick, C. -I. Meng, R. E. Huffman, V. Degen, Analysis of atomic ultraviolet lines in the diffuse aurora, submitted to J. Geophys. Res., 1988c.

Ishimoto, M., G. J. Romick, R. E. Huffman, and C. -I. Meng, Anomalous UV auroral spectra during a large magnetic disturbance, J. Geophys. Res., 94, 6955-6960, 1989a

Ishimoto, M., G. J. Romick, and C. -I Meng, Analytic estimation of O_2 Schumann-Runge absorption simulation for auroral LBH band emissions submitted to J. Geophys. Res., 1989b.

Ishimoto, M., G. J. Romick, C. -I. Meng, R. E. Huffman, Doppler shift of auroral Lyman α observed from a satellite, Geophys. Res. Lett., 16, 143, 1989c.

APPENDIX A

JOURNAL OF GEOPHYSICAL RESEARCH, VOL. 93, NO. A9, PAGES 9854–9866, SEPTEMBER 1, 1988

Auroral Electron Energy and Flux From Molecular Nitrogen Ultraviolet Emissions Observed by the S3-4 Satellite

M. ISHIMOTO AND C.-I. MENG

The Johns Hopkins University Applied Physics Laboratory, Laurel, Maryland

G. J. ROMICK

KIA Consultants Inc., Fairbanks, Alaska

R. E. HUFFMAN

Air Force Geophysics Laboratory, Hanscom Air Force Base, Bedford, Massachusetts

The UV spectra over the southern hemisphere nightside auroral oval have been obtained from an AFGL spectral/photometric experiment on board the low-altitude polar-orbiting S3-4 satellite. A detailed analysis of nightside auroral spectra from seven orbits between mid-May and June 1978 was performed to estimate the average energy and total energy flux of incident electrons. This study was based on observations of the N_2 LBH (3–10) (1928 Å) band and the N_2 VK (0–5) (2604 Å) band emission intensities and the application of model calculations by *Strickland et al.* [1983] and *Daniell and Strickland* [1986]. Comparison of the estimated quantities with the statistical satellite measurement of incident particles by *Hardy et al.* [1985] indicates that the LBH (3–10) band emission intensity can be used to estimate the total energy flux of incident electrons, similar to the N_2^+ 1N (0–0) (3914 Å) band emission intensity in the visible region. In addition, the ratio of the LBH (3–10) to the VK (0–5) band emission intensities indicates the average energy of incident auroral electrons in much the same way that the N_2^+ 1N (0–0) and O I (6300 Å) emission ratio does in the visible region. This study shows the use of different constituent emissions, model calculations, and synthetic spectra to infer the inherent possibilities in these types of studies.

1. INTRODUCTION

Ultraviolet (UV) auroral spectra have been studied on the basis of both rocket and satellite observations since the 1961 UV rocket spectrometer measurements (1100 and 3500 Å) [*Crosswhite et al.*, 1962] and the 1968 OGO-4 satellite observations (1200 to 3200 Å) [*Gerard and Barth*, 1976]. Investigations are mostly in the far UV (FUV) regions (< 1900 Å) with emphasis below 1400 Å. There are only a few observations in the near UV region (2000 to 3000 Å) [*Sharp*, 1971; *Beiting and Feldman*, 1979; *Huffman et al.*, 1980]. OGO-4 satellite observations [*Gerard and Barth*, 1976] revealed the auroral emissions in the N_2 Lyman-Birge-Hopfield (LBH) and N_2 Vegard-Kaplan (VK) band systems, the N I (1750 Å) line, and the O II (^4S-^2P) (2470 Å) line with 20-Å spectral resolution.

This article reports satellite measurements of nightside auroral emissions in both the discrete and the diffuse regions of the auroral oval under auroral activity conditions from quiescent to extremely active. All auroral oval observations used in this study were made over the winter southern hemisphere in darkness. The analysis concentrates on emission intensities and ratios of certain LBH and VK bands. In conjunction with model calculations [*Strickland et al.*, 1983; *Daniell and Strickland*, 1986], the UV data are used to estimate the average energy and the total energy flux of incident electrons across the auroral oval for each orbit. The results are in general agreement with the previously reported characteristics of particle precipitation across the auroral oval obtained by electron precipitation measurements [*Hardy et al.*, 1985].

The data used here were obtained by the Air Force Geophysics Laboratory Ultraviolet Backgrounds experiment, flown on the S3-4 satellite in 1978 [*Huffman et al.*, 1980]. That Air Force Space Test Program satellite was in a low-altitude polar orbit near the noon-midnight meridian plane, the nadir-viewing UV instruments observed the airglow, aurora, and solar scattered radiance of the Earth's atmosphere. The experiment consisted of two 1/4-m, *f*/5, Ebert-Fastie spectrometers (FUV from 1100 to 1900 Å and UV 1600 to 2900 Å) with synchronized scans. For each wavelength range, there were three selectable bandwidths at about 1, 5, and 30 Å. A separate photometer using interference filters recorded one of four (1216, 1340, 1550, and 1750 Å) wavelength bands. The initial results of the experiment and details of the sensors have been previously described by *Huffman et al.* [1980].

Paper number 7A9017.
0148-0227/88/007A-9017$05.00

2. DATA ANALYSIS

Data from 300 orbits were in easily reviewable microfiche format and covered quiescent to extremely active magnetic periods. However, in order to analyze the data in detail, the original data tapes needed to be used. In this study, we concentrate on a few orbits selected using the following criteria. First, both spectrometers were set to the same slit width in order to examine the overlapping spectral region (1600 to 1900 Å) and also to compare instrument calibration. Second, spectrometers were set at the largest slit (corresponding to a resolution of about 30 Å) in order to detect rather weak auroral emissions. Third, a photometer was set on one of the three (1340, 1550, and 1750 Å) wavelength band interference filters to continuously monitor auroral intensity variations. Finally, seven orbits, meeting all of these criteria, were selected to cover various levels of magnetic activity (Kp = 0 to 7+).

The observations of the nightside auroral oval were made at about 270 km above the winter southern hemisphere from May 1 to June 22, 1978. Solar zenith angles, geomagnetic conditions, peak intensities of the O I 1304 Å, and $L\alpha$ emissions within the oval for these seven orbits, together with the estimated particle

characteristics, are summarized in Table 1 and discussed more fully in section 4.

2.1. *Data Reduction*

The spectrometers have an intrinsic integration period for each wavelength step of 5 ms, and it takes 21 s to make one complete wavelength scan (i.e., 1100 to 1900 Å for the FUV and 1600 to 2900 Å for the UV). The number of data points was reduced by summing over 25 ms for the FUV spectrum and over 15 ms for the UV spectrum so that each spectral readout corresponds to the total counts in 1 Å. The 30-Å resolution spectra were insensitive to smoothing for any running mean below 20 Å. Running means of 6 and 15 Å were used to construct the FUV and UV spectra, respectively, in order to minimize the apparent counting statistical noise. After this spectral smoothing process, the counts were converted to rayleighs per angstrom (R/Å) using the calibrated instrument sensitivity and radiance scaling factors given in Figure 3 of *Huffman et al.* [1980]. The detector background noise was eliminated prior to calibration by subtracting 0.34 count per 5 ms for the FUV spectrometer measurements and 0.19 count per 5 ms for the UV spectrometer measurements so that spectral intensities in wavelength regions of no expected optical emission in the nightglow would yield a low signal level.

The spectral scan time of 21 s and the field of view of the spectrometers (11.5°) are quite large compared to the characteristic time and spatial scales of auroral display features, especially over the discrete auroral region. Consequently, it is necessary to correct each readout within a spectral scan in an attempt to compensate for any auroral intensity variations during each 21-s scan as the spacecraft moves across the auroral structure. We have tried to normalize each spectrum to a constant intensity by using data from the photometer that has a small field of view (1.65° or 0.12°) and an integration time of 10 ms. The satellite takes about 4.5 s to traverse the instantaneous viewing area of the spectrometers at the 100 km altitude of the auroral emission. Therefore the photometer data were smoothed by taking a running mean (4.5 s) to smear the photometer measurement over the 11.5° viewing angle of the spectrometers. The smoothed data, which typically vary across the scan by some 20% and at most by 150% in the diffuse auroral region, were then used to normalize the spectral intensities within each 21-s scan (hereafter called the photometer normalization).

Although the LBH and VK band emissions vary differently with incident particle energy, we assume that the intensity variation over the scan is greater than the relative spectral variation due to changes in characteristic energy. This assumption is the best approach available with this data set, and it appears to work well when the photometer monitors one of the LBH wavelength regions. However, the procedure is expected to be less effective for scans associated with rapid intensity variations such as across a sharp boundary of the auroral oval. Also, the normalization is completely meaningless for auroral emissions that do not vary proportionately to the monitored photometer band. For example, neither the geocoronal nor the auroral $L\alpha$ emission varies systematically with the LBH intensities transmitted by the 1550 and 1750 Å photometer filters since these filters transmit no $L\alpha$ emission. Less than 3% of the total intensity transmitted by (1340 Å) filter is due to $L\alpha$, the rest is primarily due to the O I (1304 Å) emission (see Figure 4 in *Huffman et al.* [1980]. Thus the observed $L\alpha$ emission intensity cannot be corrected with the photometer intensity variations within each spectral scan.

The two spectrometer ranges overlapped between 1600 and 1900 Å. However, the spectral data for wavelengths greater than 1750 Å from the FUV spectrometer were not used in this analysis because of the very low sensitivity in that wavelength region [*Huffman et al.*, 1980]. When the photometer normalization is applied to spectral data in the 1600 to 1750 Å region, where the two spectrometers overlapped, the match is quite good even though the two observations were made about 14 s apart. Furthermore, after the photometer normalization, the auroral spectral band systems that cover wide wavelength ranges (i.e., the LBH and the VK) match nominal synthetic spectra very well. Figure 1 shows the comparison of the normalized auroral spectra from the diffuse auroral region averaged over four scans (Figure 1*a*) with the synthetic VK band systems (Figure 1*b*) and with the synthetic LBH band systems (Figure 1*c*); the synthetic spectra are from *Degen* [1986]. Figure 1*a* also shows the combined spectra obtained from two separate FUV and UV spectrometers and the region of spectral overlap. In the overlap region, the spectra match very well; the deviation is less than 10%. The good agreement between the observed (Figure 1*a*) and the synthetic (Figures 1*b* and 1*c*) spectra lends credibility to the photometric normalization technique. In general, photometer normalization works well except in regions with drastic intensity changes, such as near the edges of the discrete auroral region.

Since the satellite altitude during these observations was about 260 km and we observed no anomalous LBH vibrational distributions, we disregarded vehicle glow [*Conway et al.*, 1987].

2.2. *Selection of Band Systems*

Auroral and airglow radiation consists of various molecular band systems such as the N_2 LBH, VK and Herman-Kaplan, the NO γ and δ, and the O_2 Herzberg I bands, as well as atomic lines such as the N I (1200, 1493, and 1744 Å), O I (1304 and 1356 Å), N II (2143 Å), and O II (2470 Å) lines. Two wavelength regions are particularly difficult to analyze. One is from 1500 to 1900 Å, where the relative emission intensities of the VK band system are uncertain. This will be described in detail in the next section. The other region is the O_2 Schumann-Runge continuum region from 1350 to 1750 Å where atmospheric O_2 absorbs the emissions coming from below 130 km [*Meier et al.*, 1982]. Therefore in this analysis, we have concentrated on the UV spectra above 1900 Å.

The major molecular band features in the UV spectra are the LBH and VK band systems. The rest of the auroral spectral features will be more easily distinguished by subtracting out the LBH and VK band systems from the observed spectra. The solid line in Figure 2 is the observed spectrum (Figure 1*a*) with the synthetic LBH and VK band systems subtracted. In the subtraction process, the intensities of the observed and synthetic peaks at 1928 Å for the LBH and at 2604 Å for the VK are matched. Because of uncertainties in the synthetic VK band emission intensities below 2000 Å, only the VK synthetic spectrum above 2050 Å was subtracted. There are obvious atomic features at 1744 Å (N I) and 2143 Å (N II) in Figure 2. Small features below 2050 Å (except the N I line at 1744 Å) may be part of the VK band system emission; however, they typically are smaller than those expected in the synthetic spectra by a factor of 2 or 3 (Figure 1*b*). The band features above 2500 Å are mainly from the O_2 Herzberg I band systems, which are commonly seen in the airglow outside the auroral regions. The secondary features between 1900 and 2600 Å consist of the NO δ and Herman-Kaplan band systems. The O II forbidden line at 2470 Å is not clearly distinguishable in this spectrum but is strong at other times. Its intensity can reach as

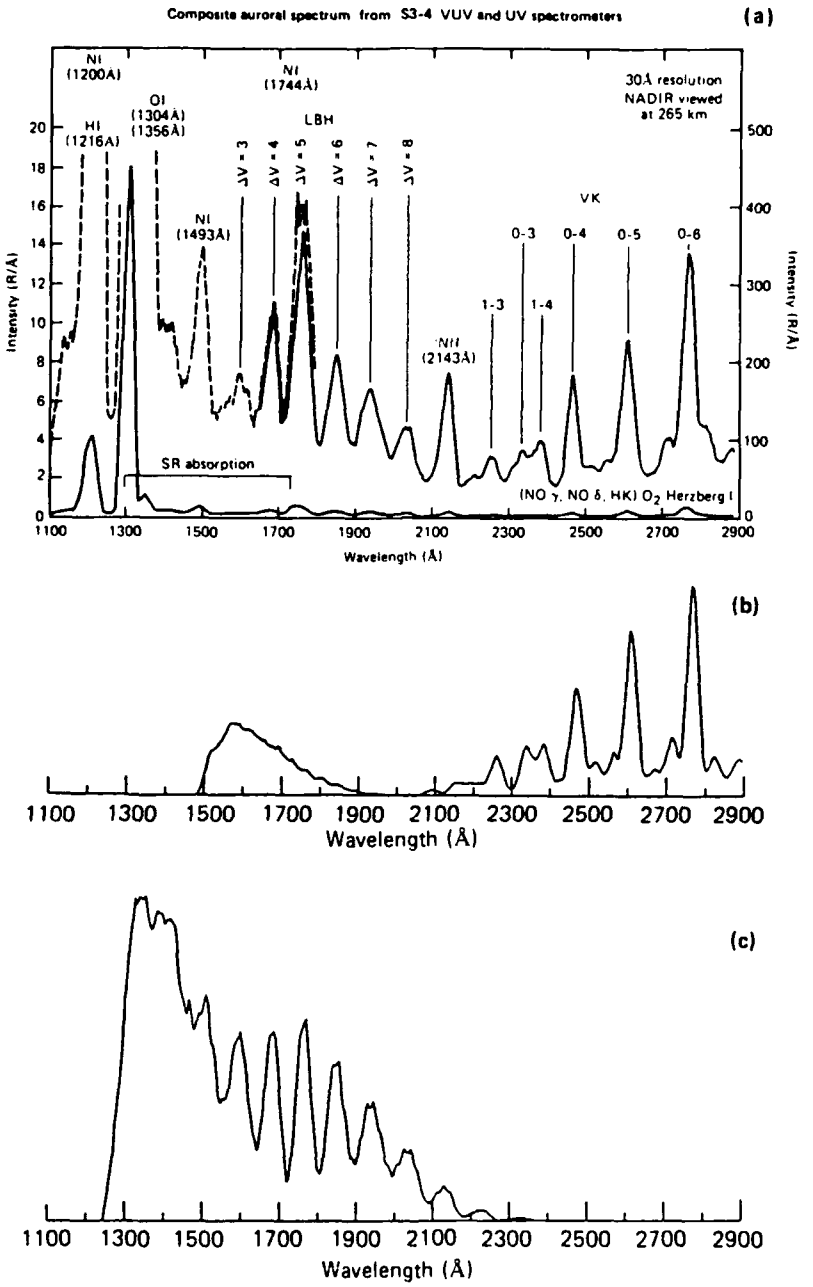

Fig. 1. Comparison of the observed UV spectrum with LBH and VK synthetic spectra from *Degen* [1986]. (*a*) Spectra of 30-Å resolution obtained by FUV (dotted line) and near-UV (solid line) spectrometers overlapping in the wavelength range 1600 to 1750 Å. These spectra are the average of four consecutive 21-s scans viewing a diffuse aurora in the southern hemisphere midnight sector from 260 km altitude at about 1836 UT on June 2, 1978. (*b*) VK synthetic spectrum assuming T_r = 400 K and the vibrational population distribution. (Note uncertainty for high v' or $\lambda < 2000$ Å; see text for details.) (*c*) LBH synthetic spectrum assuming T_r = 400 K and T_v = 400 K.

high as a few hundred rayleighs in some spectra associated with the discrete auroral region.

Taking into consideration the secondary emission band features, atomic lines, and uncertainties in the synthetic spectra, we found that the LBH (3-10) peak at 1928 Å and the VK (0-5) peak at 2604 Å are relatively free from contamination by other band systems and lines. These peaks are located outside the O_2 Schumann-Runge absorption region and have reasonably good signal strengths. Therefore these two intensities can be used as the representative emission intensities for the LBH and VK bands.

2.3. *Estimation of the LBH* (3-10) *and the VK* (0-5) *Band Intensities*

For the LBH (3-10) band intensity estimation, we integrated the observed intensity between 1916 and 1955 Å because this interval consists of LBH emission and also is the least contaminated by other emissions. The intensity of the secondary emission, i.e., NO δ, was assumed to be the same as in the nearest nightglow spectra equatorward of the oval and subtracted from this integral. For the synthetic spectra using 30-Å resolution, 99% of the LBH (3-10) band occurs in this range. In consideration of all the other

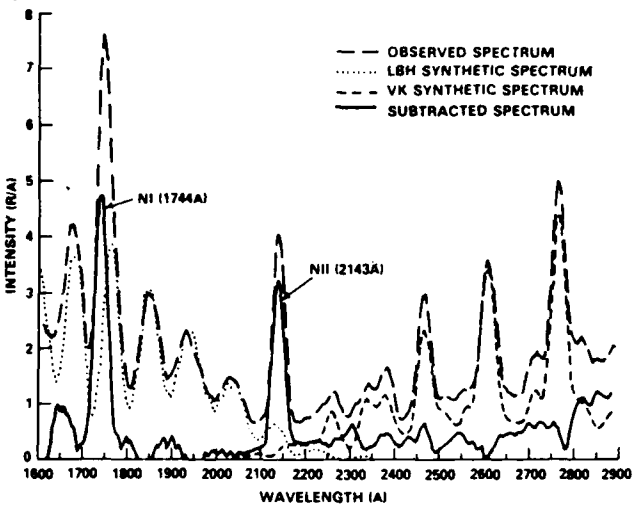

Fig. 2. The effect of subtracting LBH and VK synthetic spectra from observed UV spectra between 1600 and 2900 Å. Intensities at the two peaks of 1928 and 2604 Å in the observed spectrum are used to normalize the LBH (3-10) and VK (0-5) synthetic bands. The normalized synthetic spectra are then subtracted from the observed spectrum. In the remaining spectrum, N I at 1744 Å and N II at 2143 Å are clearly seen. The spectra below 2000 Å are suspected to come from VK emission from high vibrational levels ($v' > 6$). The spectrum between 1880 and 2750 Å s a composite of the NO δ, the N_2 Herman-Kaplan band systems, and the O II forbidden line at 2470 Å. Spectra beyond 2500 Å are mainly O_2 Herzberg I band emission seen as airglow outside the auroral region.

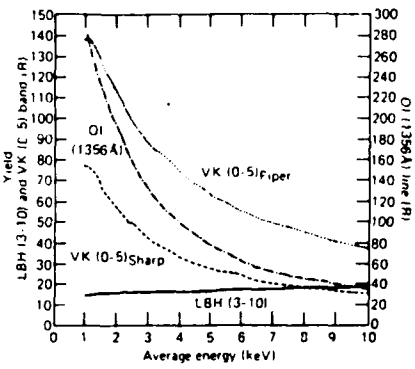

Fig. 3. The column emission rate as a function of the average energy of incident electrons calculated by Strickland: LBH (3-10), VK (0-5), and O I (1356 Å). The values are normalized for a unit flux (1 erg/cm^2 s) with a Maxwellian distribution. The MSIS-83 model atmosphere is used. The common unit for the LBH (3-10) and VK (0-5) band emission intensities is given on the left, while the unit for the O I (1356 Å) line is on the right. The subscripts of the VK $(0-5)_{Piper}$ and VK $(0-5)_{Sharp}$ correspond to the use of the atomic quenching coefficients by *Piper et al.* [1981] and *Sharp* [1971], respectively.

overlapping LBH bands, 45.8% of the integrated intensity is due to the LBH (3-10) band. Therefore, the LBH (3-10) band emission intensity was obtained from the observed intensity integrated between 1916 and 1955 Å by multiplying by 0.463.

For the VK (0-5) band intensity estimation, we integrated the observed intensity between 2591 and 2628 Å because in this interval the VK emission is least contaminated by other emissions. The intensity of the secondary emission, i.e., Herzberg I, was assumed to be the same as in the nearest nightglow spectra equatorward of the oval and subtracted from this integral. For the synthetic spectra with 30 Å resolution, 98% of the (0-5) band occurs in this range. In consideration of all the other overlapping VK bands, 95.7% of the integrated intensity is due to the (0-5) band. Consequently, the (0-5) band emission intensity was obtained by multiplying the integrated intensity between 2591 and 2604 Å by 0.976.

3. Model Considerations

3.1. *LBH Band System*

The LBH band system is located in the 1250 to 2400 Å range with a total intensity of 383 kR for an IBC III aurora [*Vallance-Jones*, 1974]. The LBH band system originates from a transition from the $a^1\Pi_g$ state to the $X^1\Sigma_g^+$ ground state. The collisional quenching for this band emission takes place below 95 km, which is lower than most auroral emission altitudes. A synthetic spectrum of this band provided by *Degen* [1986] is shown in Figure 1*c*. The model of *Strickland et al.* [1983] indicates that the peak production altitude is from 105 to 120 km, depending on the energy of the incident electrons. The LBH synthetic spectrum [*Degen*, 1986] with a 30-Å spectral resolution is not sensitive to changes in the rotational and vibrational temperature around 300 K. Consequently, we have used synthetic 30-Å spectral resolution [*Degen*, 1986] with T_r = 400 K and T_v = 400 K in this study.

Figure 3 shows the column emission intensity caused by 1 erg/cm^2 s incident flux (called yield according to Strickland) of the LBH (3-10) band as well as the VK (0-5) band and the O I (1356 Å) line as a function of the average energy of incident electrons. The energy flux with a Maxwellian distribution is more representative of the incident electron distribution in diffuse auroras as described by *Strickland et al.* [1983]. The values in Figure 3 were calculated with modified parameter values by D. J. Strickland (private communication, 1987) and differ from those in *Strickland et al.* [1983]. The cross sections of the LBH bands were replaced by those of *Ajello and Shemansky* [1985] for this calculation. The cross section of the O I (1356 Å) was adjusted by multiplying the cross section of *Stone and Zipf* [1974] by 0.6 to reflect the revision by *Zipf and Erdman* [1985]. The model atmosphere used was the MSIS-83 model by *Hedin* [1983] (year = 1985, day = 32, sec = 14,400 s, GLAT = 60°, GLON = 270°, LT = 2200, $F10.7$ = 120, AP = 20).

Because of the direct relationship of the LBH (3-10) to the incident electrons, and because it is not dependent on chemistry, atmospheric absorption, and quenching, the yield of the LBH (3-10) band can be used with the Strickland model (Figure 3) to calculate the energy flux.

3.2. *VK Band System*

The auroral VK band system extends from 1500 to 7000 Å with a total intensity of 55 kR for an IBC III aurora according to *Vallance-Jones* [1974]. The VK band system originates in the forbidden transition from the $A^3\Sigma_u^+$ state to the $X^1\Sigma_g^+$ ground state. The VK vibrational energy levels are excited by several mechanisms such as direct electron excitation from the N_2 electronic ground state, radiative cascade involving the $B^3\Pi_g$ and $C^3\Pi_u$ states, and depopulation of the $v \geq 8$ vibrational levels by the "reverse" N_2 1P transition $A^3\Sigma_u^+ \rightarrow B^3\Pi_g$ [*Degen*, 1982]. Estimated vibrational population distributions by several studies differ from each other, especially in the high vibrational levels ($v \geq 7$) [*Cartwright*, 1978]. The dominant VK band features at wavelengths >2000 Å come from low vibrational energy levels of the N_2 $A^3\Sigma_u^+$ state that are populated largely by cascade from other electronic states. The population of the high-lying vibrational levels does not affect the band features at wavelengths >2000 Å. On the other hand, the VK band features at wavelengths <2000

Å originate from the high vibrational energy levels; however, the source and magnitude of their population distribution have not been established. If present in the aurora as it appears in the synthetic spectra, the cluster of bands in the 1500 to 2000 Å range could contribute a significant background for the LBH band systems in the same wavelength region. However, auroral spectra of 4-Å resolution obtained in a rocket experiment [*Eastes and Sharp*, 1987] show little VK band emission between 1675 and 2075 Å, where the VK emission from $v' = 4$, 6, 7, and 8 would appear. In addition, the atmospheric O_2 (Schmann-Runge continuum, 1350 to 1750 Å) absorbs the emission coming from below 130 km. Therefore considering these factors, we assumed little VK emission at wavelengths <2000 Å. The rotational energy levels appear to be collisionally well thermalized at the local temperature [*Degen*, 1982].

Because of the lifetime of the A state, it is expected that quenching will affect the emission profiles of the VK band systems. This is demonstrated in the theoretical analysis by *Daniell and Strickland* [1986]. They showed that for typical auroral average energies most of the emission will come above 120 km. According to the MSIS-83 model atmosphere [*Hedin*, 1983], the thermal temperature above 120 km during the disturbed time is greater than 400 K. The characteristic shape of VK synthetic spectra using 30-Å resolution does not vary significantly with a few-hundred-degree change in the rotational temperature above 400 K. Therefore we set $T_r = 400$ K in the synthetic spectrum by *Degen* [1986] and then used his assumed vibrational population distribution in this study (Figure 1*b*). Degen determined the vibrational population distribution by matching synthetic spectra with values from various published papers. For 30-Å resolution, the spectrum above 2000 Å in Figure 1*b* seemed adequate for this study.

Figure 3 shows the VK (0-5) band column emission intensity rates as functions of incident electron energy calculated by Strickland. The emission intensities will differ, depending on the choice of the quenching rate coefficient for atmospheric atomic oxygen for the $v' = 0$ level and the atmospheric atomic oxygen density. The quenching rate coefficients were based on rocket data, 9×10^{-11} cm^{-3} s^{-1} for the $v' = 0$ level by *Sharp* [1971] (hereafter called the Sharp value), and laboratory data, 2.8×10^{-11} cm^3 s^{-1} by *Piper et al.* [1981] (hereafter called the Piper value).

The variation in the atomic oxygen densities changes the column emission intensity in a way similar to the change in the quenching rate coefficient. The dependence on the atmospheric oxygen density was demonstrated in Figure 13 of *Daniell and Strickland* [1986].

In order to get atomic oxygen densities for the aurora cases studied here, the column emission intensity ratio of the O I (1356 Å) line to the LBH (3-10) band was utilized (Figure 4). Variations in the atomic oxygen densities also change the column emission intensity of the O I line as illustrated in Figure 11 of *Strickland et al.* [1983]. In the next section, we will use this concept and the observed O I (1356 Å) line emission to deduce an appropriate atomic oxygen density. The selection of the model-energy-dependent intensity relationship for the VK (0-5) band will depend upon the LBH (3-10) and the VK (0-5) bands, a suitable atomic oxygen quenching coefficient, and the atmospheric oxygen density deduced from the observed O I (1356 Å) line.

3.3. *Relation of Total Energy Flux and Average Energy of Incident Electrons, and the Observed Emission Intensities*

The average characteristics of auroral electron precipitation from data of the DMSP and STP 78-1 satellites were statistically studied as a function of magnetic local time, latitude, and the *Kp* index by *Hardy et al.* [1985]. They obtained an average energy flux of a few ergs/cm^2 s and the average energy of incident electrons was about 3 keV for $3 < Kp < 6$ in the midnight sector.

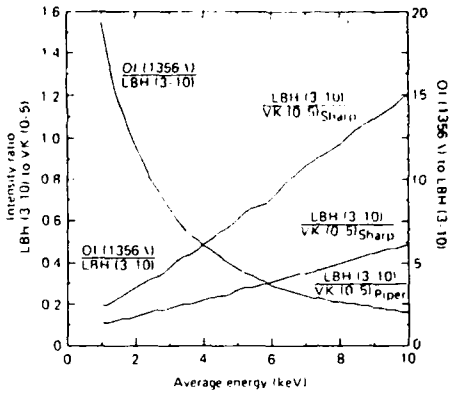

Fig. 4. Emission intensity ratios as a function of average energy of incident electrons. The ratios in solid line are deduced from the values in Figure 3. The two solid curves for the LBH (3-10) to the VK (0-5) band emission intensity ratios reflect the use of the Sharp or Piper atomic oxygen quenching coefficient. The two dotted curves demonstrate the effect of 30% atomic oxygen density of the model atmosphere (see the text for detail). The common scale of the VK (0-5) to the LBH (3-10) band emission intensity ratio is given on the left, while the scale for the O I (1356 Å) line to the LBH (3-10) band intensity ratio is given on the right. The subscripts of the VK $(0\text{-}5)_{Piper}$ and VK $(0\text{-}5)_{Sharp}$ correspond to the use of the atomic quenching coefficients by *Piper et al.* [1981] and *Sharp* [1971], respectively.

In the discrete auroral region where high total energy flux of incident electrons is expected, the S3-4 spectral data show high intensities of the LBH (3-10) band emission. Its yield is insensitive to the energy of the incident electrons (Figure 3), and thus the observed absolute emission rate is proportional to the total energy flux of incident electrons.

The LBH (3-10) band yield by an electron flux with average energy of about 3 keV is 16 R, as shown in Figure 3. The observed average LBH (3-10) band intensity for $3 < Kp < 6$ was 55 R. Thus, the average energy flux inferred from the seven orbits in the diffuse region of the southern auroral oval is 3.5 ergs/cm^2 s, which is at the higher end of the values reported by *Hardy et al.* [1985]. Considering the differences between the instantaneous and the model atmospheres, the agreement is certainly very reasonable. Thus with the Strickland model, the LBH (3-10) band intensity can provide a way of observing remotely the energy flux of auroral precipitation.

The most uncertain density in the model atmosphere is that of atomic oxygen. We can estimate the atomic oxygen density based on the observations of the O I (1356 Å) line and the LBH (3-10) and VK (0-5) band emission intensities.

In order to deduce the O I 1356-Å line intensity, the LBH bands which overlap this wavelength must be subtracted from the observed spectra. Since we do not know the altitude distribution of the LBH band emission, we cannot estimate the exact LBH band emission intensity through the O_2 SR absorption. However, we can estimate upper and lower bounds of the O I line assuming two imaginary LBH band systems.

The upper bound value of the O I intensity was estimated by subtracting our underestimated LBH band intensity around 1356 Å. Assuming the LBH emission was located in one layer at a certain altitude, we can apply the known variation of the absorption cross section as a function of wavelength [*Hudson*, 1971] to the

synthetic LBH band system spectrum and modify this synthetic spectrum to the observations between 1600 and 1680 Å. This one layer approximation always underestimates the LBH bands around the 1356 Å, where the O_2 SR cross section is large. We then subtracted this under-estimated LBH contribution from the 1356 Å observation to obtain an upper bound for pure O I (1356 Å) emission intensity.

A lower bound value for the O I intensity was estimated by subtracting our overestimated LBH band intensity around 1356 Å. In the wavelength region of 1356 Å ± 60 Å, only three nontrivial atomic lines exist, the O I 1304 Å, the O I 1356Å, and the N I 1411Å. If all the LBH band systems are subtracted from the observed spectra, these three lines should be the only ones appearing in the subtracted spectra. The two minimum intensity points between the three maximum points from the three atomic line peaks in the LBH subtracted spectrum should not be less than zero for the 30-Å resolution spectra. If we draw a straight line on the spectra between these two minimum points and assume the peak intensity of the O I line to be above this straight line at 1356 Å, we get the lower bound O I emission intensity.

Taking the middle point of the upper and lower bounds for the bottom of the O I line, we obtained the O I emission intensity. The difference between this middle point and either bound lies within 10% of the estimated O I emission intensity itself. This accuracy (within 10%) is adequate for our study. The average intensity ratio of the O I (1356Å) to the LBH (3-10) remained approximately constant at about 5 ± 1 in the diffuse auroral regions where the LBH (3-10) band intensities were more than 20 R.

Figure 4 shows the intensity ratio O I(1356Å)/LBH(3-10) as a function of the average energy of the incident electrons calculated by Strickland under a MSIS-83 model atmosphere (the values are from Figure 3). A reduction of the atmospheric oxygen density lowers the magnitude of the curve by decreasing the O I (1356 Å) line emission (see Figure 11 of *Strickland et al.* [1983] for details). The curve reads 4.5 keV for the intensity ratio of 5, observed by the S3-4 satellite. However, if the atomic oxygen density during the observations were smaller, the curve calculated for this modified oxygen density would have been reduced in magnitude, therefore the curve would have read a lower average energy for the observed intensity ratio (5).

Figure 4 also shows the intensity ratios LBH(3-10)/VK(0-5) as a function of the average energy of the incident electrons calculated by Strickland (the values are from Figure 3). These two curves in Figure 4 represent the two quenching rate coefficients with the same MSIS-83 model atmosphere. A reduction of the atmospheric oxygen density decreases the magnitude of the curve by increasing the VK (0-5) band emission, and therefore decreasing the ratio LBH/VK (see Figure 13 of *Daniell and Strickland* [1986] for details). The LBH/VK curves for Sharp and Piper quenching coefficients read 3 and 8.5 keV for the average intensity ratio of 0.4 observed by the S3-4 satellite. However, if the atomic oxygen density during the observations were smaller, the curves calculated for this oxygen density would be reduced in magnitude, and therefore yields higher average energy for the intensity ratio of 0.4.

If the atomic oxygen density during the observation was 30% less than the model atmosphere used in the Strickland calculation. (It would lower the curves O I/LBH by 30% and LBH/VK by 20% in Figure 4, according to Strickland's calculations (see Figure 11 of *Strickland et al* [1983] and Figure 13 of *Daniell and Strickland* [1986]. Then, the new curves of the O I/LBH for the intensity ratio of 5 and the LBH/VK with Sharp quenching coefficient for the intensity ratio of 0.4 would yield the same averaged energy of 3.5 keV for this reduced atomic oxygen atmosphere. Although this estimated average energy is slightly higher than the statistically averaged energy, 3 keV, reported by *Hardy et al.* [1985], we conclude that the analysis of the VK band intensity using the Sharp quenching coefficient satisfactorily links the optical measurements, the model calculations by *Strickland et al.* [1983] and *Daniell and Strickland* [1986], and the particle analysis by *Hardy et al.* [1985]. Therefore we conclude that the atomic oxygen density during our observation was 30% less than that of the MSIS-83 atmosphere used in Strickland's calculation. This shows the consistency of the observations with the results of Strickland's new LBH and VK calculations with the Sharp coefficient for the reduced atomic oxygen density.

4. Observations and Results

The seven auroral oval crossings in the midnight sector are described in this section. The observed $L\alpha$ and O I (1304 Å) emission intensities, inferred incident electron characteristics, and magnetic conditions of these orbits are presented before the description of each auroral oval pass. Table 1 lists the observation date and time, the activity indices and approximate locations of the satellite and the solar zenith angles. The emission intensities were obtained every 22 s, corresponding to the spectrometer scan cycle (the spectrometer scanning time was 21 s). Because of the small spatial (i.e., temporal) scale of emissions, the values for the discrete auroral region listed here may not necessarily be representative. However, the values for the diffuse region are representative of each orbit.

The auroral $L\alpha$ emission intensities show no correlation to the activity indices over these orbits. The geocoronal $L\alpha$ intensities show a correlation with the solar zenith angle. *Meier and Mange* [1970] reported that the geocoronal $L\alpha$ is a function of the solar zenith angle and the column hydrogen concentration at the observation point. Since the S3-4 observation altitudes were about the same for all orbits in this latitudinal region, any variation of geocoronal emission is primarily due to changes in the solar zenith angle. The O I (1304 Å) emission intensities in the diffuse region have a strong correlation with magnetic activity. The LBH and VK band emission intensities, discussed later for Figures 5*a*-5*g*, also have a correlation with magnetic activity.

The bottom part of Table 1 gives the inferred incident electron characteristics. The average energy is the incident electron energy averaged over the entire oval crossing. The highest average energy did not occur in the most disturbed period during these seven orbits. The next line, average energy flux, gives the incident energy flux averaged over the entire oval crossing. The last parameter in the table, total energy flux across the oval, gives the sum of the energy flux, each 22 s, throughout the auroral oval for each orbit in terms of ergs/cm^2 s in a 1-cm slice across the oval and also in a fan-shaped slice with 0.5 hour longitudinal width. The former value represents the emission of the exact area observed by the nadir-viewing satellite. The latter value, which is well correlated with magnetic activity, is deduced for comparison to observations of *Hardy et al.* [1985]. The total energy flux obtained for the midnight sector (2345 to 0015 MLT) varies from 3.0×10^{23} to 1.3×10^{25} keV/s sr, which is consistent with the previously reported auroral electron precipitation over these magnetic activity levels (as in Figure 8 of *Hardy et al.* [1985].

The individual orbits, described in Figures 5*a*-5*g*, illustrate the complexities in the electron energetics and proton precipitation at the various levels of magnetic activity. The figures focus on the LBH and VK bands, the auroral $L\alpha$ emission intensities, and the

TABLE 1. Summary of Geophysical Conditions

	Orbit Number						
	1216	1593	1410	1418	1401	1267	1041
Time, 1978							
month, day, hour, minute	5 30 1512	6 22 2029	6 11 0037	6 11 1401	6 11 0037	6 2 1836	5 19 2022
day, second	150 54720	173 73740	162 2220	162 50460	162 2220	153 66960	139 73320
Activity index							
Kp	2+	3+	2	1−	4+	7+	0
Ap	18	15	17	10	17	82	4
*F*10.7	143	184	110	113	110	143	131
AE	300	250	200	100	350	1200	50
Dst	−34	−12	−31	−28	−35	−57	−18
Location							
Solar zenith angle	147	133	147	120	129	143	126
Altitude, km	273	264	274	273	277	295	270
Emissions, kR							
Auroral $L\alpha$							
Discrete peak	1.2	0.4	0.0	0.0	0.3	0.1	0.1
Diffuse peak	3.8	1.3	1.0	0.6	2.2	1.0	0.5
Geocoronal $L\alpha$	2.0	2.3	1.2	2.2	1.7	2.1	3.1
O I (1304 Å)							
Discrete peak	7.0	6.0	3.0	2.5	4.0	14.0	5.5
Diffuse peak	2.3	2.2	1.3	1.0	3.0	5.0	2.6
Incident electron characteristics							
Average energy, keV	3.6	4.4	1.2	3.6	5.4	3.2	3.2
Average energy flux, ergs/cm^2 s	10.0	2.2	5.2	0.66	2.5	8.6	0.78
Total energy flux across the oval							
1 cm width ($\times 10^8$ ergs/s)	19.4	3.9	5.1	0.74	4.1	19.6	1.69
30 min longitudinal width							
($\times 10^{23}$ keV/s sr)	122	15.2	37.1	3.38	21.9	133	3.4

photometer data. The latitudinal emission intensity variations for all seven auroral oval crossings are presented. There are four panels in each diagram. The first (top) panel shows the high-time-resolution nadir-view photometer data across the auroral oval without averaging. The value in the upper right-hand corner indicates the peak transmission wavelength of the photometer filter used for that orbit. Since each filter has a rather wide bandpass with a full width half maximum of 116 to 164 Å [*Huffman et al.*, 1980], the photometer counts of the 1340-Å filter do not necessarily covary with the LBH or VK band system intensities, owing to the strong influence of the O I (1304 Å) emission. Thus photometer normalization using this particular bandpass (1340 Å) does not work as well as when using filters centered at 1550 or 1750 Å. Also, as previously mentioned, the photometer normalization to the spectral observation is not valid in a region with sudden intensity changes (more than a factor of 10 in a few seconds), such as at the edge of the discrete auroral region.

The second panel shows the deduced auroral $L\alpha$ and N I (1200 Å) emission intensities as well as the total observed $L\alpha$ emission intensity. There are several steps in the calculation of the auroral $L\alpha$ intensity from the observed spectrum. We first deduced the N I (1744 Å) emission intensity by subtracting Degen's synthetic spectrum from the observed LBH band intensities between 1715 and 1775 Å. Second, the ratio 4.0 of the cross sections of N I lines at 1200 and 1744 Å was used to estimate the N I (1200 Å) line intensity. This ratio from the laboratory [*Ajello and Shemansky*, 1985] and from atmospheric observations [*Gerard and Barth*, 1976; *Sharp and Rees*, 1972] varies from 4 to 7. The differences are primarily due to the optical thickness of the N I (1200 Å) [*Meier et al.*, 1980] and the height of the aurora. The N I (1200 Å) emission intensity deduced in this way also has to be corrected for possible changes within the spectral scan as described previously. Third, we integrated the intensities of the spectra over the wavelength interval 1200 to 1245 Å without photometer normalization (hereafter called integrated 1216 Å), and we subtracted the corrected deduced N I (1200 Å) from the integrated 1216 Å. Assuming that the geocoronal $L\alpha$ change is very smooth and that its intensity can be linearly interpolated across the auroral region, it is subtracted from the integrated 1216 Å in order to obtain the auroral $L\alpha$ intensity within each spectral scan. However, this process introduces some uncertainties into the determination of the N I (1200 Å) emission intensity because of the photometer normalization and the fixed ratio that we used for the N I line emissions at 1200 and 1744 Å. Because of the potential large error due to large intensity change across the spectrum, both $L\alpha$ and N I (1200 Å) emission intensities in the discrete auroral region were not plotted in Figures 5*a*-5*g*. In general, the deduced auroral $L\alpha$ variation across the auroral oval is as expected: a general increase toward the equatorward edge of the diffuse region and a general but not well defined overall enhancement with increasing activity.

The third panel shows the emission intensities of the LBH (3-10)

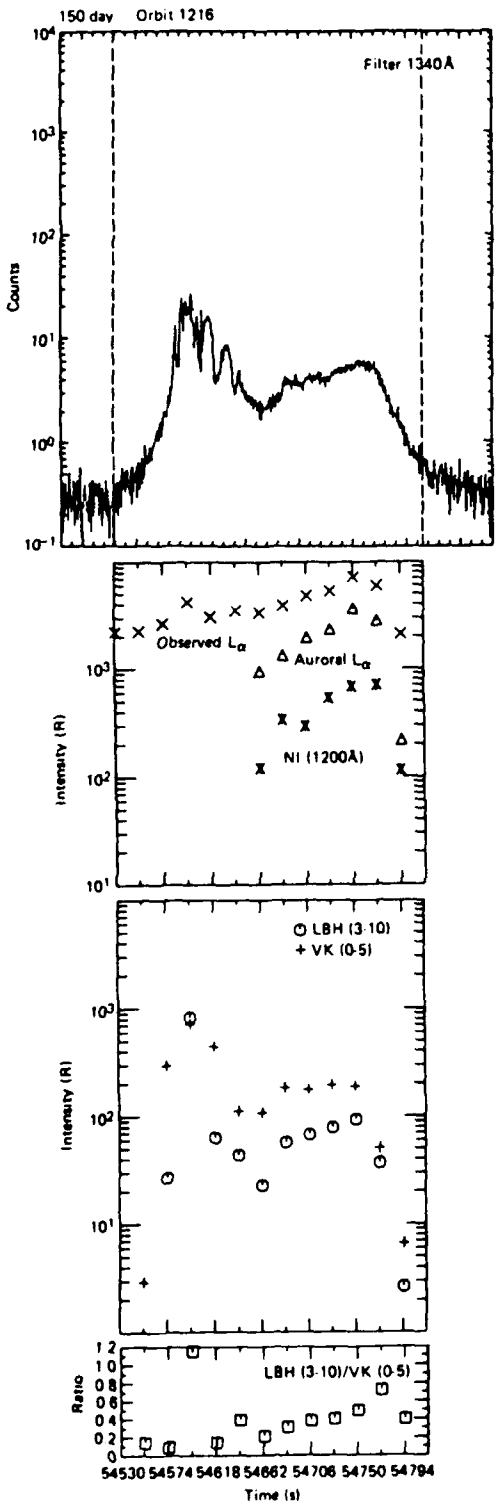

ALT (km)	277 4	276 7	275 7	274 5	273 2	271 6
GCLAT	-64 0	-60 8	-57 5	-54 3	-51 0	-47 7
GCLONG (+E)	122 5	120 5	118 9	117 5	116 3	115 2
GMLAT	-75 3	-72 2	-69 0	-65 8	-62 6	-59 4
GMLONG (+E)	200 1	195 2	191 9	189 3	187 3	185 6

Fig. 5a

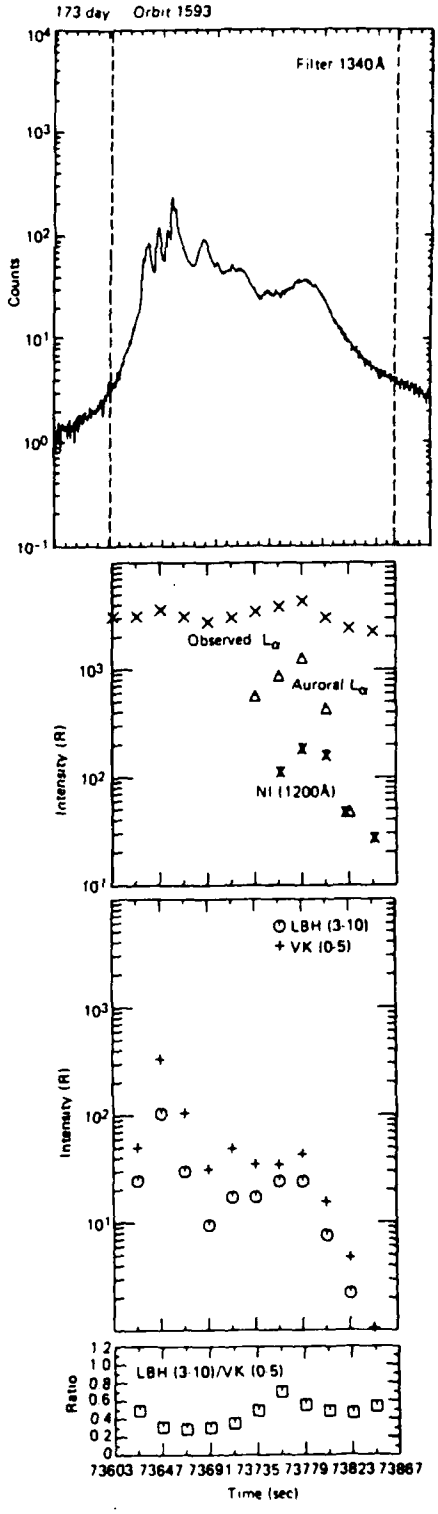

ALT (km)	269 8	270 0	270 0	269 7	269 2	268 3	267 3
GCLAT	-80 7	-78 1	-75 2	-72 2	-69 0	-65 8	-62 6
GCLONG (+E)	74 6	62 5	54 8	49 6	45 9	43 2	41 0
GMLAT	-82 8	-80 3	-77 4	-74 2	-71 0	-67 8	-64 5
GMLONG (+E)	50 5	66 0	74 6	79 7	83 0	85 1	86 7

Fig. 5b

Fig. 5. Latitudinal (time) variation of LBH (3-10) and VK (0-5) emission intensities for the seven orbits. Top panel, observed photometer counts. Second panel, both the total observed $L\alpha$ emission (cross) and the auroral $L\alpha$ emission (triangle), and the N I (1200 Å) emission (star). Third panel, LBH (3-10) (circle) and VK (0-5) (plus) band emission intensities. Fourth panel, intensity ratio of LBH (3-10) to VK (0-5) band emission intensities.

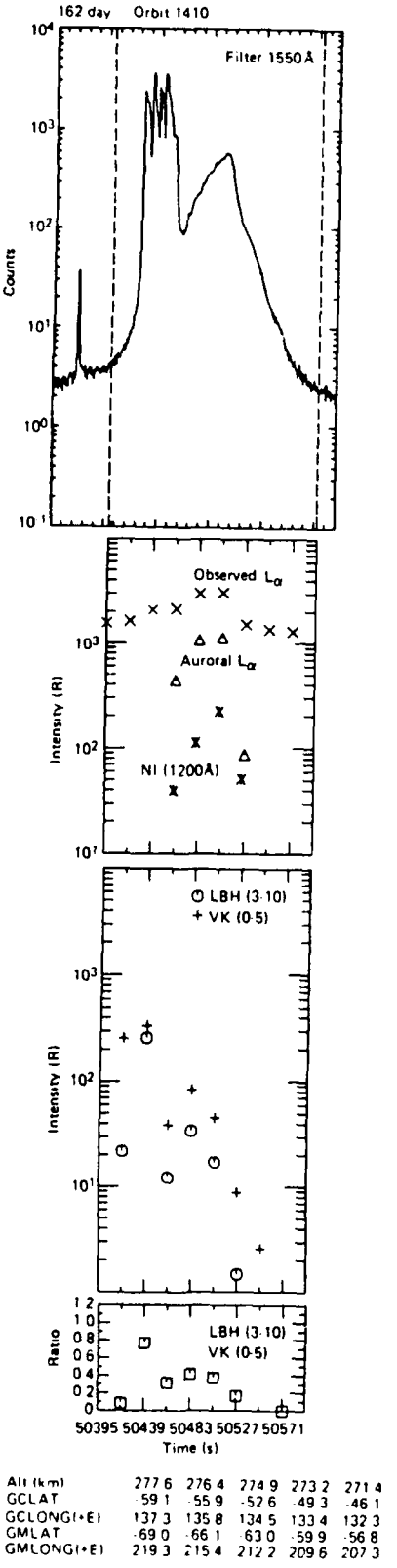

Alt (km)	277.6	276.4	274.9	273.2	271.4
GCLAT	-59.1	-55.9	-52.6	-49.3	-46.1
GCLONG(+E)	137.3	135.8	134.5	133.4	132.3
GMLAT	-69.0	-66.1	-63.0	-59.9	-56.8
GMLONG(+E)	219.3	215.4	212.2	209.6	207.3

Fig. 5c

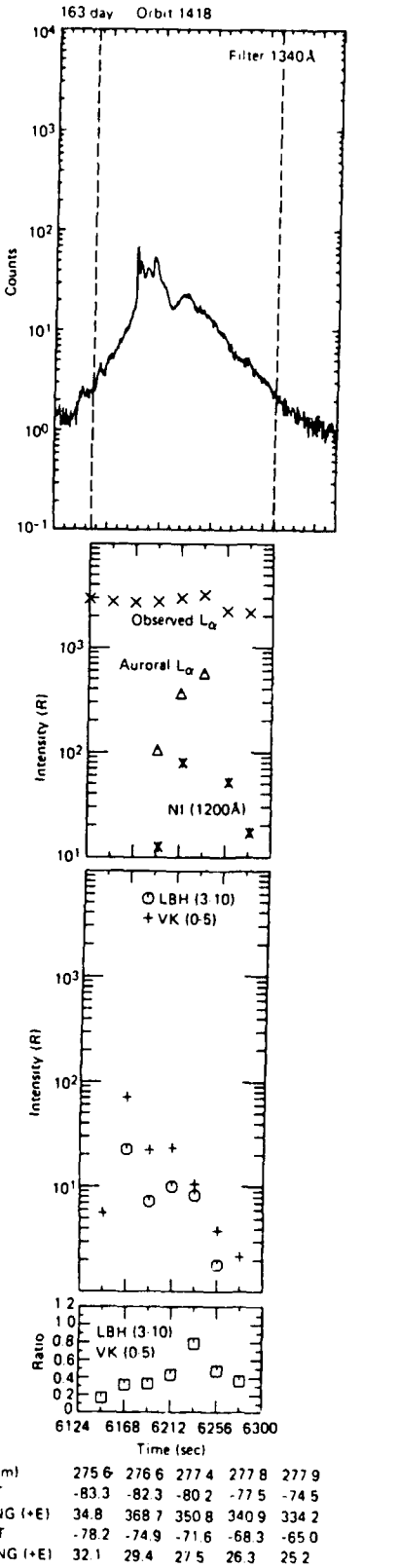

ALT (km)	275.6	276.6	277.4	277.8	277.9
GCLAT	-83.3	-82.3	-80.2	-77.5	-74.5
GCLONG (+E)	34.8	368.7	350.8	340.9	334.2
GMLAT	-78.2	-74.9	-71.6	-68.3	-65.0
GMLONG (+E)	32.1	29.4	27.5	26.3	25.2

Fig. 5d

and VK (0-5) bands. In the process of deducing these intensities, the NO δ band and the O_2 Herzberg I band emission intensities were subtracted from the 1916 to 1955 Å integral for the LBH (3-10) emission intensity and from the 2591 to 2628 Å integral for the VK (0-5) emission intensity, respectively. The background emission of the NO δ (1 to 2 R) and the O_2 Herzberg I band (3 to 9 R) within the auroral oval was determined from the airglow intensity measured just outside the equatorward edge of each auroral region. These observed intensities are only a few rayleighs for the LBH (3-10) band region and less than 10 R for the VK

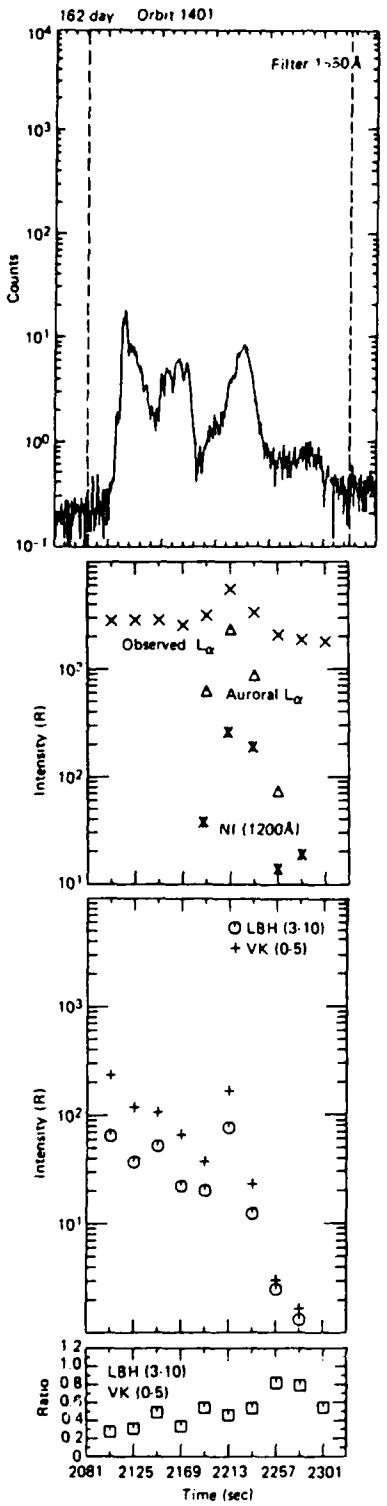

ALT (km)	281.3	282.0	282.4	282.6	282.5	282.1
GCLAT	-80.8	-78.2	-75.3	-72.2	-69.1	-65.9
GCLONG (+E)	371.5	360.3	352.9	347.8	344.0	341.2
GMLAT	-74.2	-70.9	-67.6	-64.2	-60.9	-57.6
GMLONG (+E)	35.0	35.3	35.5	35.5	35.5	35.5

Fig. 5*e*

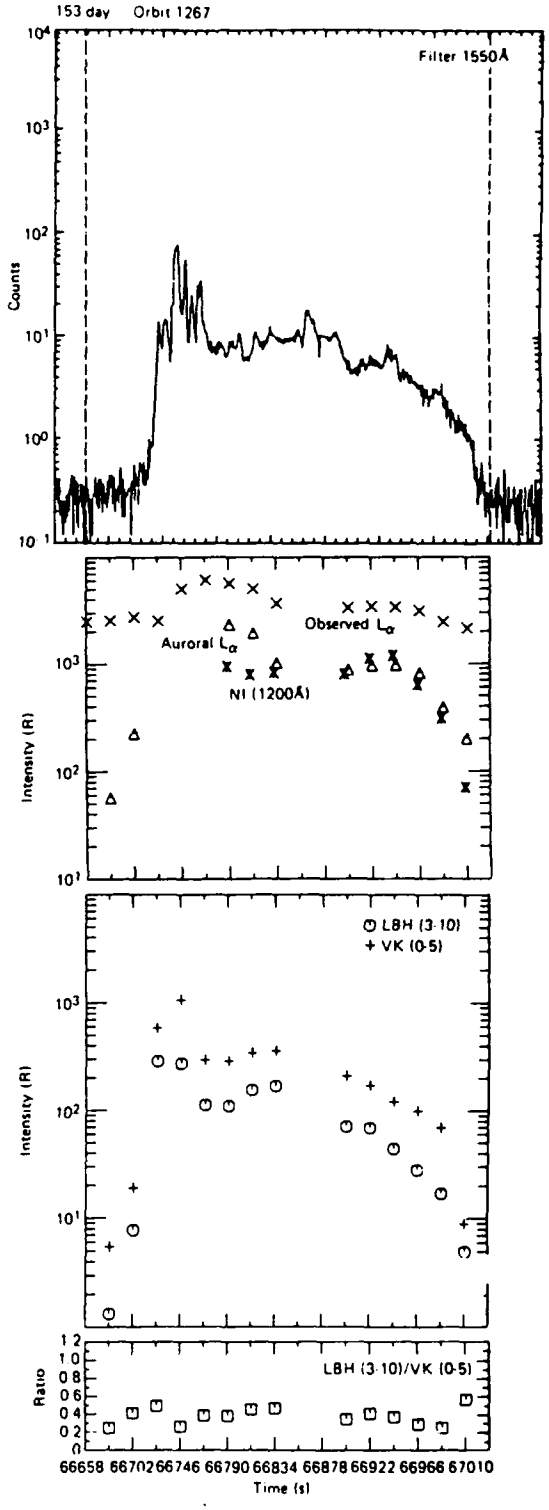

ALT (km)	281.3	281.0	280.5	279.7	278.7	277.5	276.0	274.4
GCLAT	-68.4	-65.2	-62.0	-58.8	-55.5	-52.2	-49.0	-45.7
GCLONG (+E)	75.2	72.5	70.3	68.7	67.2	65.9	64.8	63.8
GMLAT	-76.2	-72.9	-69.6	-66.2	-62.9	-59.6	-56.2	-52.9
GMLONG (+E)	115.8	117.9	119.3	120.2	120.9	121.4	121.8	122.0

Fig. 5*f*

(0–5) band region and were subtracted from the auroral spectra. The LBH and VK data in the third panel have been normalized within each spectral scan on the basis of the photometer data.

The fourth panel shows the intensity ratio of the LBH (3–10) to VK (0–5) band emissions from the third panel. In general, the ratio increases equatorward in the diffuse region, indicating hardening of the electron energy.

Figure 5*a* (orbit 1216) illustrates an oval crossing almost exactly along the 2300 MLT meridian plane in a period of weak activity ($Kp = 2+$) and near the peak of a small 250 nT substorm.

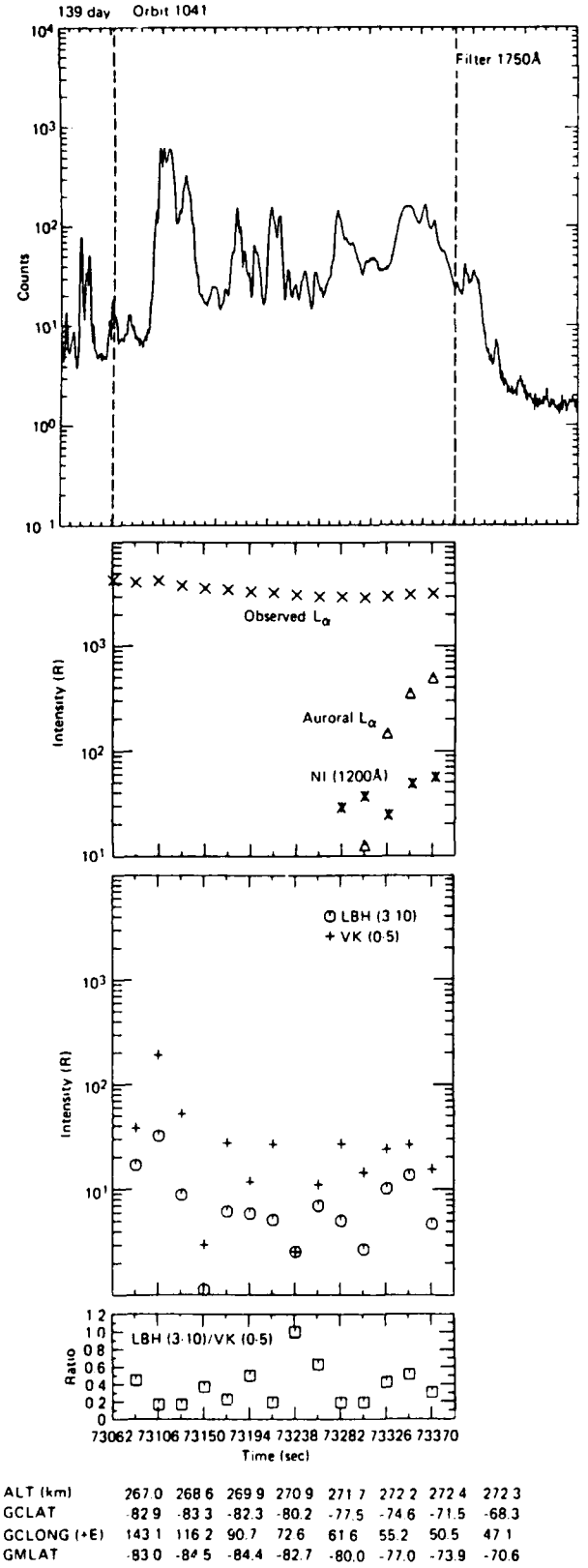

ALT (km)	267.0	268.6	269.9	270.9	271.7	272.2	272.4	272.3
GCLAT	-82.9	-83.3	-82.3	-80.2	-77.5	-74.6	-71.5	-68.3
GCLONG (+E)	143.1	116.2	90.7	72.6	61.6	55.2	50.5	47.1
GMLAT	-83.0	-84.5	-84.4	-82.7	-80.0	-77.0	-73.9	-70.6
GMLONG (+E)	328.6	356.4	29.1	56.1	70.4	77.4	81.9	85.0

Fig. 5g

The first panel shows the auroral oval extended from $-75°$ to $-60°$ geomagnetic latitude (GMLAT); a clear distinction between the discrete and diffuse auroral regions can be seen in the 1340-Å photometer intensity features.

The auroral $L\alpha$ emission intensity (second panel) in this pass is the highest among the seven orbits examined. Missing values for the auroral $L\alpha$ emission intensities are due to overestimation of the N I (1200 Å) emission intensity. The auroral N I (1200 Å) emission was subtracted as previously described. The assumed fixed ratio between the 1200 and 1744 Å emission can cause an overestimate of N I (1200 Å) at times. In the discrete region, the assumed 1200/1743 Å ratio can lead to an uncertainty in the auroral $L\alpha$ emission intensity of $\pm 50\%$; however, in the diffuse region it results in only a $\pm 10\%$ uncertainty.

The enhancement of the auroral $L\alpha$ emission (in particular, the intensity of 3.3 kR at 54,750 s in the diffuse region) indicates proton precipitation with an energy flux of 0.4 erg/cm^2 s, assuming typical average energies near 10 keV (*Edgar et al.* [1973] and the $L\alpha$ cross section from *Van Zyl and Newman* [1988]. This proton flux would produce about 7 R of the LBH (3–10) and less than 1 R of the VK (5–10) band emission intensity using the curve of Figure 7 and Table 3 by *Edgar et al.* [1973] and the $L\alpha$ cross section obtained by *Van Zyl and Newman* [1988].

The third panel shows the LBH (3–10) and VK (0–5) band emission intensities with variations similar to those of the photometer. Since the photometer filter was set at 1340 Å, the reliability of the values of the LBH and VK band emission intensities in the discrete region in the third and fourth panels is lessened, even though high intensities are present in the discrete region, with input energy fluxes exceeding 60 ergs/cm^2 s. The energy flux in the diffuse region is 2 to 8 ergs/cm^2 s. Despite a rather small Kp value (2+), the total energy flux across the oval is as large as that of the intense storm ($Kp = 7+$) recorded among the seven cases under study here. The fourth panel shows the LBH to VK band emission intensity ratio, which is an indicator of the average energy of incident electrons. Although the value in the discrete region is less reliable owing to sudden changes in auroral intensity and a less reliable 1340-Å photometer normalization, a high average energy was still inferred. The hardening of the electron energy spectrum from 1 to 7 keV is observed across the diffuse region toward lower latitude.

Figure 5*b* (orbit 1593) shows a slanted oval crossing between the 2000 and 2130 MLT meridians in a moderately active period ($Kp = 3+$, $AE = 250$ nT) during the recovery of a 700 nT substorm. The auroral oval was located between $-80°$ and $-70°$ GMLAT. Although the 1340-Å photometer did not show a distinct transition between the discrete and diffuse region, the LBH and VK emission intensity variations reveal a clear transition. The auroral $L\alpha$ emission intensity profile indicates intense proton precipitation in the equatorward part of the diffuse region. The peak energy flux (third panel) and the peak average energy (fourth panel) of incident electrons are located at a slightly higher latitude than the peak in $L\alpha$. The inferred energy flux is low despite a rather active period ($Kp = 3+$), possibly due to the observation in the early evening sector. In the fourth panel, the inferred average energy of the incident electrons does not show very high energies in the discrete region. Hard electron precipitation in the diffuse region is evident. The last data points at 73,823 and 73,855 s in the third and the fourth panels may be in considerable error owing to the low count rate.

Figure 5*c* (orbit 1410) shows an oval crossing between the 0100 and 2300 MLT meridians in a rather low activity period ($Kp = 2$) during the development of a weak <200 nT substorm. The auroral emission was bounded between $-67°$ and $-60°$ GMLAT. The photometer's 1550-Å filter used on this pass basically monitored the LBH band emission. The photometer count variation

is similar to the spectrometer LBH band emission intensities. The photometer normalization in this case should work reasonably well. Auroral $L\alpha$ emission intensities peak again slightly equatorward of the LBH and VK emission intensities. At 50,439 s, the satellite was over the discrete region for almost 22 s, corresponding to one spectrometer scan cycle; therefore, the spectrum taken there represents the discrete auroral emission. Missing values of the auroral $L\alpha$ emission intensity on the second panel are due to overestimation of the N I (1200 Å) emission intensity for geocoronal background subtraction. The observed N I (1744 Å) at that time was over 1 kR. Since the 1750-Å region in the UV and the 1200 Å region in the FUV were monitored at about the same time by the two spectrometers (the photometer correction between them was only a factor of 1.1), the photometer normalization should not really affect the determination of these two emission intensity ratios. The oversubtraction of the N I (1200 Å) suggests that the intensity ratio of 4.0 is an overestimate for this discrete aurora at 50,439 s. Over this spectral scan, the photometer normalization factor changed smoothly by a factor of 3.5 compared to 3 orders of magnitude in some other discrete regions. Therefore the determined intensities of the LBH (3–10) and VK (0–5) band emissions should be fairly accurate for this discrete auroral observation. An apparent inverted V structure in electron precipitation in the discrete auroral region can be seen on both the third and fourth panels. Even though the diffuse region was very narrow, the energy hardening is still identifiable, and the average energy of 3 keV agrees well with the value from the statistical study of electron precipitation by *Hardy et al.* [1985].

Figure 5*d* (orbit 1418) shows an oval crossing near the 2300 MLT meridian in a very quiet period ($Kp = 1-$, $AE = 50$ nT) with no substorm activity in the previous 12 hours. The auroral oval was bounded between $-83°$ and $-80°$ GMLAT. The spectrometer recorded the weakest O I 1304 Å and $L\alpha$ line emission among the seven auroral oval crossings examined. The missing points of the auroral $L\alpha$ and LBH band emissions at 6146 and 6278 s are located below the 10 R minimum value of the figure. The inferred electron energy flux was peaked more poleward than the auroral $L\alpha$ emission and the average energy of incident electrons; however, the ratio at 6234 s may be inaccurate because of the low LBH and VK band intensities. The observed intensities of the LBH and VK band emissions were very small over the whole pass compared to other passes. Even so, energy hardening of electron precipitation in the diffuse auroral region is still recognizable.

Figure 5*e* (orbit 1401) shows an oval crossing along the 2300 MLT meridian in an active period ($Kp = 4+$, $AE = 400$ nT) during a period of continuous substorm activity. The oval was 9° wide bounded between $-79°$ and $-70°$ GMLAT. The photometer data do not show a clear distinction between the discrete and the diffuse auroral regions. The 1550-Å photometer observation provides reasonably good normalization for the LBH and VK band emission intensities except at 2103 s, where the emission intensities rose suddenly at the polar edge of the discrete aurora. Despite the active period, the signals were weak and the inferred energy fluxes were less than those in orbit 1410 at weak geomagnetic activity. The signals after 2257 s may not be reliable owing to a very low count rate. Nevertheless, the hardening of electron energy in the diffuse region is again obvious.

Figure 5*f* (orbit 1267) shows an oval crossing between the 2000 and 2200 MLT meridians in an extremely active period ($Kp = 7+$) near a peak of a very intense substorm activity. The AE index indicates that the observation was made after substorm breakup and 5 hours into intense continuous substorms. The AE value reached 1200 nT, and the oval was bounded between $-73°$ and $-53°$ GMLAT with a peak intensity of O I (1304 Å) of 14 kR in the discrete auroral region and 5 kR in the diffuse auroral region (Table 1). The inferred total energy flux was the largest among the seven auroral oval crossings examined. The 1550-Å photometer measurements do not show a clear distinction between the discrete and the diffuse regions; a narrow discrete region may be inferred. Two spectrometer data points at 66,856 and 66,878 s are missing in the original record. The proton precipitation was not significantly enhanced despite the active period. If we compare this with the intensity profiles of the LBH and VK band emissions, we can conclude that relatively more auroral $L\alpha$ emission was detected at the equatorward part of the oval. There is an intensity peak of the $L\alpha$ emission at the equatorward edge of the diffuse region at 66,966 s. The inferred electron energy flux in the oval crossing is between 2 and 20 ergs/cm^2 s. The hardening of electron energy is not seen, and a relatively constant average level is observed over the whole oval.

Figure 5*g* (orbit 1041) shows a slanted crossing between the 1700 and 2100 MLT meridians in a quiescent period ($Kp = 0$, $AE <$ 20 nT) with no indication of substorm activity. The oval was located above about $-69°$ GMLAT with a width of at least $\sim 15°$. The spectrometer count rate associated with this quiescent period is very low. Consequently, half of the data points for the auroral $L\alpha$ line and the LBH and VK band emission intensities are not very accurate. The average energy flux as well as the total energy flux over the whole oval are very low, as shown in Table 1. The energy flux is slightly higher in the discrete region near 2 erg/cm^2 s at 73,106 s. Even with the low signals, the proton precipitation is enhanced near the equatorward edge, and the electron energy also hardens near the edge of the diffuse region.

In summary, these seven orbits indicate that the O I (1304 Å) line emission intensity and the inferred characteristics of incident electrons are correlated with geomagnetic activity. The geocoronal $L\alpha$ line emission intensity variations are a function of solar zenith angle. The auroral $L\alpha$ line emission intensity, which is an indicator of proton precipitation, does not correlate well with the geomagnetic activity. Morphologically, the auroral $L\alpha$ emission is more intense near the equatorward edge of the diffuse region. The intensities of the LBH (3–10) and VK (0–5) band emissions are not always correlated with the geomagnetic activity. The average energy flux, total energy flux, and average energy across each oval crossing inferred from the emissions (in Table 1) are consistent with those from a statistical study of electron precipitation [*Hardy et al.*, 1985]. The increase in average electron energy was seen near the equatorward edge of the diffuse regions in most of the oval crossings.

5. Conclusions and Comments

The nadir-viewing UV spectral/photometric measurement from the S3-4 satellite at 270 km provides data to study the energetics of incident electrons in the nighttime aurora. The observations of seven selected auroral oval crossings and model calculations revealed several salient features.

1. The observed emission intensities of the LBH (3–10) band, the VK (0–5) band, and the O I (1356 Å) line in the diffuse auroras were consistent with what would be inferred from a modified version of the model calculation by *Strickland et al.* [1983], provided (1) The average energy of incident electrons was 3 ± 1 keV as reported by *Hardy et al.* [1985] in his statistical study, (2) The atmospheric atomic oxygen density was 30% less than the model atmosphere (MSIS-83) used in the model calculation by Strick-

land, and (3) The atomic oxygen quenching coefficient for the VK (0–5) band by *Sharp* [1971] is used.

2. The LBH (3–10) band emission intensity is a good indicator of the average energy flux of the incident electrons. The modified model calculation produces 16 R of the LBH (3–10) band emission per erg/cm^2 s of incident electrons.

3. The intensity ratio of the LBH (3–10) to VK (0–5) emissions is a good indicator of the average energy of the incident electrons in the auroral region.

4. In the midnight sector the auroral $L\alpha$ emission is most intense near the equatorward edge of the diffuse auroral region, which is in agreement with the accepted morphology of proton precipitation and observations of ground-based Balmer emissions.

An application of the observed characteristics in the apparent near independency of the LBH band emission intensities outside the O_2 Schumann-Runge continuum on the incident electron energy (> 1 keV at least) is that auroral oval images in such LBH bands (such as the (3–10)) could be used to deduce the total energy flux precipitated within the oval. With less uncertainty and simultaneous observation of the accurate atomic oxygen densities and further understanding of the quenching rate coefficient, the simultaneous auroral oval images of LBH and VK band emissions could provide average energy contours of the oval precipitation.

The S3-4 data hold promise for future studies of the relation between proton precipitation and associated emissions. In addition, higher-resolution data (5-Å resolution) should permit a more detailed study of the relative intensities of the various N I, N II, and O II lines and $L\alpha$ emissions as well as provide detailed information on the population distributions of the VK for the high-lying vibrational levels.

Acknowledgments. We are grateful to D. J. Strickland for running his program of electron aurora for us. This research is supported by Directorate of Chemical and Atmospheric Sciences grant AFOSR 86-0057 to The Johns Hopkins University Applied Physics Laboratory.

The Editor thanks I. C. McDade and another referee for their assistance in evaluating this paper.

REFERENCES

Ajello, J. M., and D. E. Shemansky, A reexamination of important N_2 cross sections by electron impact with application to the dayglow: The Lyman-Birge-Hopfield band system and N I (119.99 nm), *J. Geophys. Res. 90*(A10), 9845-9861, 1985.

Beiting, E. J., and P. D. Feldman, Ultraviolet spectrum of the aurora (2000–2800 Å), *J. Geophys. Res., 84*, 1287-1296, 1979.

Cartwright, D. C., Vibrational populations of the excited states of N_2 under auroral conditions, *J. Geophys. Res., 83*(A2), 517-531, 1978.

Conway, R. R., R. R. Meier, D. F. Strobel, and R. E. Huffman, The far ultraviolet vehicle glow of the S3-4 satellite, *Geophys. Res. Lett., 14*, 628-631, 1987.

Crosswhite, H. M., E. C. Zipf, Jr., and W. G. Fastie, Far-ultraviolet auroral spectra, *J. Opt. Soc. Am., 6*, 643, 1962.

Daniell, R. E., Jr., and D. J. Strickland, Dependence of auroral middle UV emissions on the incident electron spectrum and neutral atmosphere, *J. Geophys. Res., 91*(A1), 321-327, 1986.

Degen, V., Synthetic spectra for auroral studies: The N_2 Vegard-Kaplan band system, *J. Geophys. Res., 87*(A12), 10,541-10,547, 1982.

Degen, V., Dialup facility for gerlerating auroral and airglow synthetic spectra, Rep. UAG-R(305), Geophys. Inst., Fairbanks, Alaska, April 1986.

Eastes, R. W., and W. E. Sharp, Rocket-borne spectroscopic measurements in the ultraviolet aurora: The Lyman-Birge-Hopfield bands, *J. Geophys. Res., 92*(A9), 10,095-10,100, 1987

Edgar, B. C., W. T. Miles, and A. E. S. Green, Energy deposition of protons in molecular nitrogen and applications to proton auroral phenomena, *J. Geophys. Res., 78*(28), 6595-6606, 1973.

Gerard, J.-C., and C. A. Barth, OGO-4 observations of the ultraviolet auroral spectrum, *Planet. Space Sci., 24*, 1059-1063, 1976.

Hardy, D. A., M. S. Gussenhoven, and E. Holdman, A statistical model of auroral electron precipitation, *J. Geophys. Res., 90*(A5), 4229-4248, 1985.

Hedin, A. E., A revised thermospheric model based on mass spectrometer and incoherent scatter data: MSIS-83, *J. Geophys. Res., 88*(A12), 10,170-10,188, 1983.

Hudson, R. D., Critical review of ultraviolet photoabsorption cross section for molecules of astrophysical and aeronomic interest, *Rev. Geophys., 9*(2), 305-406, 1971.

Huffman, R. E., F. J. LeBlanc, J. C. Larrabee, and D. E. Paulsen, Satellite vacuum ultraviolet airglow and auroral observations, *J. Geophys. Res., 85*(A5), 2201-2215, 1980.

Meier, R. R., and P. Mange, Geocoronal hydrogen: An analysis of the Lyman-Alpha airglow observed from OGO-4, *Planet. Space Sci., 18*, 803-821, 1970.

Meier, R. R., D. J. Strickland, P. F. Feldman, and E. P. Gentieu, The ultraviolet dayglow, I, Far UV emission of N and N_2, *J. Geophys. Res., 85*(A5), 2177-2184, 1980.

Meier, R. R., R. R. Conway, P. D. Feldman, D. J. Strickland, and E. P. Gentieu, Analysis of nitrogen and oxygen far ultraviolet auroral emissions, *J. Geophys. Res., 87*(A4), 2444-2452, 1982.

Piper, L. G., G. E. Caledonia, and J. P. Kennealy, Rate constants for deactivation of $N_2(A\ ^3\Sigma_u^+,\ v' = 0,1)$ by O, *J. Chem. Phys., 75*, 2847-2852, 1981.

Sharp, W. E., Rocket-borne spectroscopic measurements in the ultraviolet aurora: Nitrogen Vegard-Kaplan bands, *J. Geophys. Res., 76*, 987-1005, 1971.

Sharp, W. E., and M. H. Rees, The auroral spectrum between 1200 and 4000 Å, *J. Geophys. Res.*, 77, 1810, 1972.

Stone, E. J., and E. C. Zipf, Electron impact excitation of the ^3S and ^5S states of atomic oxygen, *J. Chem. Phys., 60*, 4237, 1974.

Strickland, D. J., J. R. Jasperse, and J. A. Whalen, Dependence of auroral FUV emissions on the incident electron spectrum and neutral atmosphere, *J. Geophys. Res., 88*(A10), 8051-8062, 1983.

Vallance-Jones, A., *Aurora*, D. Reidel, Hingham, Mass., 1974.

Van Zyl, B., and H. Neumann, Lyman-α emission cross sections for low-energy H and H^+ collisions with N_2 and O_2, *J. Geophys. Res., 93*, 1023-1027, 1988.

Zipf, E. C., and P. W. Erdman, Electron-impact excitation of atomic oxygen: Revised cross section values, *Eos Trans. AGU, 66*(18), 321, 1985.

R. E. Huffman, Air Force Geophysics Laboratory, Hanscom Air Force Base, Bedford, MA 01731.

M. Ishimoto and C.-I. Meng, The Johns Hopkins University Applied Physics Laboratory, Johns Hopkins Road, Laurel, MD 20707.

G. J. Romick, KIA Consultants Inc., Fairbanks, AK 99775.

(Received March 19, 1987;
revised March 3, 1988;
accepted March 23, 1988.)

APPENDIX B

ULTRAVIOLET SPECTRA IN THE DIFFUSE AURORAL REGION

M. Ishimoto,* G. J. Romick,† R. E. Huffman,‡ and C.-I. Meng*

*Applied Physics Laboratory, The Johns Hopkins University
Johns Hopkins Road, Laurel, Maryland 20707

†KIA Consultants Inc.
Fairbanks, Alaska 99775

‡Air Force Geophysics Laboratory, Hanscom Air Force Base
Bedford, Massachusetts 01731

ABSTRACT

Ultraviolet spectra over the southern hemisphere nightside auroral oval were obtained from the AFGL spectral/photometric experiment on board the polar-orbiting S3-4 satellite at 270 km between mid-May and June 1978. Spectra with 30-Å resolution from seven auroral oval crossings were selected to analyze the diffuse auroral region under various magnetic activities (K_p = 0 to 7+). The observed spectra were compared with synthetic spectra and model calculations of the LBH and VK band systems for various studies. The large range of wavelengths (1100–2900 Å) measured allowed the analysis of band and line intensities such as the LBH and VK band systems and the NI (1744-Å), NII (2143-Å), and OI (1356-Å) lines.

Certain wavelengths can be used to determine the energy and flux characteristics of the auroral electron precipitation over the auroral oval and provide quantitatively important information on atmospheric parameters. Of the latter, emphasis here is on the atomic oxygen quenching coefficient for the VK band ($v' = 0$), the atomic oxygen column density, the NII (2143-Å) line emission cross section, the impact of O_2 SR absorption on specific emissions, and the presence and importance of heavy particle precipitation. This study illustrates the range of information that can be obtained by the synthesis of atmospheric emissions model calculations and laboratory measurements.

1. INTRODUCTION

All auroral oval observations used in this study were made over the winter southern hemisphere auroral region in darkness under a wide range of auroral conditions. The data were obtained by the Air Force Geophysics Laboratory "Ultraviolet Backgrounds" experiment, flown on the S3-4 satellite in 1978.[1] The satellite was in a low-altitude polar orbit near the noon-midnight meridian plane, and the nadir-viewing UV instruments observed the airglow, aurora, and solar scattered radiance of the earth's atmosphere. The experiment consisted of two simultaneous scans of ¼-m, f/5, Ebert-Fastie spectrometers: the FUV (formerly VUV) from 1100 to 1900 Å and the UV from 1600 to 2900 Å. For each wavelength range, there were three selectable bandwidths at about 1, 5, and 30 Å. A separate photometer using interference filters recorded one of four (1216-, 1340-, 1550-, and 1750-Å) wavelength bands.

The initial results of the experiment and details of the sensors and data analysis have been previously described.[1-4] One phase of the data analysis focuses on the emission intensities and ratios of certain Lyman-Birge-Hopfield (LBH) and Vegard-Kaplan (VK) bands, which, in conjunction with model calculations,[5,6] are used to estimate the average energy and the total energy flux of incident electrons across the auroral oval. The results are in general agreement with previously reported characteristics of particle precipitation across the auroral oval obtained by electron precipitation measurements.[7] The study also concentrates on the three atomic line intensities, NI (1744 Å), NII (2143 Å), and OI (1356 Å). Using the intensity correlation between these lines and the LBH (3–10) band, the emission mechanisms for these lines has been investigated, and the emission cross section of the NII line has been evaluated using other known cross sections (the LBH band and the NI (1744-Å) line) obtained from laboratory studies.[8] In addition, we have demonstrated how these emissions can be used to monitor the atomic oxygen concentrations, the heavy particle precipitation, and the O_2 Schumann-Runge (SR) absorption effects on the observed spectra.

In this study, a few orbits were selected using the following criteria. First, both spectrometers were set to the same slit width in order to examine the overlapping spectral region (1600 to 1900 Å) and also to compare instrument calibration. Second, spectrometers were set at the largest slit (corresponding to a resolution of about 30 Å) in order to detect rather weak auroral emissions. Third, a photometer was set on one of the three (1340-, 1550-, and 1750-Å) wavelength band interference filters to monitor continuously auroral intensity variations. Finally, seven orbits, meeting all of these criteria, were selected to cover various levels of magnetic activity (K_p = 0 to 7+).

Observations of the nightside auroral oval were made at about 270 km above the winter southern hemisphere from May 1 to June 22, 1978. Solar zenith angles, geomagnetic conditions, peak intensities of the OI 1304-Å line, and Lα emissions within the oval for these seven orbits, together with the estimated particle characteristics, are summarized in Table 1 and discussed more fully in Section 4.

2. DATA ANALYSIS

2.1. Data reduction

The spectrometers have an intrinsic integration period for each wavelength step of 5 ms, and it takes 21 s to make one complete wavelength scan (i.e., 1100 to 1900 Å for the FUV and 1600 to 2900 Å for the UV).[2] The 30-Å resolution spectra were insensitive to smoothing for any running mean below 20 Å. After such spectral smoothing the counts were converted to rayleighs per angstrom (R/Å) using calibrated instrument sensitivity and radiance scaling factors.[1]

Table 1. Summary of Geophysical Conditions

Orbit No.	1216	1593	1410	1418	1401	1267	1041
Time (1978)							
Month Day Hour Min.	5 30 15 12	6 22 20 29	6 11 0 37	6 11 14 1	6 11 0 37	6 2 18 36	5 19 20 22
Day Second	150 54720	173 73740	162 2220	162 50460	162 2220	153 66960	139 73320
Activity index							
K_p	2+	3+	2	1−	4+	7+	0
A_p	18	15	17	10	17	82	4
F10.7	143	184	110	113	110	143	131
AE	300	250	200	100	350	1200	50
Dst	−34	−12	−31	−28	−35	−57	−18
Location							
Solar zenith angle	147	133	147	120	129	143	126
Altitude (km)	273	264	274	273	277	295	270
Emissions (kR)							
Auroral Lα							
Discrete peak	1.2	0.4	0.0	0.0	0.3	0.1	0.1
Diffuse peak	3.8	1.3	1.0	0.6	2 2	1.0	0.5
Geocoronal Lα	2.0	2.3	1.2	2.2	1.7	2.1	3.0
OI (1304 Å)							
Discrete peak	7.0	6.0	3.0	2.5	4.0	14.0	5.5
Diffuse peak	2.3	2.2	1.3	1.0	3.0	5.0	2.6
Inferred incident electron characteristics							
Average energy (keV)	3.6	4.4	1.2	3.6	5.4	3.2	3.2
Average energy flux (erg cm^{-2} s^{-1})	10.0	2.2	5.2	0.66	2.5	8.6	0.78
Total energy flux across the oval							
1 cm width ($\times 10^8$ erg s^{-1})	19.4	3.9	5.1	0.74	4.1	19.6	1.69
30 min longitudinal width ($\times 10^{23}$ keV s^{-1} sr^{-1})	122	15.2	37.1	3.38	21.9	133	3.4

The spectral scan time of 21 s and the field of view of the spectrometers (11.5°) are quite large compared to the characteristic time and spatial scales of auroral display features, especially over the discrete auroral region. We have tried to normalize each spectrum to a constant intensity by using data from the photometer that has a small field of view (1.65° or 0.12°) and an integration time of 10 ms. The smoothed photometer data, which typically vary across the spectral scan by some 20% and at most by 150% in the diffuse auroral region, were then used to normalize the spectral intensities within each 21-s scan. This is the best approach available with this data set and it appears to work well when the photometer monitors one of the LBH wavelength regions. However, the procedure is expected to be less effective for scans associated with rapid intensity variations such as across a sharp boundary of the auroral oval. Also, the normalization is completely meaningless for auroral emissions that do not vary proportionately to the monitored photometer band. For example, neither the geocoronal nor the auroral emission varies systematically with the LBH intensities transmitted by the 1550- and 1750-Å photometer filters since these filters transmit no Lα emission.

The two spectrometer ranges overlapped between 1600 and 1900 Å. However, the spectral data for wavelengths greater than 1750 Å from the FUV spectrometer were not used in this analysis because of the very low sensitivity in that wavelength region.[1] When the photometer normalization is applied to spectral data in the 1600- to 1750-Å region, where the two spectrometers overlapped, the match is quite good even though the two observations were made about 14 s apart. Further, after photometer normalization, the auroral spectral band systems that cover wide wavelength ranges (i.e., the LBH and the VK) match nominal synthetic spectra very well. Figure 1 shows the comparison of the normalized auroral spectra from the diffuse auroral region averaged over four scans (Fig. 1a) with the synthetic VK band systems (Fig. 1b) and with the synthetic LBH band systems (Fig. 1c); the synthetic spectra are from Degen.[9] Figure 1a also shows the combined spectra obtained from two separate FUV and UV spectrometers and the region of spectral overlap. In the overlap region, the spectra match very well; the deviation is less than 10%. The good agreement between the observed (Fig. 1a) and the synthetic (Figs. 1b and 1c) spectra lends credibility to the photometric normalization technique. In general, photometer normalization works well except in regions with drastic intensity changes, such as near the edges of the discrete auroral region.

Since the satellite altitude during these observations was about 260 km and we observed no anomalous LBH vibrational distributions, we disregarded vehicle glow.[10]

2.2. Band systems

Auroral and airglow radiation consists of various molecular band systems such as the N_2 LBH, VK and Herman-Kaplan, the NO γ and δ, and the O_2 Herzberg I bands, as well as atomic lines

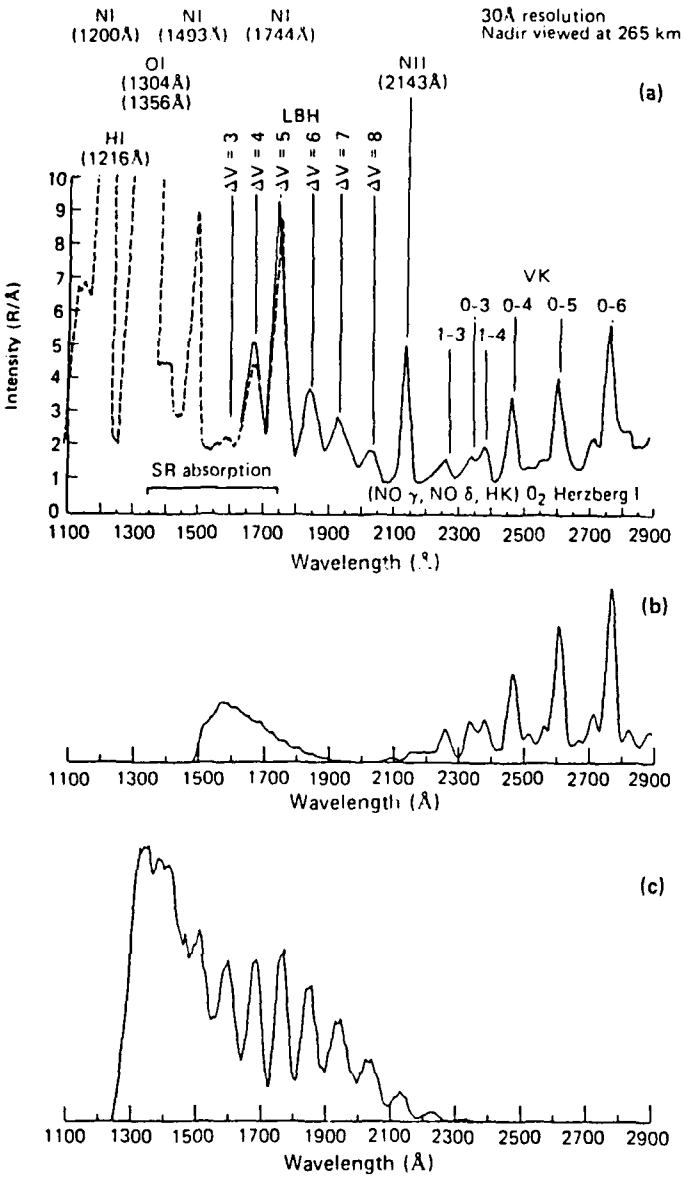

Figure 1. Comparison of the observed UV spectrum with LBH and VK synthetic spectra from Degen.[9] (a) Spectral average of four consecutive 21-s scans of 30-Å resolution obtained by FUV (dotted line) and near-UV (solid line) spectrometers overlapping in the wavelength range 1600 to 1750 Å. (b) VK synthetic spectrum assuming T_r = 400 K and the vibrational population distribution. (c) LBH synthetic spectrum assuming T_r = 400 K and T_v = 400 K.

such as the NI (1200-, 1493-, and 1744-Å), OI (1304- and 1356-Å), NII (2143-Å), and OII (2470-Å) lines. Two wavelength regions are particularly difficult to analyze. One is from 1500 to 1900 Å, where the relative emission intensities of the VK band system are uncertain. This will be described in detail in the next section. The other region, particularly for nadir-viewing observations, is the O_2 SR continuum region from 1350 to 1750 Å, where atmospheric O_2 absorbs the emissions coming from below 130 km.[11] Therefore, for much of this analysis, we have concentrated on the UV spectra above 1900 Å.

The major molecular band features in the UV spectra are the LBH and VK band systems. The rest of the auroral spectral features will be more easily distinguished by subtracting out the LBH

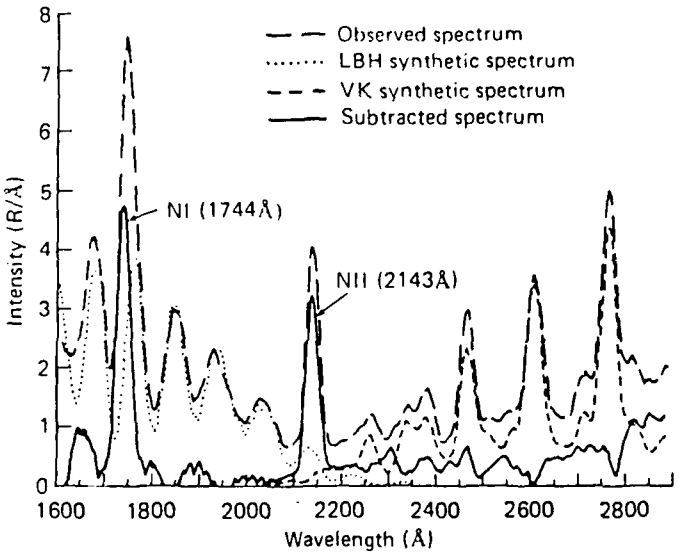

Figure 2. The effect of subtracting LBH and VK synthetic spectra from observed UV spectra between 1600 and 2900 Å. Intensities at the two peaks of 1928 and 2604 Å in the observed spectrum are used to normalize the LBH (3-10) and VK (0-5) synthetic bands. The normalized synthetic spectra are then subtracted from the observed spectrum.

and VK band systems from the observed spectra. The solid line in Fig. 2 is the observed spectrum (Fig. 1a) with the synthetic LBH and VK band systems subtracted. In the subtraction process, the intensities of the observed and synthetic peaks at 1928 Å for the LBH and at 2604 Å for the VK are matched. Because of uncertainties in the synthetic VK band emission intensities below 2000 Å, only the VK synthetic spectrum above 2050 Å was subtracted. There are obvious atomic features at 1744 Å (NI) and 2143 Å (NII) in Fig. 2. Small features below 2050 Å (except the NI line at 1744 Å) may be part of the VK band system emission; however, they typically are smaller than those expected in the synthetic spectra by a factor of 2 or 3 (Fig. 1b). The band features above 2500 Å are mainly from the O_2 Herzberg I band systems, which are commonly seen in the airglow outside the auroral regions. The secondary features between 1900 and 2600 Å mainly consist of the NO δ and Herman-Kaplan band systems.

Taking into consideration the secondary emission band features, atomic lines, and uncertainties in the synthetic spectra, we found that the LBH (3-10) peak at 1928 Å and the VK (0-5) peak at 2604 Å are relatively free from contamination by other band systems and lines. These peaks are located outside the O_2 SR absorption region and have reasonably good signal strengths. Therefore, their two peak intensities can be used as the representative emission intensities for the LBH and VK bands.

2.3. Atomic lines

The NI 1744-Å line intensity was obtained by subtracting the synthetic LBH band system matched to the 1928-Å peak from the observed spectra, assuming O_2 SR absorption was negligible (e.g., a few percent even if the 1928-Å peak and the synthetic VK band system spectrum matched at the 2604-Å peak from the observed 30-Å resolution spectra).

To get the true OI line emission intensity at 1356 Å, the LBH band intensities underneath must be subtracted from the observed spectra. In the wavelength region between 1325 and 1725 Å, the emissions below 150 km were substantially absorbed by atmospher-

ic O_2 (O_2 SR continuum). Thus, the synthetic LBH band system spectra must be modified to include the effect of the O_2 SR absorption between the emission layers and the spectrometer at 270 km. The technique we used is described in detail in Ishimoto et al.,[3] and results in an estimate of the 1356-Å OI emission intensity within 10% error, which is adequate for this study.

3. MODEL CONSIDERATIONS

3.1. LBH band system

The LBH band system is located in the 1250- to 2400-Å range, with a total intensity of 383 kR for an IBC III aurora.[12] The LBH band system originates from a transition from the $a^1\pi_g$ state to the $X^1\Sigma_g^+$ ground state. The collisional quenching for this band emission takes place below 95 km, which is lower than most auroral emission altitudes. A synthetic spectrum of this band is shown in Fig. 1c. The model of Strickland et al.[5] indicates that the peak production altitude is from 105 to 120 km, depending on the energy of the incident electrons. The LBH synthetic spectrum, with a 30-Å spectral resolution, is not sensitive to changes in the rotational and vibrational temperature around 300 K. Consequently, we have used the synthetic 30-Å spectral resolution with T_r = 400 K and T_v = 400 K.

Figure 3 shows the column emission intensity caused by 1 erg cm^2 s^{-1} incident flux (or "yield" according to Strickland) of the LBH (3-10) band as well as the VK (0-5) band and the OI (1356-Å) line as a function of the average energy of incident electrons. The energy flux with a Maxwellian distribution is more representative of the incident electron distribution in diffuse auroras.[5] The values in Fig. 3 were therefore calculated with modified parameter values by Strickland (private communication, 1987). The cross sections of the LBH bands were replaced by those of Ajello and Shemansky[8] for this calculation. The cross section of the OI (1356-Å) emission was adjusted by multiplying the cross section of Stone and Zipf[13] by 0.6 to reflect the revision by Zipf and Erdman.[14] The model atmosphere used was the MSIS-83 model by Hedin.[15]

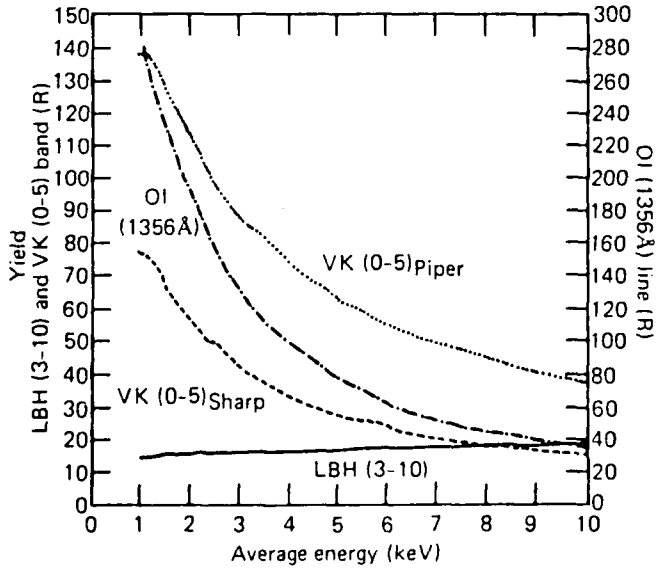

Figure 3. The column emission rate as a function of the average energy of incident electrons calculated by Strickland: LBH (3-10), VK (0-5), and OI (1356 Å). The values are normalized for a unit flux (1 erg cm^{-2} s^{-1}) with a Maxwellian distribution. The MSIS-83 model atmosphere is used. The common unit for the LBH (3-10) and VK (0-5) band emission intensities is given on the left, while the unit for the OI (1356-Å) line is on the right. The subscripts of the VK $(0\text{-}5)_{Piper}$ and VK $(0\text{-}5)_{Sharp}$ correspond to the use of the atomic quenching coefficients by Piper et al.[20] and Sharp (1971),[19] respectively.

3.2. VK band system

The auroral VK band system extends from 1500 to 7000 Å, with a total intensity of 55 kR for an IBC III aurora.[12] The VK band system originates in the forbidden transition from the $A^3\Sigma_u^+$ state to the $X^1\Sigma_g^+$ ground state. The VK vibrational energy levels are excited by several mechanisms such as direct electron excitation from the N_2 electronic ground state, radiative cascade involving the $B^2\pi_g$ and $C^3\pi_u$ states, and depopulation of the $v \geq 8$ vibrational levels by the "reverse" N_2 $1P$ transition $A^2\Sigma_u^+ \rightarrow B^3\pi_g$.[16] Estimated vibrational population distributions by several studies differ from each other, especially in the high vibrational levels ($v \geq 7$).[17] The dominant VK band features at wavelengths of >2000 Å come from low vibrational energy levels of the N_2 $A^3\Sigma_u^+$ state that are populated largely by cascade from other electronic states. The population of the high-lying vibrational levels does not affect the band features at wavelengths of >2000 Å. On the other hand, the VK band features at wavelengths of >2000 Å originate from the high vibrational energy levels; however, auroral spectra of 4-Å resolution, obtained in a rocket experiment,[18] show little VK band emission between 1675 and 2075 Å, where the VK emission from v' = 4, 6, 7, and 8 would appear. Consequently, we assumed little VK emission at wavelengths of >2000 Å. The rotational energy levels appear to be collisionally well thermalized at the local temperature.[16]

The characteristic shape of VK synthetic spectra using a 30-Å resolution does not vary significantly, with a few-hundred-degree change in the rotational temperature above 400 K. Therefore, we set T_r = 400 K in the synthetic spectrum by Degen,[9] and then used his assumed vibrational population distribution (Fig. 1b), which was obtained by matching synthetic spectra with values from various published papers. For a 30-Å resolution, the spectrum above 2000 Å in Fig. 1b seemed adequate for this study.

Figure 3 shows the VK (0-5) band column emission intensity rates as functions of incident electron energy calculated by Strickland. The emission intensities will differ, depending on the choice of the quenching rate coefficient for atmospheric atomic oxygen for the v' = 0 level and the atmospheric atomic oxygen density. Quenching rate coefficients were based on rocket data (9×10^{-11} cm^{-3} s^{-1} for the v' = 0 level)[19] and laboratory data (2.8×10^{-11} cm^3 s^{-1}).[20]

To obtain atomic oxygen densities for the auroral cases studied here, the column emission intensity ratio of the OI (1356-Å) line to the LBH (3-10) band was used (Fig. 4). Variations in the atomic oxygen densities also change the column emission intensity of the OI line.[5] Below we use this concept and the observed OI (1356-Å) line emission to deduce an appropriate atomic oxygen density. The selection of the model-energy-dependent intensity relationship for the VK (0-5) band will depend upon the LBH (3-10) and the VK (0-5) bands, a suitable atomic oxygen quenching coefficient, and the atmospheric oxygen density deduced from the observed OI (1356-Å) line.

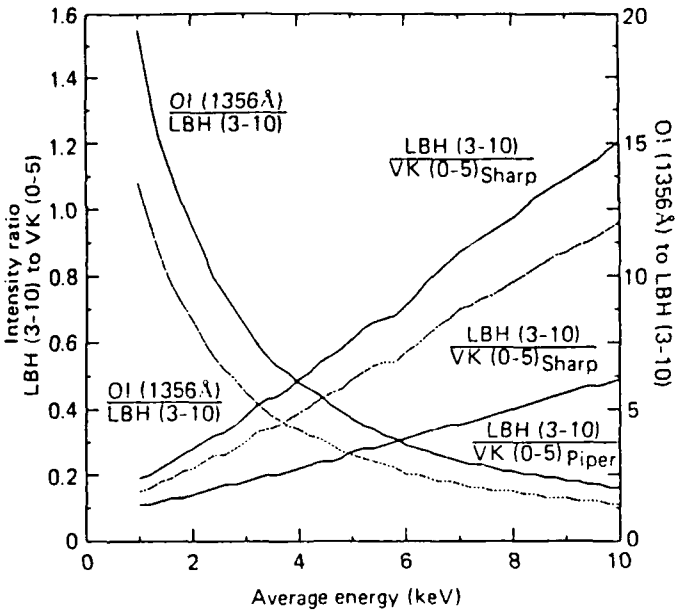

Figure 4. Emission intensity ratios as a function of average energy of incident electrons. The ratios in solid line are deduced from the values in Fig. 3. The two solid curves for the LBH (3-10) to the VK (0-5) band emission intensity ratios reflect the use of the Sharp or Piper atomic oxygen quenching coefficient. The two dotted curves demonstrate the effect of 30% atomic oxygen density of the model atmosphere (see the text for detail). The common scale of the VK (0-5) to the LBH (3-10) band emission intensity ratio is given on the left, while the scale for the OI (1356-Å) line to the LBH (3-10) band intensity ratio is given on the right. The subscripts of the VK $(0\text{-}5)_{Piper}$ and VK $(0\text{-}5)_{Sharp}$ are the same as for Fig. 3.

3.3. Relation of total energy flux and average energy of incident electrons, and the observed emission intensities

The average characteristics of auroral electron precipitation from DMSP and STP 78-1 satellite data were statistically studied as a function of magnetic local time, latitude, and the K_p index by Hardy et al.[7] They obtained an average energy flux of a few erg cm^{-2} s^{-1}, and the average energy of incident electrons was about 3 keV for $3 < K_p < 6$ in the midnight sector.

In the discrete auroral region where high total energy flux of incident electrons is expected, the S3-4 spectral data show high intensities of the LBH (3-10) band emission. Its yield is insensitive to the energy of the incident electrons (Fig. 3), and thus the observed absolute emission rate is proportional to the total energy flux of incident electrons.

The LBH (3-10) band yield by an electron flux with average energy of about 3 keV is 16 R, as shown in Fig. 3. The observed average LBH (3-10) band intensity for $3 < K_p < 6$ was 55 R. Thus, the average energy flux inferred from the seven orbits in the diffuse region of the southern auroral oval is 3.5 erg cm^{-2} s^{-1}, which is at the higher end of the values reported.[7] Considering the differences between the instantaneous and the model atmospheres, the agreement is certainly reasonable. Thus, with the appropriate model, the LBH (3-10) band intensity can provide a way of observing remotely the energy flux of auroral precipitation.

The most uncertain density in the model atmosphere is that of atomic oxygen. We can estimate the atomic oxygen density based on the observations of the OI (1356-Å) line and the LBH (3-10) band emission intensities.

Figure 4 shows the intensity ratio OI (1356 Å)/LBH (3-10) as a function of the average energy of the incident electrons calculated by Strickland under an MSIS-83 model atmosphere (the values are from Fig. 3). A reduction of the atmospheric oxygen density lowers the magnitude of the curve by decreasing the OI (1356-Å) line emission. The curve reads 4.5 keV for the intensity ratio of 5.0, which was observed from the S3-4 satellite. However, if the atomic oxygen density during the observations were smaller, the curve calculated for this modified oxygen density would have been reduced in magnitude; therefore the curve would have read a lower average energy for the observed intensity ratio (5.0).

Figure 4 also shows the intensity ratios LBH (3-10)/VK (0-5) as a function of the average energy of the incident electrons calculated by Strickland. These two curves in Fig. 4 represent the two quenching rate coefficients with the same MSIS-83 model atmosphere. A reduction of the atmospheric oxygen density decreases the magnitude of the curve by increasing the VK (0-5) band emission, and therefore decreasing the ratio LBH/VK.[6] The LBH/VK curves for the Sharp and Piper quenching coefficients read 3 and 8.5 keV for the average intensity ratio of 0.4 observed by the S3-4 satellite. However, if the atomic oxygen density during the observations were smaller, the curves calculated for this oxygen density would be reduced in magnitude, and therefore would yield higher average energy for the intensity ratio of 0.4.

If the atomic oxygen density during the observation were 30% less than the model atmosphere used in the Strickland calculation, it would lower the OI/LBH curve by 30% and the LBH/VK curve by 20%, as shown by the dotted curves in Fig. 4. Then, the new curves of the OI/LBH for the intensity ratio of 5.0 and the LBH/VK with Sharp quenching coefficient for the intensity ratio of 0.4 would yield the same averaged energy of 3.5 keV for this reduced atomic oxygen atmosphere. Although this estimated average energy is slightly higher than the statistically averaged energy, 3 keV,[7] we conclude that the analysis of the VK band intensity using the Sharp quenching coefficient satisfactorily links the optical measurements, the model calculations by Strickland et al.[5] and Daniell and Strickland,[6] and the particle analysis by Hardy et al.[7] This implies that the atomic oxygen density during our observation was 30% less than that of the MSIS-83 atmosphere used in Strickland's calculation.

4. OBSERVATIONS AND RESULTS

4.1. Overview of the individual orbit data

The observed Lα and OI (1304-Å) emission intensities, inferred incident electron characteristics, and magnetic conditions of seven auroral oval crossings are presented in Table 1 along with the date and time, the activity indexes, and approximate locations of the satellite and the solar zenith angles. The emission intensities were obtained every 22 s, corresponding to the spectrometer scan cycle (the spectrometer scanning time was 21 s).

The auroral Lα emission intensities show no correlation to the activity indexes over these orbits. The geocoronal Lα intensities show a correlation with the solar zenith angle. The geocoronal Lα has been reported to be a function of the solar zenith angle and the column hydrogen concentration at the observation point.[21] Since the S3-4 observation altitudes were about the same for all

orbits in this latitudinal region, any variation of geocoronal emission is primarily due to changes in the solar zenith angle. The OI (1304-Å) emission intensities in the diffuse region have a strong correlation with magnetic activity. The LBH and VK band emission intensities also correlate with magnetic activity.

The bottom part of Table 1 gives the inferred incident electron characteristics. The average energy is the incident electron energy averaged over the entire oval crossing. The highest average energy did not occur in the most disturbed period during these seven orbits. The next line, average energy flux, gives the incident energy flux averaged over the entire oval crossing. The last parameter in the table, total energy flux across the oval, gives the sum of the energy flux, each 22 s, throughout the auroral oval for each orbit in terms of erg cm^{-2} s^{-1} in a 1-cm slice across the oval and also in a fan-shaped slice with a 0.5-h longitudinal width. The former value represents the emission of the exact area observed by the nadir-viewing satellite. The latter value, which is well correlated with magnetic activity, is deduced for comparison to previous observations.[7] The total energy flux obtained for the midnight sector (2345 to 0015 MLT) varies from 3.0×10^{23} to 1.3×10^{25} keV s^{-1} sr^{-1}, which is consistent with the previously reported auroral electron precipitation over these magnetic activity levels.

Three individual orbits (Fig. 5) have been selected to describe the complexities in the electron energetics and proton precipitation at the various levels of magnetic activity involved in the seven orbits. The figure focuses on the LBH and VK bands, the auroral Lα emission intensities, and the photometer data. There are four panels in each diagram. The top panel shows the high-time-resolution nadir-view photometer data across the auroral oval without averaging. The value in the upper right-hand corner indicates the peak transmission wavelength of the photometer filter used for that orbit.

The second panel shows the deduced auroral Lα emission intensity as well as the total observed Lα intensity from the observed spectrum. We first deduced the NI (1744-Å) emission intensity by subtracting Degen's synthetic spectrum from the observed LBH band intensities between 1715 and 1775 Å. Second, the ratio 4.0 of the cross sections of NI lines at 1200 and 1744 Å was used to estimate the NI (1200-Å) line intensity. This ratio from the laboratory[8] and from atmospheric observations[22,23] varies from 4.0 to 7.0. The differences are primarily due to the optical thickness of the NI (1200-Å) emission[24] and the height of the aurora. The NI (1200-Å) emission intensity deduced in this way also has to be corrected for possible changes within the spectral scan as described previously. Third, we integrated the intensities of the spectra over the wavelength interval 1200 to 1245 Å without photometer normalization, and we subtracted the corrected deduced NI (1200 Å) from this value. Assuming that the geocoronal Lα change is very smooth and that its intensity can be linearly interpolated across the auroral region, it is also subtracted to obtain the auroral Lα intensity within each spectral scan. However, this process introduces some uncertainties into the determination of the NI (1200-Å) and auroral Lα emission intensities because of the photometer normalization and the fixed ratio that we used for the NI line emissions at 1200 and 1744 Å. In general, the deduced auroral Lα variation across the auroral oval is as expected: a general increase toward the equatorward edge of the diffuse region and a general, but not well-defined, overall enhancement with increasing activity.

The third panel shows the emission intensities of the LBH (3-10) and VK (0-6) bands. In the process of deducing these intensities, the NO δ band and the O_2 Herzberg I band emission intensities were subtracted by using the airglow intensities measured just outside the equatorward edge of each auroral region. These observed intensities are only a few rayleighs for the LBH (3-10) band region and less than 10 R for the VK (0-5) band region and were subtracted from the auroral spectra. The LBH and VK data in the third panel have been normalized within each spectral scan on the basis of the photometer data.

The fourth panel shows the intensity ratio of the LBH (3-10) to VK (0-5) band emissions from the third panel. In general, the ratio increases to a peak value in the diffuse region before declining, thus indicating hardening of the electron energy in the diffuse region and softening just at the equatorward edge.

In summary, these seven orbits indicate that the OI (1304-Å) line emission intensity and the inferred characteristics of incident electrons are well correlated with geomagnetic activity. The geocoronal Lα line emission intensity variations are a function of the solar zenith angle. The auroral Lα line emission intensity, which is an indicator of proton precipitation, does not correlate well with the geomagnetic activity. Morphologically, the auroral Lα emission is more intense near the equatorward edge of the diffuse region. The intensities of the LBH (3-10) and VK (0-5) band emissions are not always correlated with the geomagnetic activity. The average energy flux, total energy flux, and average energy across each oval crossing inferred from the emissions (in Table 1) are consistent with those from a statistical study of electron precipitation.[7] The increase in average electron energy before its final decrease was seen near the equatorward edge of the diffuse regions in most of the oval crossings.

4.2. NI (1744-Å) and NII (2143-Å) lines and emission cross sections

The simultaneous dissociation and excitation of N_2 by secondary electrons is believed to be responsible for both atomic line emissions. The LBH band system is also produced by the direct electron excitation of N_2. Because of the short radiative lifetime of these excitations, collisional deactivation is negligible above 95 km. Therefore, the column emission rate can be expressed as

$$I^j = \int\int n(z)\sigma^j(E)\psi(E,z)dEdz \quad , \tag{1}$$

where $n(z)$ is the atmospheric N_2 density, $\sigma^j(E)$ is the j-th emission cross section, and $\psi(E,z)$ is the secondary electron flux. According to model calculations[25] and rocket measurements,[26] the energy spectra of the auroral electron flux around the excitation-peak altitude are insensitive to both neighboring altitudes and the incident characteristic energy. Therefore, we can separate the altitude integration from the energy integration as an approximation given by

$$I^j = N(\bar{z}) \int \sigma^j(E)\psi(E,\bar{z})dE \quad , \tag{2}$$

where $\psi(E,\bar{z})$ is the secondary electron energy flux averaged at $\bar{z}$,

$N(\bar{z}) = \int n(z)dz$ is the column N_2 density, and

$\bar{z}$ is a representative altitude for the emission.

According to the MSIS-86 model atmosphere,[15] the N_2 densities, and therefore $N(\bar{z})$, do not differ significantly from each other over the range in the magnetic activities during these observations. Defining the effective cross section as in Eq. (3),

$$\sigma^j_{\text{eff}} = \int \sigma^j(E)\psi(E,\bar{z})dE \quad , \tag{3}$$

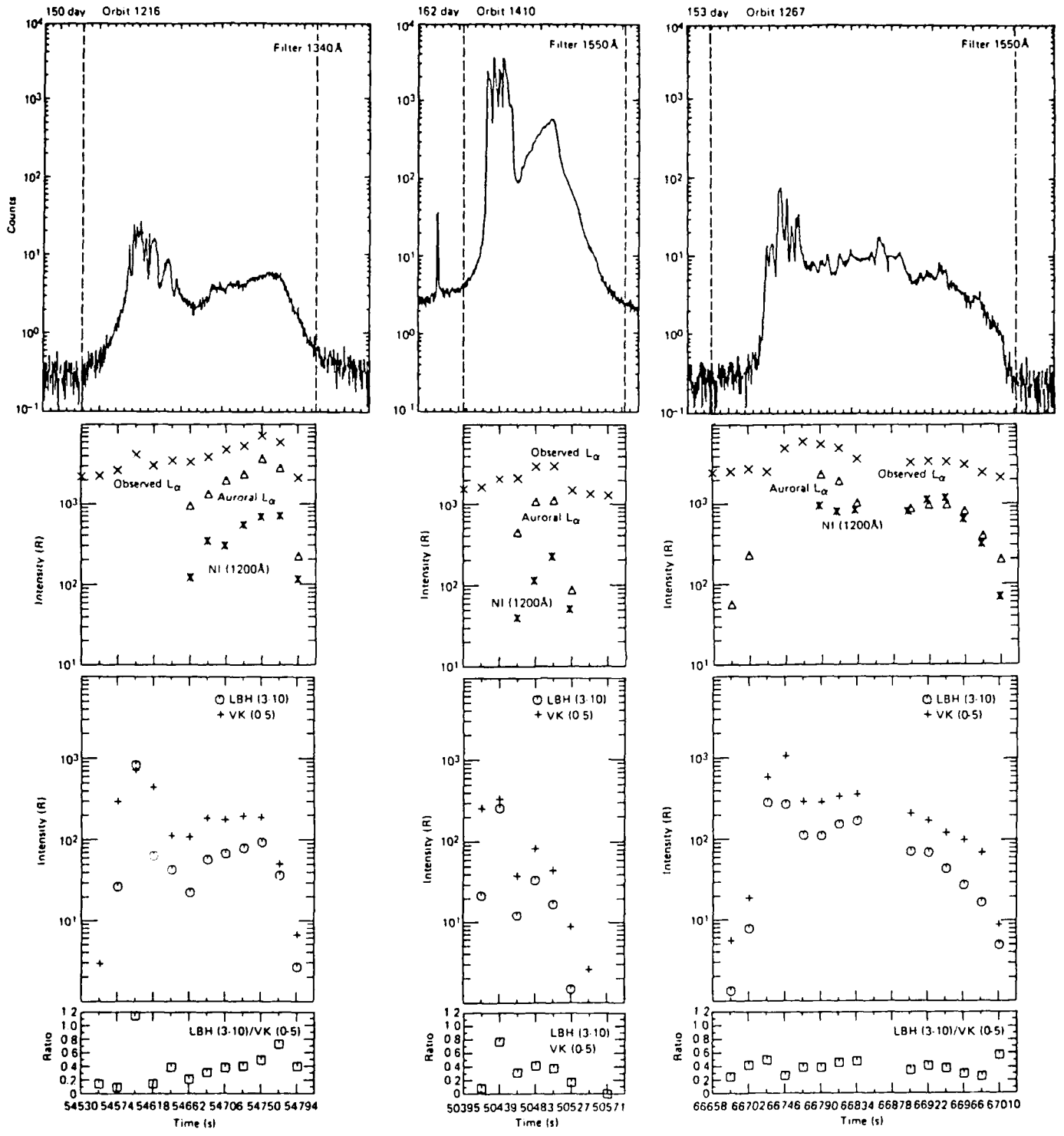

ALT (km)	277.4	276.7	275.7	274.5	273.2	271.6
GCLAT	-64.0	-60.8	-57.5	-54.3	-51.0	-47.7
GCLONG (+E)	122.5	120.5	118.9	117.5	116.3	115.2
GMLAT	-75.3	-72.2	-69.0	-65.8	-62.6	-59.4
GMLONG (+E)	200.1	195.2	191.9	189.3	187.3	185.6

277.6	276.4	274.9	273.2	271.4	
-59.1	-55.9	-52.6	-49.3	-45.1	
137.3	135.8	134.5	133.4	132.3	
-69.0	-66.1	-63.0	-59.9	-56.8	
219.3	215.4	212.2	209.6	207.3	

281.3	281.0	280.5	279.7	278.7	277.5	276.0	274.4
-68.4	-65.2	-62.0	-58.8	-55.5	-52.2	-49.0	-45.7
75.2	72.5	70.3	68.7	67.2	65.9	64.8	63.8
-76.2	-72.9	-69.6	-66.2	-62.9	-59.6	-56.2	-52.9
115.8	117.9	119.3	120.2	120.9	121.4	121.8	122.0

Figure 5. Latitudinal (time) variation of LBH (3-10) and VK (0-5) emission intensities for the seven orbits. Top panel: observed photometer counts. Second panel: the total observed emission (X), the auroral Lα emission (Δ), and the NI (1200-Å) emission (*). Third panel: LBH (3-10) (O) and VK (0-5) (+) band emission intensities. Fourth panel: intensity ratio of LBH (3-10) to VK (0-5) band emission intensities.

one can show that the column emission rate of the NI and NII lines and the LBH (3-10) band emission is proportional to this effective cross section,

$$I^j = N(\bar{z})\sigma^j_{\text{eff}} \tag{4}$$

$$\text{or} \quad I^j/I^k = \sigma^j_{\text{eff}}/\sigma^k_{\text{eff}} \tag{5}$$

$$\text{or} \quad I^j = (\sigma^j_{\text{eff}}/\sigma^k_{\text{eff}})I^k \quad . \tag{6}$$

Figures 6a-c show the correlation observed among the two atomic lines and the LBH (3-10) band emission intensities. The average intensity ratios, with their standard deviation of the [NI]/[LBH], [NII]/[LBH], and [NI]/[NII], are 1.12 ± 0.25, 1.31 ± 0.18, and 0.89 ± 0.19, respectively. The constant relationship between these three emissions supports the argument that the primary excitation mechanism for each is the same (i.e., direct electron excitation with no complicated chemical process involved).

Figures 7a-c show the energy spectra of the electron energy flux, the laboratory-measured cross sections, and the weighted cross sections. The electron energy flux here, $\psi(E,\bar{z})$, is from Feldman et al.[26] The cross sections of the LBH (3-10) band and the NII (2143-Å) line are from Ajello and Shemansky[8] and Erdman and Zipf.[27] Ajello and Shemansky published the cross sections of the NI (1744 Å) at only 100- and 200-eV electron impact. We applied the energy dependency of their cross section for the NI (1200-Å) to the NI (1744-Å) emission. The weighted cross section is defined as

$$\sigma_w(E) = \sigma(E) \times \psi(E,\bar{z}) \quad .$$

The effective cross section is redefined as

$$\sigma^j_{\text{eff}} = \int_0^{200\text{eV}} \sigma^j_w(E)dE \quad . \tag{7}$$

Note that the effective cross section increases, at most, up to 10% by extending the integration upper bound to 2 keV. Using the relation expressed in Eq. (5), the estimated column emission intensity ratios for the NI (1744-Å) and the NI (2143-Å) to the LBH (3-10) band are 1.8 and 3.6×10^{-3}, respectively.

The relative intensity ratios of the NI line emission to the LBH line emission from our observations (1.4) agree reasonably well with this theoretical prediction (1.8) for electron excitation of this emission. On the other hand, the relative intensity ratio of the NII to the LBH from our observations (1.3) does not agree with the laboratory value of the cross section (3.6×10^{-3}).[27] However, the estimated cross section from our results on NII (5×10^{-18} cm^2) agrees with the value determined from rocket observations (4×10^{-18} cm^2),[28] and subsequent revisions.[29,30] If the NII emission comes from the dissociative excitation of N_2 and its lifetime is as short as is predicted, then the absolute cross section should be two orders of magnitude greater than that measured by Erdman and Zipf.[27]

Major variations from the observed ratios in Figs. 6a-c can be used to investigate other possible excitation mechanisms. One orbit at high magnetic activity has been studied in detail, with the conclusion that at times the signature of incident heavy particles such as O^+ or O may be observable.[4]

4.3. OI (1356-Å) line excitation

Two direct electron excitation mechanisms are responsible for the OI (1356-Å) line emission: excitation of O and dissociative

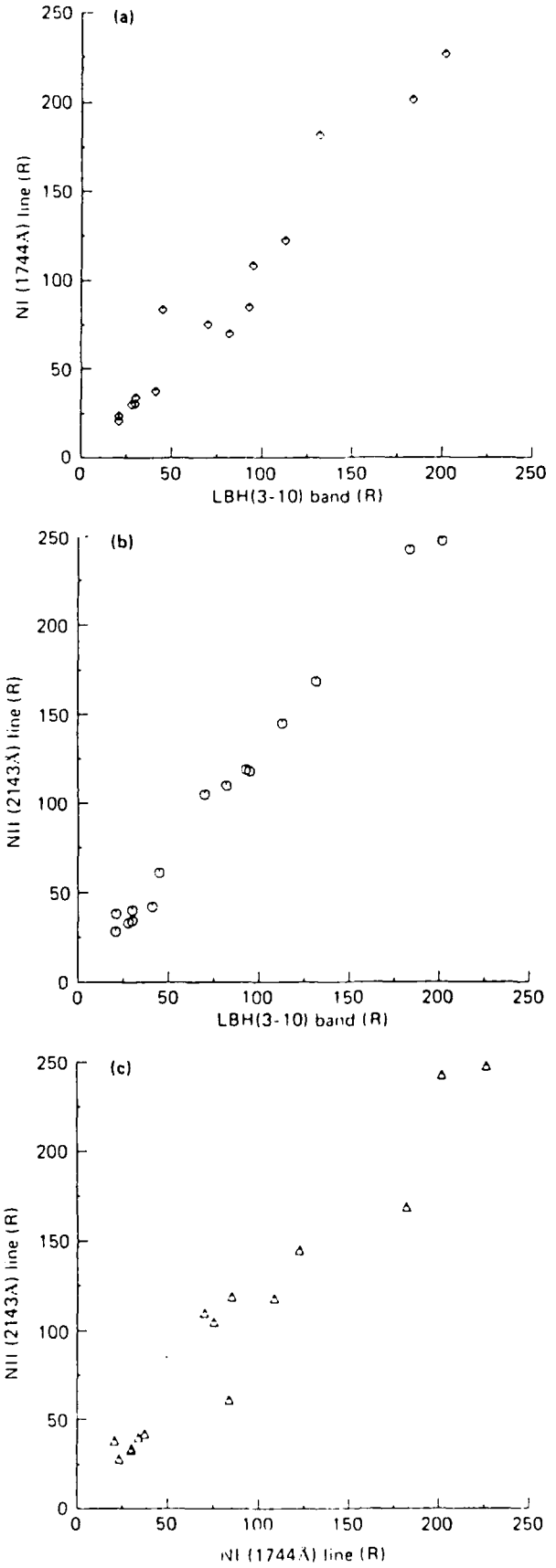

Figure 6. Intensity relationship between the NI (1744-Å), NII (2143-Å), and LBH (3-10) emissions: (a) NI (1744 Å) vs. LBH (3-10), (b) NII (2143 Å) vs. LBH (3-10), and (c) NI (1744 Å) vs. NII (2143 Å).

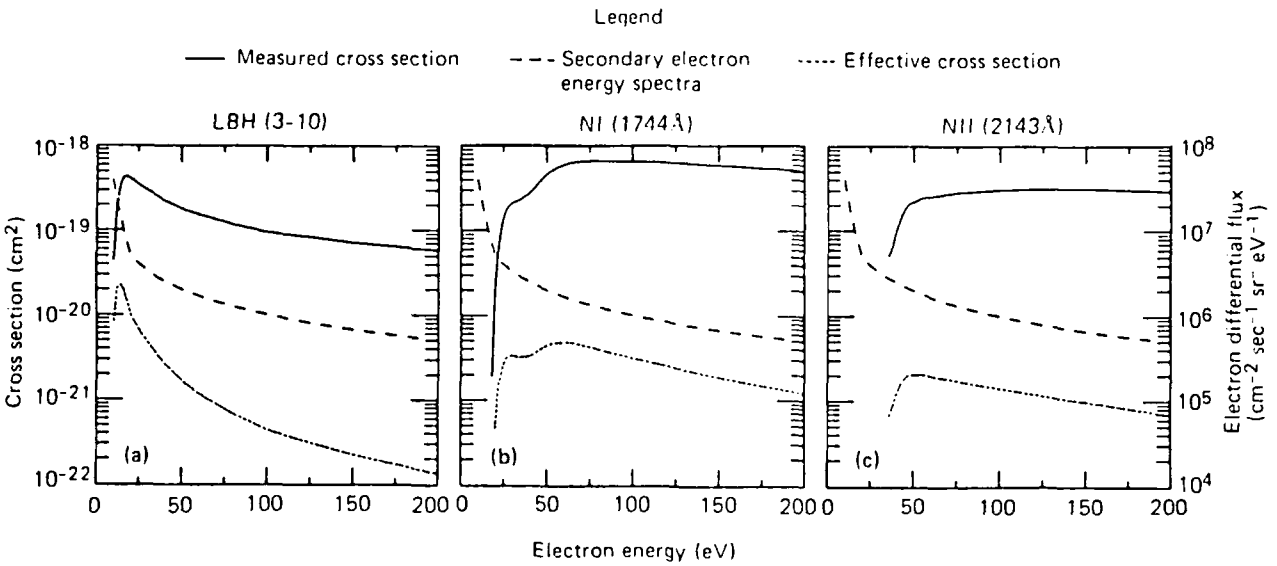

Figure 7. The electron impact cross sections (solid lines), the secondary electron flux (broken line) from Feldman and Doering,[26] and the effective emission cross sections (dotted lines), as defined in the text. The units for cross sections and electron flux as a function of electron energy are shown on the left and right axes, respectively. (a) LBH (3-10), the electron impact emission cross section is from Ajello and Shemansky.[8] (b) NI (1744 Å), the electron impact emission cross section is from Ajello and Shemansky.[8] (c) NII (2143 Å), the electron impact emission cross section is from Erdman and Zipf.[27]

excitation of O_2. Although the former mechanism is the major one, the latter mechanism becomes important if the incident electron energy is high ($\geq$ 5 keV) and reaches low in the atmosphere. For example, for 5-keV electrons, the emission from O_2 reaches 30% of that from O (Strickland, private communication). However, most 1356-Å emission from O_2 dissociation is absorbed by O_2 before it gets to the satellite at 270 km. Therefore, all the OI (1356-Å) emissions observed by S3-4 nadir-viewing spectrometers should be predominantly from atomic oxygen.

The excitation cross sections of the OI (1356-Å) line and the dependence of the LBH band system on electron energy (and, therefore, the intensity ratio of the two) are nearly independent of the secondary electron energy spectrum and depend only on the relative abundance of O and N_2.[31] The O and N_2 column densities of the MSIS-86 model atmosphere at the time of the five auroral crossings do not differ significantly from one pass to the other. Since neither the O or N_2 density changes substantially according to the MSIS-86 model, the intensity ratio of the OI (1356-Å) line to the LBH (3-10) band should be nearly constant.

Figures 8a-c show the observed OI (1356-Å) line and the NII (2143-Å) line. The average observed intensity ratio of the OI (1356-Å) line to the LBH (3-10) band was 4.92, with the standard deviation of 1.53. This ratio is close to the value (4.0) measured in an aurora rocket.[31]

5. CONCLUSIONS AND COMMENTS

The nadir-viewing UV spectral/photometric measurement from the S3-4 satellite at 270 km provides data to study the energetics of incident electrons in the nighttime aurora. The observations of selected auroral oval crossings combined with model calculations revealed several salient points.

- The observed emission intensities of the LBH (3-10) band, the VK (0-5) band, and the OI (1356-Å) line in the diffuse auroras were consistent with what would be inferred from a modified version of the model calculation by Strickland et al.[5] and imply:
  - — The average energy of incident electrons was 3 ± 1 keV as reported by Hardy et al.[7]
  - — The atmospheric atomic oxygen density was 30% less than the model atmosphere (MSIS-83) used in the calculation by Strickland.
  - — The atomic oxygen quenching coefficient for the VK (0-5) band is that given by Sharp.[19]
- The LBH (3-10) band emission intensity is a good indicator of the average energy flux of the incident electrons. The modified Strickland calculation produces 16 R of the LBH (3-10) band emission per erg cm^{-2} s^{-1} of incident electrons.
- The intensity ratio of the LBH (3-10) to VK (0-5) emissions is a good indicator of the average energy of the incident electrons in the auroral region when combined with model calculations.
- In the midnight sector the auroral Lα emission is most intense near the equatorward edge of the diffuse auroral region, which is in agreement with the accepted morphology of proton precipitation and observations of ground-based Balmer emissions.

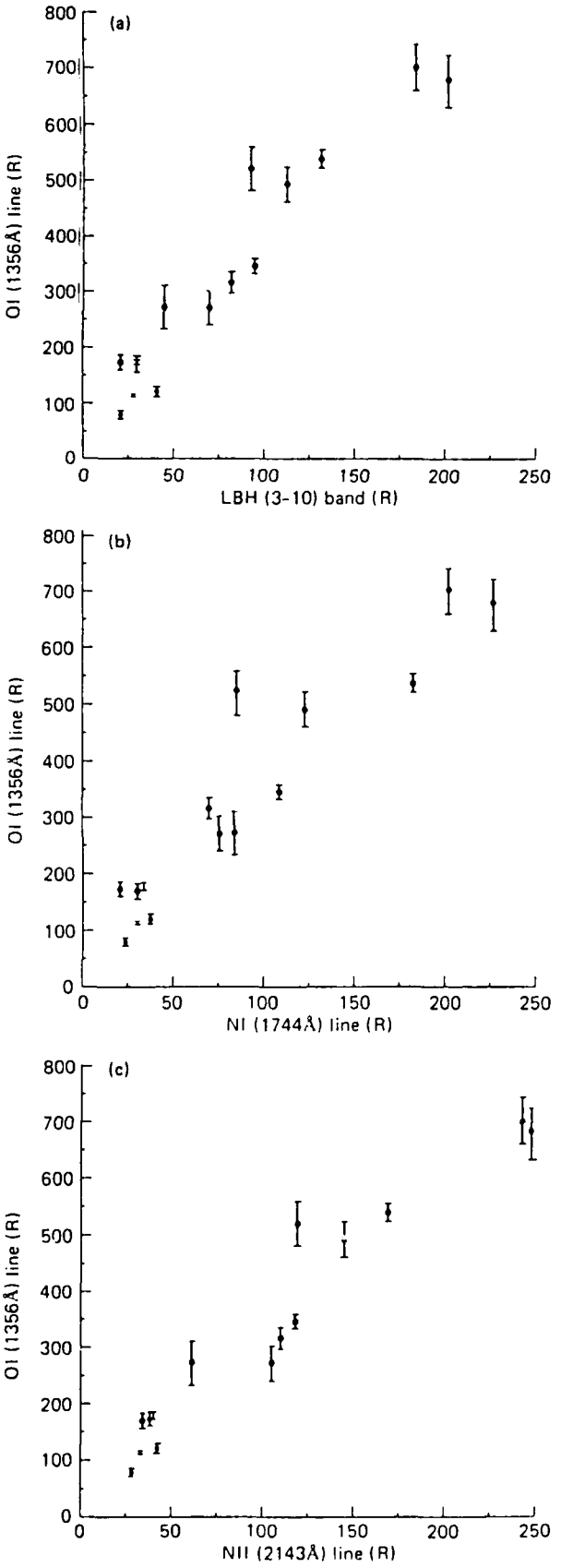

Figure 8. Intensity relationship of the OI (1356-Å) line to the NI (1744-Å) and the NII (2143-Å) line, and the LBH (3-10) band emissions: (a) OI (1356 Å) vs. LBH (3-10), (b) OI (1356 Å) vs. NI (1744 Å), and (c) OI (1744 Å) vs. NII (2143 Å).

- Intensities of the NI (1744-Å), the NII (2143-Å), and the OI (1356-Å) lines, and the LBH (3-10) band at 1928 Å show a constant proportionality to each other. The correlation of these emission intensities is consistent with the predominant emission mechanism being a direct electron impact on N_2 and O.

- The inferred NII (2143-Å) line emission cross section agrees with previously reported results[28,30] and is two orders of magnitude larger than the laboratory measurement by Erdman and Zipf.[27]

An application of the apparent near independency of the LBH band emission intensities, outside the O_2 SR continuum, on the incident electron energy (>1 keV at least) is that auroral oval images in such LBH bands (such as the (3-10)) could be used to deduce the total energy flux precipitated within the oval. With less uncertainty and simultaneous observation of the accurate atomic oxygen densities and with further understanding of the quenching rate coefficient, the simultaneous oval images of LBH and VK band emissions could provide average energy contours of the oval precipitation. Variation in the ratios of the atomic to molecular emissions, coupled with changes in both vibrational and rotational temperatures of the molecular bands from those expected for electron precipitation, can be used to detect regions of heavy particle precipitation. Thus, the use of ultraviolet emissions can lead to techniques for mapping the precipitation type, boundaries, and time variation on a global basis.

6. REFERENCES

1. R. E. Huffman, F. J. LeBlanc, J. C. Larrabee, and D. E. Paulsen, "Satellite vacuum ultraviolet airglow and auroral observations," J. Geophys. Res. 85(A5), 2201-2215 (1980).

2. M. Ishimoto, G. J. Romick, R. H. Huffman, and C.-I. Meng, "Auroral electron energy and flux from molecular nitrogen ultraviolet emissions observed by the S3-4 satellite," J. Geophys. Res. (in press, 1988).

3. M. Ishimoto, G. J. Romick, C.-I. Meng, R. E. Huffman, and V. Degen, "Analysis of atomic ultraviolet lines in the diffuse aurora," J. Geophys. Res. (in press, 1988).

4. M. Ishimoto, G. J. Romick, C.-I. Meng, and R. E. Huffman, "Anomalous UV auroral spectra during a large magnetic disturbance," J. Geophys. Res. (in press, 1988).

5. D. J. Strickland, J. R. Jasperse, and J. A. Whalen, "Dependence of auroral FUV emissions on the incident electron spectrum and neutral atmosphere," J. Geophys. Res. 88(A10), 8051-8062 (1983).

6. R. E. Daniell, Jr. and D. J. Strickland, "Dependence of auroral middle UV emissions on the incident electron spectrum and neutral atmosphere," J. Geophys. Res. 91(A1), 321-327 (1986).

7. D. A. Hardy, M. S. Gussenhoven, and E. Holdman, "A statistical model of auroral electron precipitation," J. Geophys. Res. 90(A5), 4229-4248 (1985).

8. J. M. Ajello and D. E. Shemansky, "A reexamination of important N_2 cross sections by electron impact with application to the dayglow: the Lyman-Birge-Hopfield band system and NI (119.99 nm)," J. Geophys. Res. 90(A10), 9845-9861 (1985).

9. V. Degen, Dialup Facility for Generating Auroral and Airglow Synthetic Spectra, Geophysical Institute Report, UAG-R(305) (Apr 1986).

10. R. R. Conway, R. R. Meier, D. F. Strobel, and R. E. Huffman, "The far ultraviolet vehicle glow of the S3-4 satellite," Geophys. Res. Lett. 14, 628-631 (1987).

11. R. R. Meier, R. R. Conway, P. D. Feldman, D. J. Strickland, and E. P. Gentieu, "Analysis of nitrogen and oxygen far ultraviolet auroral emissions," J. Geophys. Res. 87(A4), 2444-2452 (1982).

12. A. Vallance-Jones, Aurora, D. Reidel Publishing Company, Boston (1974).

13. E. J. Stone and E. C. Zipf, "Electron impact excitation of the ^3S and ^5S states of atomic oxygen," J. Chem. Phys. 60, 4237 (1974).

14. E. C. Zipf and P. W. Erdman, "Electron-impact excitation of atomic oxygen: Revised cross section values, EOS 66(18), 321, 1985.

15. A. E. Hedin, "A revised thermospheric model based on mass spectrometer and incoherent scatter data: MSIS-83," J. Geophys. Res. 88(A12), 10170-10188 (1983).

16. V. Degen, "Synthetic spectra for auroral studies: the N_2 Vegard-Kaplan band system," J. Geophys. Res. 87(A12), 10541-10547 (1982).

17. D. C. Cartwright, "Vibrational populations of the excited states of N_2 under auroral conditions," J. Geophys. Res. 83(A2), 517-531 (1978).

18. R. W. Eastes and W. E. Sharp, "Rocket-borne spectroscopic measurements in the ultraviolet aurora: the Lyman-Birge-Hopfield bands," J. Geophys. Res. 92(A9), 10095-10100 (1987).

19. W. E. Sharp, "Rocket-borne spectroscopic measurements in the ultraviolet aurora: nitrogen Vegard-Kaplan bands," J. Geophys. Res. 76, 987-1005 (1971).

20. L. G. Piper, G. E. Caledonia, and J. P. Kennealy, "Rate constants for deactivation of $N_2(A\ ^3\Sigma_u^+, v' = 0,1)$ by O," J. Chem. Phys. 75, 2847-2852 (1981).

21. R. R. Meier and P. Mange, "Geocoronal hydrogen: An analysis of the Lyman-alpha airglow observed from OGO-4," Planet. Space Sci. 18, 803-821 (1970).

22. J.-C. Gerard and C. A. Barth, "OGO-4 observations of the ultraviolet auroral spectrum," Planet. Space Sci. 24, 1059-1063 (1976).

23. W. E. Sharp and M. H. Rees, "The auroral spectrum between 1200 and 4000 Å," J. Geophys. Res. 77, 1810 (1972).

24. R. R. Meier, D. J. Strickland, P. F. Feldman, and E. P. Gentieu, "The ultraviolet dayglow 1. Far UV emission of N and N_2," J. Geophys. Res. 85(A5), 2177-2184 (1980).

25. M. H. Rees and K. Maeda, "Auroral electron spectra," J. Geophys. Res. 78, 8391 (1973).

26. P. D. Feldman, J. P. Doering, and J. H. Moore, "Rocket measurements of the secondary electron spectrum in an aurora," J. Geophys. Res. 76, 1738 (1971).

27. P. W. Erdman and Z. C. Zipf, "Dissociation excitation of the $N^+(^5S)$ state by electron impact on N_2: excitation function and quenching," J. Geophys. Res. 91(A10), 11345-11351 (1986).

28. W. E. Sharp, "The ultraviolet aurora: the spectrum between 2100 Å and 2300 Å," Geophys. Res. Lett. 5, 703 (1978).

29. A. Dalgarno, G. A. Victor, and T. W. Hartquist, "The auroral 2145 Å feature," Geophys. Res. Lett. 8, 603 (1981).

30. D. E. Siskind and C. A. Barth, "Rocket observation of the NII 2143 Å emission in an aurora," Geophys. Res. Lett. 14, 479-482 (1987).

31. P. D. Feldman and E. P. Gentieu, "The ultraviolet spectrum of an aurora 530-1520 Å," J. Geophys. Res. 87, 2453 (1982).

APPENDIX C

ANALYSIS OF ATOMIC ULTRAVIOLET LINES IN THE DIFFUSE AURORA

M. Ishimoto,[1], G. R. Romick[2], C. -I. Meng[1],

R. E. Huffman[3], V.Degen[2]

[1]The Johns Hopkins University

Applied Physics Laboratory

Laurel, Maryland 20707

[2]University of Alaska

Geophysical Institute

Fairbanks, Alaska 99701

[3]The Air Force Geophysics Laboratory

Hanscom Air Force Base

Bedford, Massachusetts 01731

Submitted to Journal of Geophysical Research

March 1988

ABSTRACT

Ultraviolet spectra were obtained in five different auroral oval crossings with various levels of geomagnetic activity from the polar-orbiting low altitude S3-4 satellite over the winter southern hemisphere in 1978. Three atomic line intensities (the NI line at 1744 Å, the NII line at 2143 Å and the OI line at 1356 Å) were deduced from the 30Å resolution observations by subtracting the synthetic spectra of N_2 LBH and VK band systems matched to the observed molecular bands. In the diffuse auroral region the intensity ratio of these lines to the LBH (3-10) band are relatively constant with associated incident electron average energy of 1-6 keV. This constant proportionality among the LBH (3-10) band, the NI (1744Å) and NII (2143Å) lines indicates that the excitation mechanism is primarilly the same, namely the direct impact of electrons on N_2. The inferred cross section for the NII line at 2143 Å is 5×10^{-18} cm^2, which agrees with the value estimated by Sharp (1978) and Siskind and Barth (1987) but is still two orders of magnitude larger than the laboratory measurements (Erdman and Zipf, 1986). The intensity correlation of the OI (1356Å) line and the LBH (3-10) band indicate that the direct excitation of O is the predominant OI (1356Å) emission mechanism for the particle energy covered in this study.

INTRODUCTION

Two 1/4 m Ebert-Fastie ultraviolet spectrometers and a photometer with filter wheel were on board the S3-4 polar orbiting satellite. The instruments were nadir-viewing and in this study the data were obtained on the night side from an altitude of 260-270 km over the southern winter hemisphere in 1978. The emissions taken at this altitude are high enough not to be affected by the UV vehicle glow (Conway et al., 1988). The detailed instrumentation and spectral analysis technique were described by Huffman et al. (1980) and Ishimoto et al. (1988), respectively. The FUV spectrometer covered from 1100 to 1900 Å, while the UV spectrometer covered from 1600 to 2900 Å. In an attempt to compensate for the slow scanning time (21s) and large field of view of the spectrometers relative to the spatial (i.e., temporal in observations) scale of the aurora, the spectral measurements were adjusted using the continuous photometer observations. (see Ishimoto et al., 1988 for details). In the diffuse auroral region, the photometer-corrected spectra from the FUV and UV spectrometers agreed very well over the overlapping wavelength band which were obtained about 15 seconds apart. The synthetic spectra of N_2 LBH and VK band systems also agreed quite well with the observed spectra.

Fifteen diffuse auroral spectra with 30 Å resolution from five auroral oval crossings were selected for detail analysis. The magnetic activity during these crossings varied from Kp=2 to 7+. The three atomic line intensities, namely the NI line at 1744 Å, the NII line at 2143 Å and the OI line at 1356 Å in the diffuse aurora are the main interest for the analysis,

since the line intensities were obtained directly by subtracting this major N_2 band system emissions, the LBH and the VK, from the observed spectra.

In our previous molecular band analysis (Ishimoto et al., 1988), the ratio of the LBH (3-10) to the VK (0-5) band intensities was an indicator of the average energy of the incident electrons. Figure 1 shows the correlation between these two band intensities observed in the 15 spectra. In the diffuse aurora, the average energy inferred from the ratio does not vary drastically (see Figure 1). The average ratio is 0.4. In addition, no correlation was found between the three atomic line intensities and either the ratio of the LBH (3-10) to VK (0-5) band intensity or the VK (0-5) band intensity.

The LBH band system is excited solely by direct electron impact on N_2 (Meier et al., 1980). No important chemical process biasing this excitation has been reported. The (3-10) band at 1928Å, which comprises 1.37 % of the entire LBH band system intensity, (Vallance Jones, 1970), was selected to represent the LBH band system, since it is free from the contamination by other emissions and absorptions.

The NI (1744Å) line emission is produced mainly by the simultaneous dissociation and excitation of N_2 by secondary electrons. The cross sections of the NI (1744Å) line and the LBH band were measured by Ajello and Shemansky (1985). The NII (2143Å) line emission is believed to be produced also by the simultaneous dissociation and excitation of N_2 by secondary electrons (Dick, 1978). The cross sections determined on the basis of auroral rocket experiments by Sharp (1978) and Siskind and Barth were $4 \times 10^{-18} cm^2$ and $1\text{-}2 \times 10^{-18}$ cm^2, respectively. However, the cross section measured in the

laboratory by Erdman and Zipf (1987) was ~ 3 x $10^{-21}cm^2$, which is three orders of magnitude less than the rocket observations.

The auroral OI (1356Å) line intensity is produced by direct excitation by secondary electrons. Therefore, the intensity ratio of the OI line to the N_2 LBH band is highly valuable as an indicator of the atmospheric oxygen concentration (Feldman and Gentieu, 1982). The claimed excitation mechanisms of the three atomic lines have the same cause, simply direct secondary electron excitation on the atmospheric constituents. Thus, by using the column emission intensity correlation between these lines and the LBH (3-10) band, we should be able to investigate the following:

1. Whether the electron impact dissociative mechanism is the predominant mechanism for the excitation of the NI and NII line emissions.
2. What is the value of the emission cross section of the NII line using other known cross sections (the LBH band and the NI (1744Å)line by Ajello and Shemansky, 1985).
3. Whether the direct electron impact excitation of O is the predominant OI emission mechanism

DATA PROCESSING

Fifteen spectra from five different passes of the diffuse aurora observations (Kp = 2 - 7+) were selected for this analysis. All the spectra have LBH (3-10) band intensities greater than 20 R above the noise level.

Figure 2 shows a composite auroral spectrum with 30 Å resolution from the Far UV and UV spectrometers. The major band systems are the N_2 LBH

(1300-2500Å) and the N_2 VK (1400Å and longer). From the previous analysis (Ishimoto et al., 1988), the LBH (3-10) band at 1928 Å and the VK (0-5) band emissions at 2604 Å with 30 Å resolution were shown to be free from other emission contaminations. The best-fit LBH and VK synthetic spectra (Degen, 1986) are also shown in Figure 2. Subtraction of the synthetic spectra from the observed spectra reveals specific atomic line features. Figure 2 illustrates the procedure for the deduction of the atomic line intensities.

The NII 2143 Å line emission intensity was obtained by subtracting the synthetic LBH band system spectrum matched at the 1928 Å peak, and the synthetic VK band system spectrum matched at the 2604 Å peak from the observed 30 Å resolution spectra. Variation within reasonable values (300-600°K) for the vibrational and rotational temperatures do not affect the overall shape of the LBH and VK synthetic spectra. Consequently 400°K was used for both vibrational and rotational temperatures.

The VK band emissions at wavelengths below 2000 Å are the result of direct electron impact excitation to the higher vibrational levels ($v' \geq 4$). Higher resolution (8 Å) S3-4 data, which is under investigation, shows little VK band emission at these wavelengths. Auroral rocket measurements with 4 Å resolution by Eastes and Sharp (1987) showed minuscule VK band system emission between 1675 and 2000 Å. The emissions below 1675 Å are from even higher vibrational levels. Therefore, in the light of the above evidence we assumed in this analysis no appreciable VK emissions below 2000 Å.

The NI 1744Å line intensity was obtained by subtracting the synthetic LBH band system matched to the 1928 Å peak from the observed spectra, assuming O_2 Schumann-Runge (SR) absorption was negligible (e.g. a few percent even if the 1928Å emission comes from 105 km).

In order to get the true OI line emission intensity at 1356Å, the LBH band intensities underneath must be subtracted from the observed spectra. In the wavelength region between 1325 and 1725 Å, the emissions below 150 km were substantially absorbed by atmospheric O_2 (O_2 Schumann-Runge continuum). Thus, the synthetic LBH band system spectra must be modified to include the effect of the O_2 SR absorption between the emission layers and the spectrometers at 270 km. Since we do not know the altitude distribution of the LBH band emission, we cannot estimate the exact LBH band emission intensity through the O_2 SR absorption. However, we can estimate upper and lower bounds for the OI line assuming two LBH band system intensities.

The upper bound value of the OI intensity was estimated by subtracting an under estimated LBH band intensity around 1356 Å. Assuming the LBH emission was located in one layer at a certain altitude, we can apply the known variation of the absorption cross section as a function of wavelength (Hudson, 1971) to the synthetic LBH band system spectrum and modify this synthetic spectrum to the observations between 1600 and 1680 Å. This single layer approximation always underestimates the LBH bands around 1356Å, where the O_2 SR cross section is large. We then subtracted this underestimated LBH contribution from the 1356 Å observation to obtain an upper bound for pure OI (1356 Å) emission intensity.

A lower bound value for the OI intensity was estimated by subtracting the overestimated LBH band intensity around 1356 Å. In the wavelength region of 1356 Å ± 60 Å, only three non-trivial atomic lines exist, the OI 1304 Å, the OI 1356Å and the NI 1411Å. If all the LBH band systems are subtracted from the observed spectra, these three lines should be the only ones appearing in the subtracted spectra. The two minimum intensity points

between the three maximum intensity points from the three atomic line peaks in the LBH subtracted spectrum should not be less than zero for the 30 Å resolution spectra. If we draw the straight line on the spectra between these two minimum points and assume the peak intensity of the OI line to be above this straight line at 1356 Å, we can obtain the lower bound OI emission intensity.

Taking the middle point of the upper and lower bounds for the bottom of the OI line, we obtained the OI emission intensity. The difference between this middle point and either upper or lower bound lies within 10% of the estimated OI emission intensity itself. This accuracy (within 10%) is adequate for our study.

After subtracting the modified LBH synthetic spectrum, the remaining spectrum shows the existence of the OI line emission at 1641 Å. The intensity ratio of this OI line to the 1304 line remained at around 1-7 x 10^{-3} compared to 3 x 10^{-3} from the dayglow spectra reported by Meier and Conway (1985). This is further confirmation of the 1641Å emission intensity and the previously reported intensity ratio.

RESULTS

A. NI (1744Å) and NII (2143Å) lines

The simultaneous dissociation and excitation of N_2 by secondary electrons is believed to be responsible for both nitrogen atomic line emissions. The LBH band system is also produced by direct electron excitation of N_2. Because of the short radiative lifetime of these excitations, collisional deactivation is negligible above 95 km. Therefore, the column emission rate can be expressed by the equation,

$$I^j = \int \int n(z)\, \sigma^j(E)\, \Psi(E,z)\, dE\, dz \qquad (1)$$

where n(z) is the atmospheric N_2 density, σ^j (E) is the j-th emission cross section and Ψ (E,z) is the secondary electron flux. According to model calculations (Rees and Maeda, 1973) and rocket measurements (Feldman et al., 1971), the energy spectra of the auroral electron flux around the excitation-peak altitude are insensitive to both neighboring altitudes and the incident characteristic energy. Therefore, we can separate the altitude integration from the energy integration as an approximation.

$$I^j = N(\bar{z}) \int \sigma^j(E)\, \Psi(E, \bar{z})\, dE \qquad (2)$$

where $\Psi(E, \bar{z})$ is the secondary electron energy flux averaged at $\bar{z}$

$N(\bar{z}) = \int n(z)\, dz$ is the column N_2 density, and

$\bar{z}$ is a representative altitude for the emission.

According to the MSIS-86 model atmosphere (Hedin, 1986), the N_2 densities, therefore N $(\bar{z})$, at the time of the five orbits of current interest do not differ significantly from each other over the range in the magnetic activity. Defining the effective cross section by equation,

$$\sigma^j_{eff} = \int \sigma^j(E)\, \Psi(E,\bar{z})\, dE, \qquad (3)$$

one can show that the column emission rate of the NI and NII lines and the LBH (3-10) band emission is proportional to this effective cross section.

$$I^j = N(\bar{z})\, \sigma^j_{eff} \qquad (4)$$

or $$I^j / I^k = \sigma^j_{eff} / \sigma^k_{eff} \qquad (5)$$

or $$I^j = (\sigma^j_{eff} / \sigma^k_{eff})\, I^k \qquad (6)$$

Figures 3 a-c show the correlation observed among the two atomic nitrogen lines and the LBH (3-10) emission intensities. The average intensity ratios with their standard deviation of the [NI]/[LBH], [NII]/[LBH] and [NI]/[NII] ratios are 1.12 ± 0.25, 1.31 ± 0.18 and 0.89 ± 0.19, respectively.

The constant relationship between these emissions support the argument that the primary excitation mechanism for these three emissions is the same, i.e., the direct electron excitation with no complicated chemical process involved.

Figure 4a-c shows the energy spectra of the electron energy flux, the laboratory measured cross sections and the weighted cross sections for the LBH (3-10) band and the two emission lines. The electron energy flux here, $\Psi(E,\bar{z})$ was from Feldman et al. (1971). The cross sections of the LBH (3-10) band and the NII (2143Å) are from Ajello and Shemansky (1985) and Erdman and Zipf (1987), respectively. Ajello and Shemansky (1985) published the cross sections of the NI (1744Å) only for 100 and 200 eV electron impact. We applied their energy dependency of the cross section of the NI (1200Å) to the NI (1744Å). The weighted cross section is defined as:

$$\sigma_w(E) = \sigma(E) \times \Psi(E, \bar{z}) \ .$$

The effective cross section is redefined as:

$$\sigma^j_{eff} = \int_0^{200eV} \sigma^j_w(E)\, dE. \qquad (7)$$

Note that the effective cross section increases at most, up to 10% by extending the integration upper bound to 2 keV. Using the relation expressed in equation (5), the estimated column emission intensity ratios for the NI (1744Å) and the NII(2143Å) to the LBH (3-10) band are 1.8 and 3.6×10^{-3}, respectively.

The relative intensity ratios of the NI to the LBH from our observations (1.4) agree reasonably well with this theoretical prediction (1.8). On the other hand, the relative intensity ratio of the NII to the LBH from our observations (1.3) does not agree with the theoretical prediction (3.6×10^{-3}) using Erdman and Zipf (1987) cross section. However, the estimated cross section ($5 \times 10^{-18} cm^2$) from the above calculations agrees with the value determined from the rocket observation by Sharp (1978) ($4 \times 10^{-18} cm^2$, revised in Dalgarno et al, 1981 and $1\text{-}2 \times 10^{-18}$ cm^2 by Siskind and Barth(1987). If the NII emission comes from the dissociative excitation of N_2 and its life time is as short as predicted by Erdman and Zipf (1987), then the absolute cross section should be two orders of magnitude greater than that measured by Erdman and Zipf (1987).

B. OI (1356Å) line

Two direct electron excitation mechanisms are responsible for the OI (1356Å) line emission: excitation of O and dissociative excitation of O_2. Although the former mechanism is the major one, the latter mechanism becomes important if the incident electron energy is high ($\gtrsim$ 5keV) and penetrates to low altitudes in the atmosphere. For example, for 5keV electrons, the emission from O_2 reaches 30 % of that from O (Strickland, private communication). However, most 1356Å emission from O_2 dissociation is absorbed by O_2 before it reaches the satellite altitude at 270km. Therefore, all the OI (1356Å) emission observed by S3-4 nadir-viewing spectrometers should be predominantly from atomic oxygen.

According to Feldman and Gentieu (1982), the excitation cross sections of the OI (1356Å) line and the LBH band system dependence on

electron energy and hence the intensity ratio of the two is nearly independent of the secondary electron energy spectrum and depends only on the relativeabundance of O and N_2. The O and N_2 column densities of the MSIS-86 model atmosphere (Hedin, 1986) at the time of the five auroral oval crossings do not differ significantly from one pass to the other. Since neither the O or N_2 density changes substantially according to the MSIS-86 model, the intensity ratio of the OI (1356Å) line to the LBH (3-10) band should be nearly constant.

Figure 5a-c show the correlations of the observed OI (1356Å) line intensity with the LBH (3-10) band, the NI (1744Å) line and the NII (2143Å) line. The average observed intensity ratio of the OI (1356Å) line to the LBH (3-10) band was 4.92 with the standard deviation of 1.53. This ratio is close to the value of 4 measured by rocket (Feldman and Gentieu, 1982).

CONCLUSIONS

The spectra with 30 Å resolution from five different polar region passes over the diffuse aurora taken by a polar orbiting satellite at 270 km over the winter southern hemisphere in 1978 were analyzed. Intensities of the NI (1744Å) and the NII (2143Å) lines and the LBH (3-10) band at 1928 Å show a constant proportionality to each other. The correlation of these emission intensities is consistent with the predominant emission mechanism being the direct electron impact on N_2, given similar average incident electron spectra and no drastic changes in atmospheric conditions over these satellite orbits. The inferred NII line emission cross section agrees with that by Sharp (1978) and Sikind and Barth (1987), but is larger by two orders of magnitude over the laboratory measurement by Erdman and Zipf (1986). The intensity ratio of the OI (1356Å) line to the LBH (3-10) band agrees with that measured by a rocket (Feldman and Gentieu, 1982). The correlation of these two emissions indicates that the direct impact on atomic oxygen is the predominant mechanism for the OI (1356Å) line emission for these average electron energies.

REFERENCES

Ajello, J. M. and D. E. Shemansky, A reexamination of important N_2 cross sections by electron impact with application to the dayglow: The Lyman-Birge-Hopfield band system and NI (119.99 nm), J. Geophys. Res., 90, A10, 9845- 9861, 1985.

Conway, R. R., R. R. Meier, D. F. Strobel, R. E. Huffman, The far ultraviolet vehicle glow of the S3-4 satellite, Geophys. Res. Lett., 14, 628-631, 1987.

Dalgarno, A., G. A. Victor, and T. W. Hartquist, The auroral 2145 Å feature, Geophys. Res. Lett., 8, 603, 1981.

Degen, V., Dialup Facility for Generating Auroral and Airglow Synthetic Spectra, publ. by Geophysical Institute Report, UAG-R(305), April, 1986.

Dick, K. A., The auroral 2150 Å feature: A contribution from lines of singly ionized atomic nitrogen, Geophys. Res. Lett., 5, 273, 1978.

Eastes, R. W. and W. E. Sharp, Rocket-borne spectroscopic measurements in the ultraviolet aurora: The Lyman-Birge-Hopfield Bands, J. Geophys. Res., 92, A9, 10095-10100, 1987.

Erdman, P. W. and Z. C. Zipf, Dissociation Excitation of the $N^+(^5S)$ State by Electron Impact on N_2: Excitation Function and Quenching, J. Geophys. Res., 91, A10, 11345-11351, 1986.

Feldman, P. D., J. P. Doering, and J. H. Moore, Rocket measurements of the secondary electron spectrum in an aurora, J. Geophys. Res., 76, 1738, 1971.

Feldman, P. D. and E. P. Gentieu, The ultraviolet spectrum of an aurora 530-1520 Å, J. Geophys. Res., 87, 2453, 1982.

Hedin, A. E., MSIS-86 thermospheric model, J. Geophys. Res., 92, A5, 4649-4662, 1986.

Hudson, R. D., Critical review of ultraviolet photoabsorption cross section for molecules of astrophysical and aeronomic interest, Rev. Geophys. Space Phys., 9, 2, 305-406, 1971.

Huffman, R. E., F. J. LeBlanc, J. C. Larrabee, and D. E. Paulsen, Satellite vacuum ultraviolet airglow and auroral observations, J. Geophys. Res., 85, A5, 2201-2215, 1980.

Ishimoto, M., G. J. Romick, R. H. Huffman, and C.-I. Meng, Auroral Electron Energy and Flux from Molecular Nitrogen Ultraviolet Emissions Observed by the S3-4 Satellite, J. Geophys. Res., , (submitted).

Meier, R. R. and R. R. Conway, The ^1D–^3S transition in atomic oxygen: A new method of measuring the O abundance in planetary thermospheres, Geophys. Res. Lett., 12, 9, 601-604, 1985.

Meier, R. R., D. J. Strickland, P. F. Feldman, and E. P. Gentieu, The ultraviolet dayglow 1. Far UV emission of N and N_2, J. Geophys. Res., 85, A5, 2177-2184, 1980.

Rees, M. H. and K. Maeda, Auroral Electron Spectra, J. Geophys. Res., 78, 8391, 1973.

Sharp, W. E., The ultraviolet aurora: the spectrun between 2100 Å and 2300 Å, Geophys. Res. Lett., 5, 703, 1978.

Siskind, D. E. and C. A. Barth, Rocket Observation of the NII 2143 Å Emission in an Aurora, Geophys. Res. Letters, 14, 4, 479-482, 1987.

Vallance-Jones, A., Aurora, publ. by D. Reidel Publishing Company, Boston, 1974.

FIGURE CAPTIONS

Figure 1 Intensity relationship between the LBH (3-10) band and the VK(0-5) band emissions observed in the 15 selected spectra from the nadir-viewing S3-4 satellite. Two points, (62,20) and (63,20), overlap.

Figure 2 A VUV and UV composite spectrum and the best-fit LBH and VK synthetic spectra. The dotted line represents the difference spectrum obtained by subtracting the synthetic spectra from the observed spectrum.

Figure 3 Intensity relationship between the NI (1744Å), NII (2143Å) and LBH (3-10) emissions.

Figure 3a: NI(1744Å) vs. LBH (3-10)

Figure 3b: NII(2143Å) vs. LBH(3-10)

Figure 3c: NI(1744Å) vs. NII(2143Å). Two points, (30, 33) and (30, 34), overlap.

Figure 4 The electron impact cross sections (solid lines), the secondary electron flux (broken line) from Feldman and Doering (1971), and the effective emission cross sections (dotted lines) defined in the text. The units for cross sections and electron flux as a function of electron energy are shown on the left and right ordinate, respectively.

Figure 4a LBH (3-10), the electron impact emission cross sections is from Ajello and Shemansky (1985)

Figure 4b NI (1744Å), the electron impact emission cross sections is from Ajello and Shemansky (1985)

Figure 4c NII (2143Å), the electron impact emission cross section is from Erdman and Zipf (1986).

Figure 5 Intensity relationship of the OI (1356Å) line to the NI (1744Å) and NII (2143Å) line, and the LBH (3-10) band emissions.

Figure 5a OI (1356Å) vs. LBH (3-10)

Figure 5b OI (1356Å) vs. NI (1744Å)

Figure 5c OI (1356Å) vs. NII (2143Å)

THE JOHNS HOPKINS UNIVERSITY
APPLIED PHYSICS LABORATORY
LAUREL MARYLAND

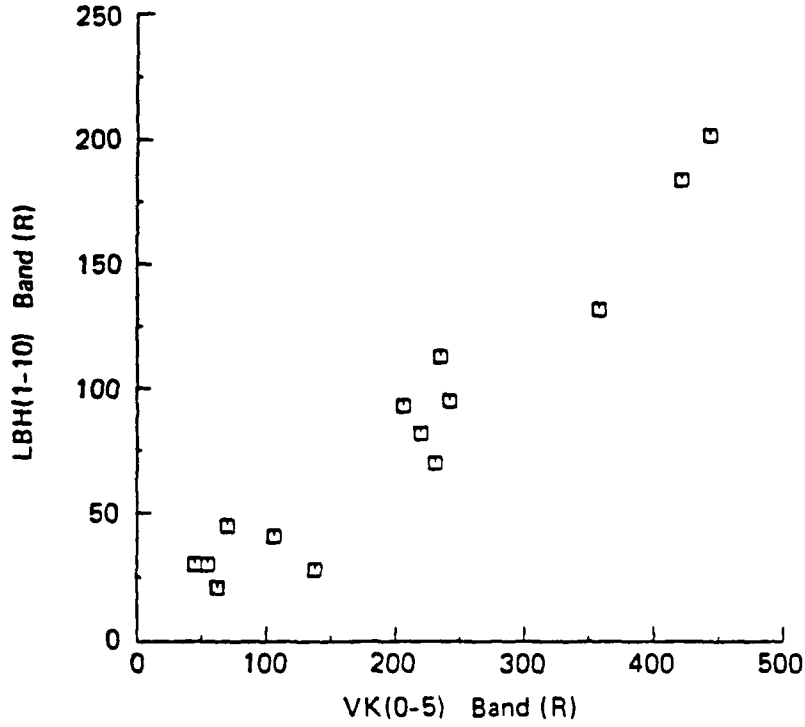

Figure 1

THE JOHNS HOPKINS UNIVERSITY
APPLIED PHYSICS LABORATORY
LAUREL MARYLAND

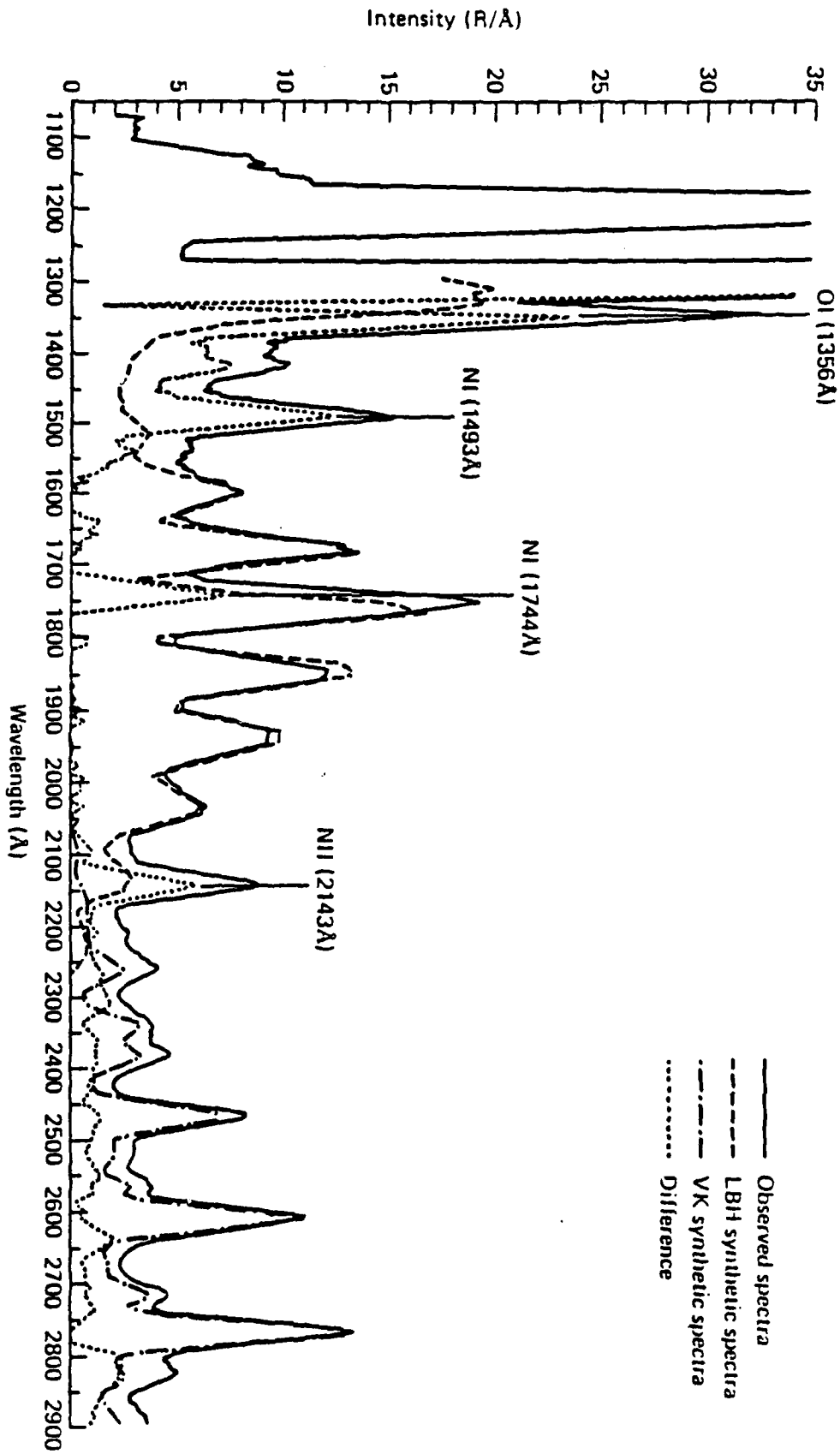

Figure 2

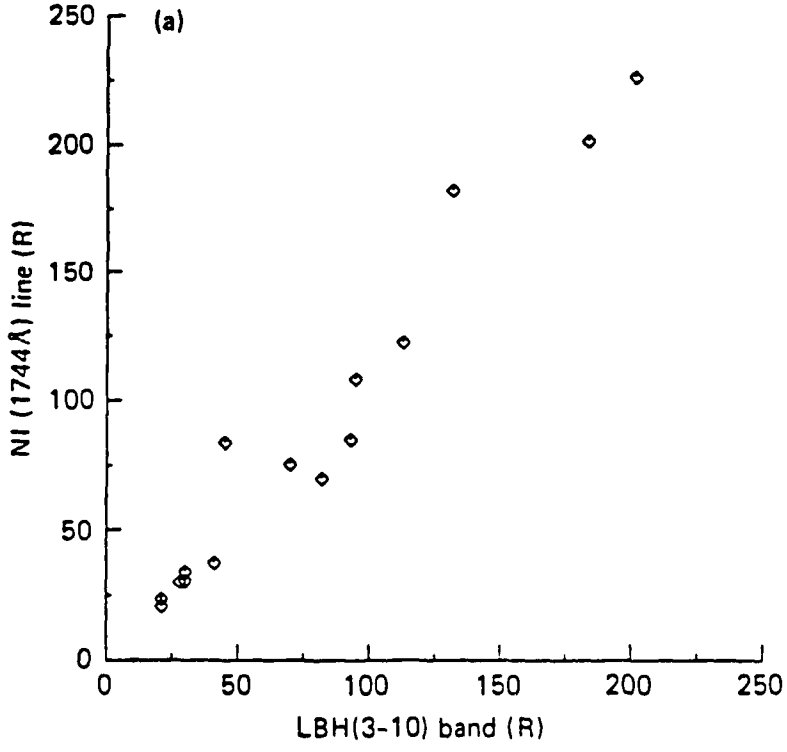

Figure 3a

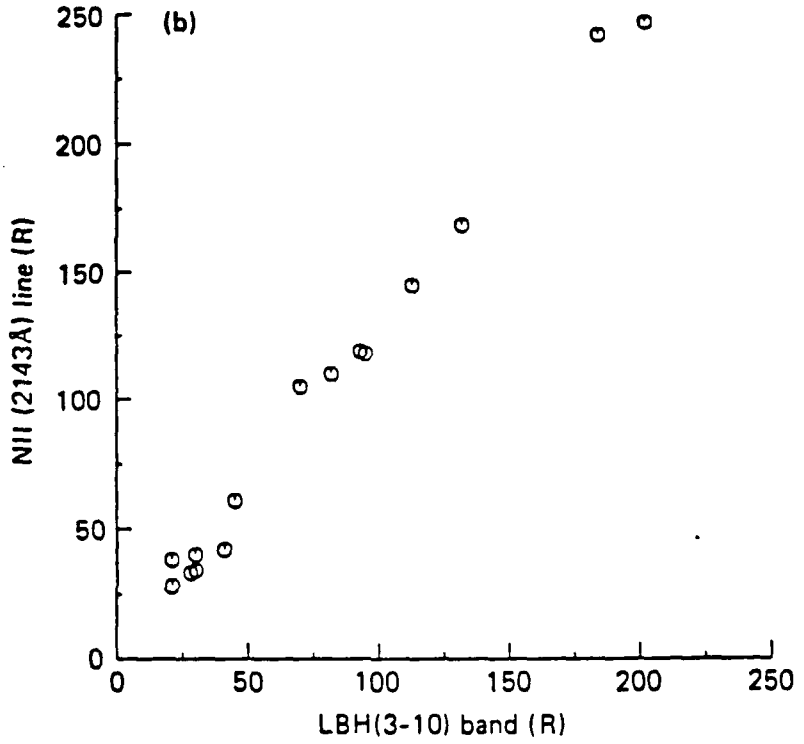

Figure 3b

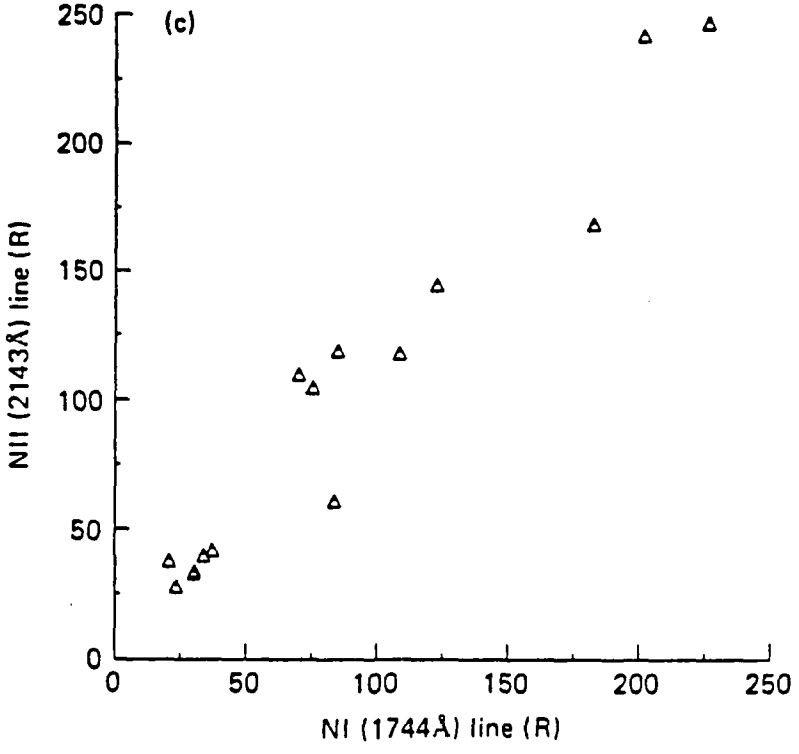

Figure 3c

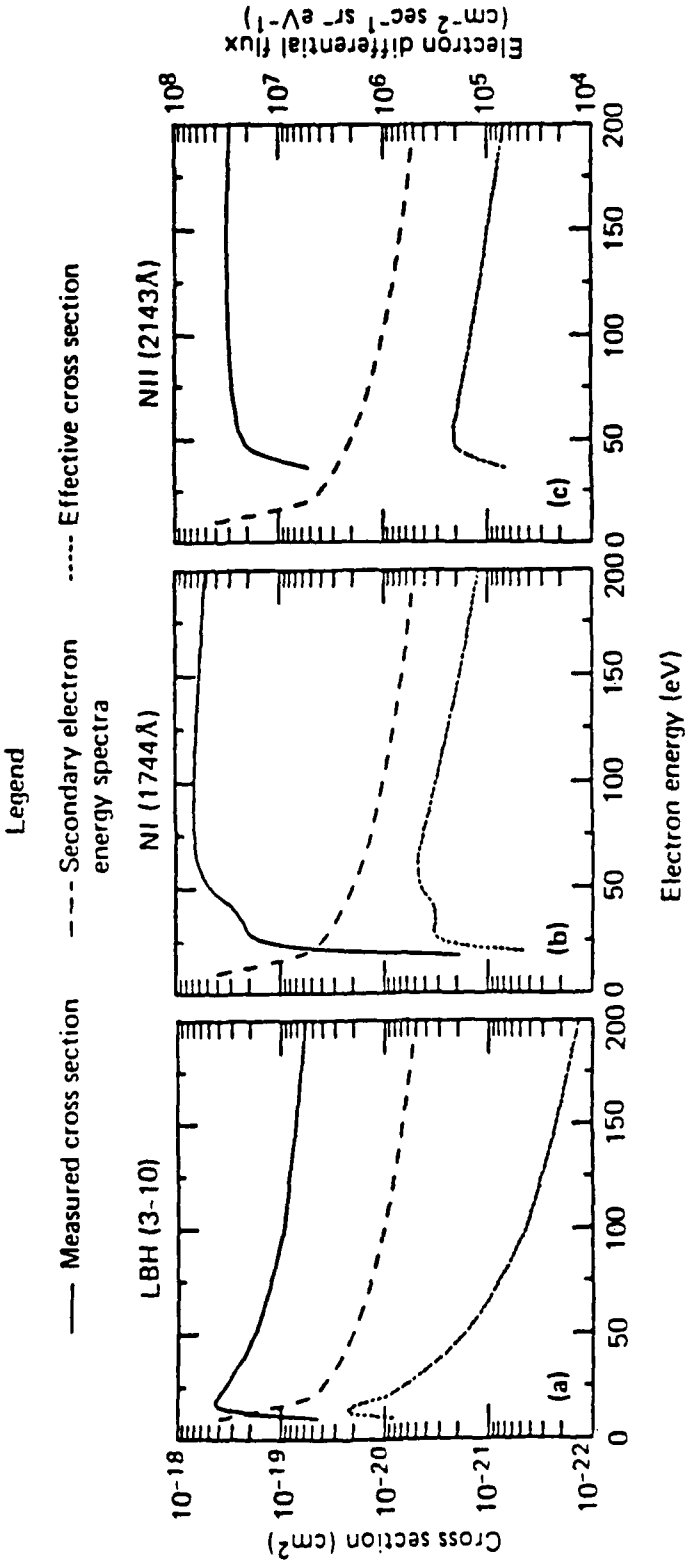
Legend
Measured cross section
Secondary electron energy spectra
Effective cross section
LBH (3-10)
NI (1744Å)
NII (2143Å)
(a)
(b)
(c)
Cross section (cm²)
Electron energy (eV)
Electron differential flux (cm⁻² sec⁻¹ sr⁻ eV⁻¹)

Figure 4

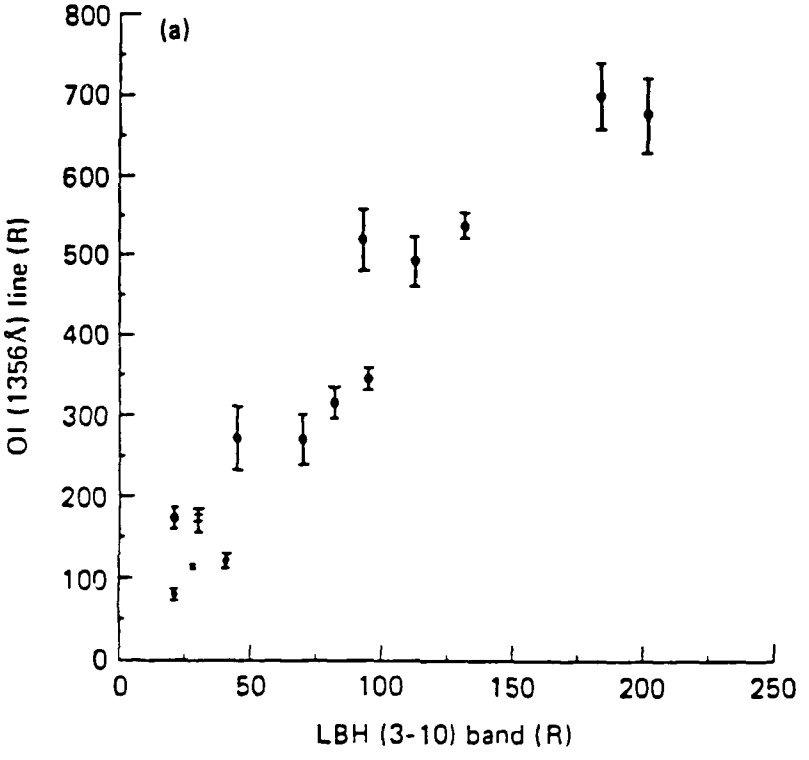
(a)
800
700
600
500
400
300
200
100
0
OI (1356Å) line (R)
0
50
100
150
200
250
LBH (3-10) band (R)

Figure 5a

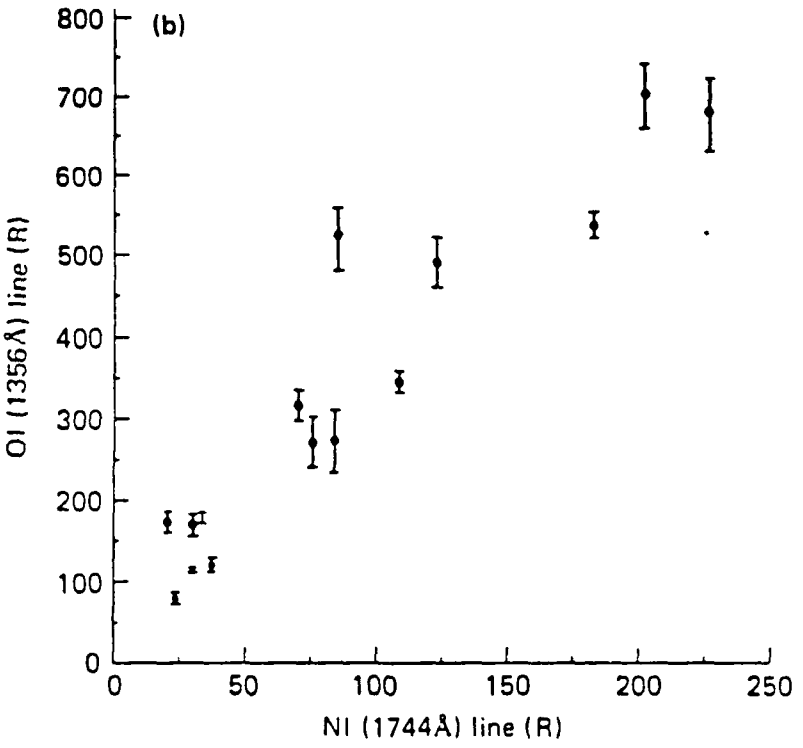
(b)
800
700
600
500
400
300
200
100
0
OI (1356Å) line (R)
0
50
100
150
200
250
NI (1744Å) line (R)

Figure 5b

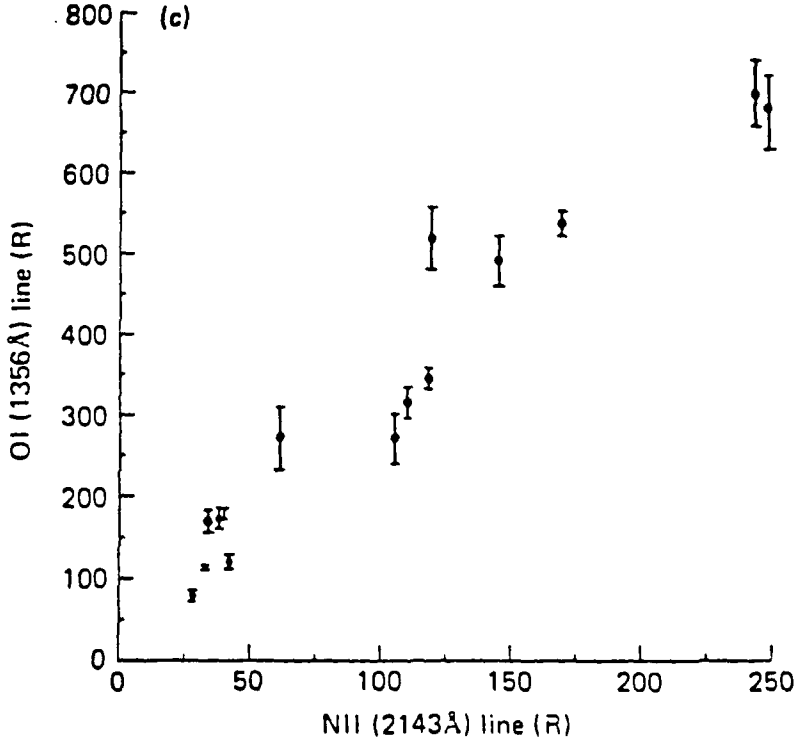
(c)
800
700
600
500
400
300
200
100
0
0
50
100
150
200
250
OI (1356Å) line (R)
NII (2143Å) line (R)

Figure 5c

APPENDIX D

JOURNAL OF GEOPHYSICAL RESEARCH, VOL. 94, NO. A6, PAGES 6955-6960, JUNE 1, 1989

Anomalous UV Auroral Spectra During a Large Magnetic Disturbance

M. ISHIMOTO AND C.-I. MENG

Applied Physics Laboratory, Johns Hopkins University, Laurel, Maryland

G. R. ROMICK

Geophysical Institute, University of Alaska, Fairbanks

R. E. HUFFMAN

Air Force Geophysics Laboratory, Hanscom Air Force Base, Massachusetts

Ultraviolet and far ultraviolet auroral spectra (1100–2900 Å) were taken during a very disturbed period (K_p = 7+) on June 2, 1978, by the S3-4 polar-orbiting satellite over the nightside, winter southern hemisphere polar region. The spectra from the equatorward section (-53° to -60° geomagnetic latitude) of the auroral precipitation showed many striking differences from those of the diffuse aurora in other orbits or the poleward section of the diffuse auroral region (-60° to -65° geomagnetic latitude) on the same orbit. The differences are as follows: (1) intensity ratios of the nitrogen atomic lines (1744 Å and 2143 Å) to the Lyman-Birge-Hopfield (LBH) (3-10) band were 2 instead of 1; (2) intensity ratio of the oxygen line (1356 Å) to the LBH (3-10) band was 15 instead of 4; (3) rotational temperature of the Vegard-Kaplan band system was 1000 K instead of 400 K; and (4) effective vibrational temperature of the LBH band system was above 3000 K instead of below 1000 K. These and other characteristics are consistent with the assumption that observed spectra may originate from two different altitude regimes. Emissions from low altitudes (approximately 120 km) were produced by typical keV diffuse auroral-electron precipitation, and those from high altitudes (approximately 200 km) were produced by keV heavy particle precipitation. The lack of significant enhancement of Lyman α emission indicates a very weak proton precipitation. We believe that these low-latitude anomalous ultraviolet spectral features are likely due to the keV ion-atom oxygen precipitation, previously observed by a mass spectrometer at 800 km.

INTRODUCTION

During large magnetospheric disturbances, various emission lines and bands have been observed at rather low latitudes (<60° GMLAT) for many decades [*Loomis*, 1861]. The spectral characteristics of the lower latitude atmospheric emissions due to precipitating particles are quite different from those of the aurora excited by keV electrons in the auroral zone. *Tinsley et al.* [1986] summarized these characteristics: (1) N_2^+ first-negative (1 N) emission with high vibrational development, (2) a high ratio (greater than 10) of red (6300 Å) to green (5577 Å) atomic oxygen lines, and (3) prominence of atomic/ionic lines of O, O^+, N, and N^+ as compared to molecular bands.

The N_2^+ first-negative 1 N emission with increased population in the higher vibrational levels (called vibrational enhancement, which is the characteristic of heavy particle precipitation) has been observed at low latitudes. These vibrationally enhanced N_2^+ 1 N emissions sometime extend to higher geomagnetic latitudes and merge into the expanded auroral oval during large storms. The emission intensity increases with the geomagnetic latitude (GMLAT), but the vibrational enhancement decreases with latitude [*Tinsley et al.*, 1982]. While N_2^+ 1 NG emissions in the low latitudes below 40° GMLAT are attributed to neutral atom precipitation from the ring current, emissions in the latitudes above 40° are attributed to direct ion and neutral atom precipitations [*Tinsley*, 1979]. This morphology agrees with the precipitation of keV heavy particles (mainly H^+ and O^+) up to 0.4 erg cm^{-2} s^{-1} sr^{-1} measured by *Shelley et al.* [1972].

In this paper we report the observation of auroral UV spectra taken at 270 km between the 2100 and 2300 magnetic local time meridians during an extremely active period (K_p = 7+, AE = 1300 nT) and near the peak of a very intense continuous substorm activity ($K_p \geq 7$, over 12 hours) on June 2, 1978. The southern auroral oval was located between -73° and -53° GMLAT. Anomalous auroral UV spectra were detected over the equatorward part of the diffuse auroral region (approximately -55° to -60° GMLAT). The spectral characteristics are high atomic to molecular emission intensity ratios and high vibrational and rotational temperatures in the N_2 molecular bands. We can conclude that these emissions resulted from keV O^+ precipitation based on the comparison with results of laboratory measurements and model calculations.

OBSERVATION AND DATA PROCESS

UV spectra were taken by two nadir-viewing ¼-m Ebert-Fastie spectrometers on board the S3-4 polar-orbiting satellite at 270 km. The detailed instrumentation and spectral analysis technique were described by *Huffman et al.* [1980] and *Ishimoto et al.* [1988], respectively. The observed UV spectra (1100-2900 Å) contain various molecular bands, such as the N_2 Lyman-Birge-Hopfield (LBH) and Vegard-Kaplan (VK) bands, and numerous N, N^+, and O lines. In the previous analysis with 30-Å spectral resolution data [*Ishimoto et al.*, 1988] we found that the LBH (3-10) band at 1928 Å and the VK (0-5) band at 2604 Å were sufficiently free from other emission contaminations to be used as the representative intensity for their respective band systems.

Paper number 88JA03920.
0148-0227/89/88JA-03920$02.00

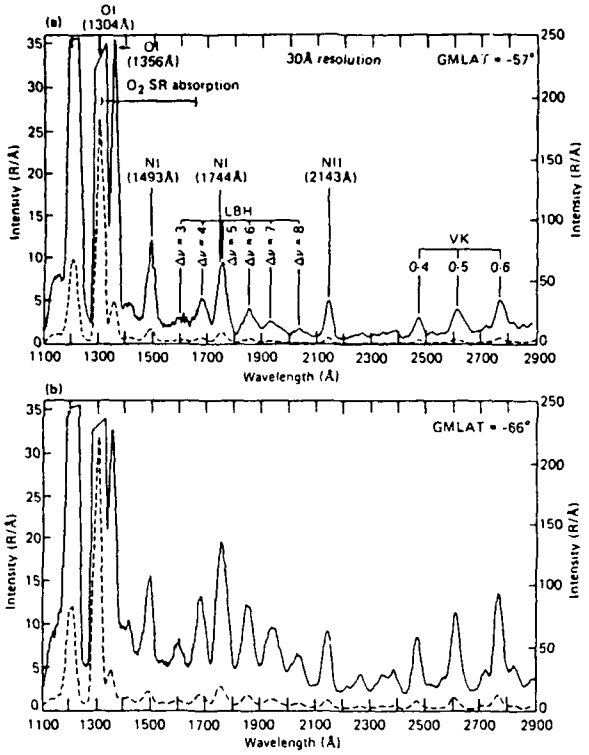

Fig. 1. The spectra from the (*a*) low-latitude part and (*b*) high-latitude part of the diffuse auroral oval. Two scales for intensities are plotted, with units for the solid curve (expanded) on the left and units for the dotted curve (compressed) on the right.

The N I 1744-Å, N II 2143-Å and O I 1356-Å line intensities were deduced by subtracting the LBH and VK band system intensities from the observed spectra (see *Ishimoto et al.* [1988] for the detailed procedure).

Twenty spectra over the diffuse auroral region from five auroral oval crossings were examined. The LBH (3-10) band intensity greater than 20 R was used as a criterion in the selection. This corresponds to a minimum signal-to-noise ratio of 5. Among the spectra examined, it is found that five taken from the equatorward part of the auroral oval during a very disturbed period were quite different from the rest. The characteristics of these anomalous spectra (hereafter designated as the lower-latitude aurora, LLA) will be compared with the three diffuse auroral spectra obtained from the poleward part of the same diffuse oval (hereafter designated as higher-latitude aurora, HLA). The latter are similar to spectra of diffuse auroral region from other oval crossings in less magnetically active periods.

Spectral Analysis

The contrast between the LLA and HLA spectra is shown in Figure 1. The LBH (3-10) band intensity in the HLA, an indicator of the energy flux of the incident electrons [*Strickland et al.*, 1983], was higher than in the LLA. Similarly, the auroral Lyman α (Lα) line emission intensity was 2000 R compared with 900 R in the LLA. Thus, while the intensity of molecular band systems, is smaller in the LLA than in the HLA, their atomic line intensities are comparable. We noticed five prominent LLA spectral characteristics: (1) the high-intensity ratio of atomic line emission to molecular emission, (2) the high rotational temperature (T_r) of the VK ($v' = 0$) band system, (3) the high effective vibrational temperature (T_v) of the LBH band system, (4) the presence of O_2 Schuman-Runge (SR) absorption, and (5) the lack of significant enhancement of the Lα line. Discussions of characteristics 1-4 follows:

1. The ratio between the line intensities (O I 1356 Å, N I 1744 Å, and N II 2143 Å) and the LBH (3-10) band intensity for five LLA spectra differs from that of the other 15 diffuse auroral spectra including the 3 HLA from the same orbit (Figure 2). The intensity ratios for the atomic lines to the LBH (3-10) bands increased by the factor of 2 to 3 for the LLA spectra (Table 1).

2. The VK band system originates in the forbidden transition from the $A^3\Pi_u^+$ state. The VK vibrational energy levels are excited by several mechanisms, such as direct electron excitation from the N_2 electronic ground state, radiative cascade involving the $B^3\Pi_g$ and $C^3\Pi_u$ states, and depopulation of the vibrational levels greater than or equal to 8 by the "reverse" N_2 1 P transition [*Degen*, 1982]. Since the VK emission analyzed here is coming predominantly from the zeroth vibrational level, which is populated by cascade, the T_v is irrelevant for this emission. The rotational energy levels appear to be collisionally well thermalized to the local temperature [*Degen*, 1982]. In a previous paper using the S3-4 data [*Ishimoto et al.*, 1988] the T_r for the diffuse auroral region emissions (i.e., HLA) was about 400 K.

The effective T_r for the HLA and LLA spectra were obtained by using the average of the three HLA spectra and of the five LLA spectra from the same orbit in comparison to synthetic VK spectra. The differences between the observed and synthetic spectra are represented by solid lines in Figure 3. The observed spectra shown in Figure 3 have had the airglow, mainly the O_2 Herzberg

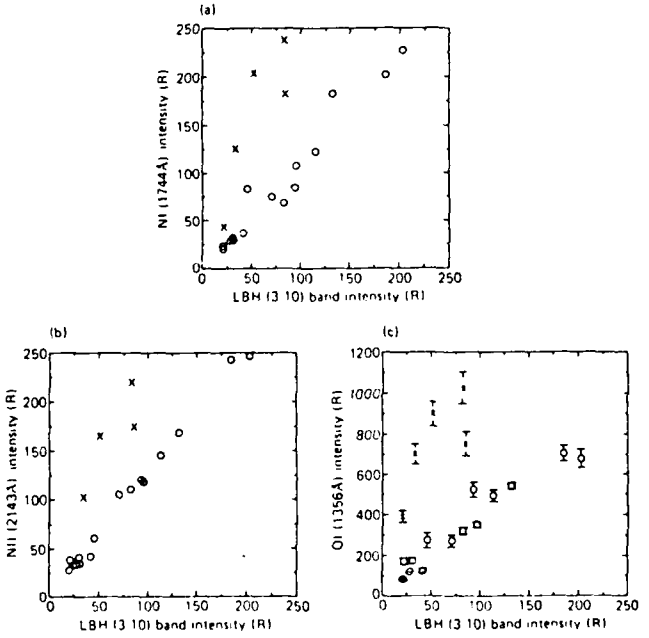

Fig. 2. Correlation between the N I 1744-Å, N II 2143-Å, and O I 1356-Å line intensities and the LBH (3-10) band intensity for the 15 diffuse auroral spectra (circles) and the 5 lower-latitude auroral spectra (crosses): (*a*) the N I 1744-Å line versus the LBH (3-10) band; (*b*) The N II 2143-Å line versus the LBH (3-10) band; and (*c*) The O I 1356-Å line versus the LBH (3-10) band. (Error bars represent the upper and lower values of the O I 1356-Å intensity. These were determined from the subtraction of the LBH bands with two extreme (high and low) altitude distributions for O_2 Schumann-Runge absorption.) Note the difference between the 5 lower-latitude auroral and the 15 diffuse auroral emission intensities in all three graphs.

TABLE 1. Average Values of the Intensity Ratios in LLA and 15 Diffuse Auroral Spectra

	LLA, Average	Diffuse Aurora, Average
[N I 1744 Å]/[LBH (3-10)]	2.90	1.12
[N II 2143 Å]/[LBH (3-10)]	2.53	1.29
[O I 1356 Å]/[LBH (3-10]	14.72	4.19

I band system, subtracted. The intensity of the HLA spectrum was normalized to the same intensity as the LLA at 2600 Å. In this comparison the three peaks of the VK band ($v' = 0$) at 2462, 2604, and 2762 Å show broader widths in the LLA spectrum. The peak at 2462 Å has a small contribution from the Herman-Kaplan band [*Beiting and Feldman*, 1979] and possibly the O II 2470-Å line [*Gerard and Barth*, 1976]. In Figure 3*b*, the comparison of the LLA spectrum and a synthetic spectrum [*Degen*, 1986] with a T_r of 400 K shows the broader peaks in the LLA spectrum. In Figure 3*c*, the comparison between two synthetic VK spectra with T_r of 1000 and 400 K gives a similar difference, *i.e.*, broader peaks in the 1000 K spectrum. The difference spectra in Figures 3*a*–3*c* show similar patterns at wavelengths longer than 2300 Å. A comparison (Figure 3*d*) of the LLA spectrum with a synthetic spectrum for a T_r of 1000 K shows a good match between the two peaks at 2604 and 2762 Å, indicating that the LLA can be well represented by a T_r of 1000 K.

The neutral temperatures at 120, 165, 200 km, and in the exosphere are 450, 1000, 1250, and 1650 K, respectively, according to the MSIS 86 model atmosphere with atmospheric conditions for this particular oval crossing ($F10.7 = 143$, $Ap = 82$, LT = 0000). Since the T_r of the VK band corresponds to the local N_2 temperature [*Degen, 1982*], the observed VK emission with a T_r of 1000 K would correspond to a model altitude of 165 km if the entire emission originated from a single altitude. A typical altitude for the peak in the auroral VK emission is 120 ± 5 km depending on atmospheric O density (D. J. Strickland, private communication, 1988). The inferred altitude of 165 km is much higher than the altitude for typical auroral VK emission.

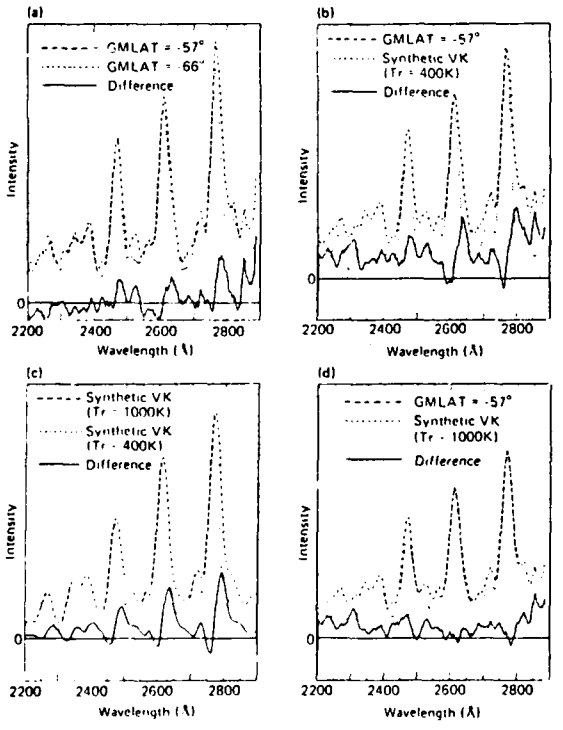

Fig. 3. Comparison of the observed and synthetic spectra of the VK band system and their differences (solid line). (*a*) The observed LLA and HLA observed spectra. The LLA spectrum shows broader widths of the VK band ($v' = 0$) at 2462, 2604, and 2762 Å. The solid line represents the remainder after subtracting the HLA spectrum from the LLA spectrum. (*b*) The LLA spectrum and a synthetic spectrum with T_r of 400 K. (*c*) Two synthetic VK spectra with T_r of 1000 and 400 K, respectively. (*d*) The LLA spectrum and a synthetic spectrum with T_r of 1000 K.

3 and 4. The LBH band system, located between 1250 and 2400 Å, represents a transition from the $a^1\Pi_g^+$ state to the ground state. The collisional quenching of this emission takes place below 95 km, which is lower than most auroral emission altitudes. A synthetic spectrum at 30-Å resolution [*Degen*, 1986] shows little dependence on T_r, even up to 3000 K; here we used 400 K for T_r.

The LBH band emission between 1300 and 1620 Å is subject to significant absorption by O_2 (SR absorption) for auroral emission below 130 km. Figure 4*a* shows the comparison of the LBH bands between the HLA and LLA spectra with airglow (mainly the NO δ band) subtracted, although its intensity is insignificant. Both spectra show O_2 SR absorption. The peak at 1750 Å consists of the LBH bands and the N I 1744 Å line. The peaks at 1600, 1680, 1840, 1930, and 2020 Å are mostly pure LBH bands. In this figure, the peak of the HLA spectrum (dashed line) at 1930 Å is normalized to that of the LLA spectrum (solid line). Enhancement of LLA at 1840 and 1680 Å is very obvious. The 1680-Å peak is affected by O_2 SR absorption, but only about 10% even if the emission came from 105 km altitude. Figure 4*b* shows the contrast of the synthetic LBH spectra [*Degen*, 1986] between the T_v of 3000 K (solid line) and 400 K (dashed line) without taking into account the O_2 SR absorption. A comparison of the spectra in the region of small O_2 SR absorption in Figures 4*a* and 4*b* indicates a high T_v for the spectrum from the LLA. The synthetic LBH spectra with a high T_v and O_2 SR absorption is demonstrated in Figure 4*c*, which will be described in detail in the next section.

The characteristics of the lower-latitude aurora from -53° to -60° GMLAT in the midnight sector during a large magnetic disturbance can be summarized as follows:

1. The LBH (3-10) band emission was less intense than that from the poleward part of the diffuse aurora during the same orbit.
2. The Lα line emission intensity, indicative of proton precipitation, was less intense than that from the poleward part of the diffuse oval.
3. The intensity ratios of the nitrogen atomic lines (N I 1744 Å and N II 2143 Å) to the LBH (3-10) band emission were enhanced by a factor of 2 to 3 over those from the typical diffuse auroral region.
4. The intensity ratio of the O I (1356 Å) line to the LBH (3-10) band emission was enhanced by a factor of 3 to 4 over spectra from the typical diffuse auroral region.
5. The inferred T_r of the VK ($v' = 0$) band was 1000 K, in contrast to 400 K for the poleward part of the diffuse auroral oval.
6. The inferred T_v of the LBH system was 3000 K, in contrast to 400 K for the poleward part of the same oval.
7. The LBH bands in the 1300-1620 Å region show the effect of O_2 SR absorption.

DISCUSSION

Typical diffuse auroral emissions are caused predominantly by electron precipitation with energy spectra characterized by a Max-

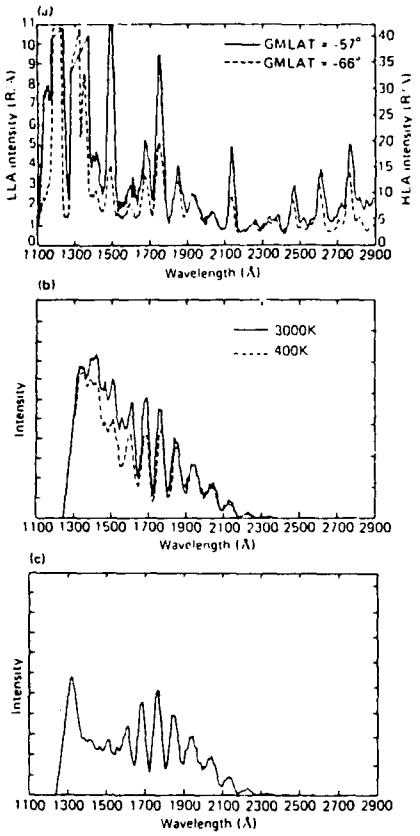

Fig. 4. Comparison of the observed and synthetic spectra of the LBH band system. (*a*) The LBH bands of the HLA and LLA spectra. The LLA spectrum has airglow emissions, mainly the NO δ band, subtracted. Both spectra show the effects of O_2 SR absorption in the 1300- to 1700-Å region. (*b*) The contrast between the synthetic LBH spectra for T_r of 3000 K (solid line) and T_r of 400 K (dashed line), without taking into account the O_2 SR absorption. (*c*) The synthetic spectra for a composite T_v of 400 K and 5000 K. The composite LBH spectrum is a blend of 80% of 400 K and 20% of 5000 K. The spectrum for a T_v of 400 K was modified by O_2 SR absorption as if it originated at 108 km. No SR absorption is applied to the 5000 K spectrum.

wellian distribution of an average energy of 3 keV [*Hardy et al.*, 1985]. The peak emission height is about 110–120 km for the LBH and VK emissions, respectively [*Strickland et al.*, 1983; *Daniell and Strickland*, 1986]. The LBH emissions from this altitude are subject to O_2 SR absorption. The contribution of proton precipitation to the entire auroral emission including the emission from electron precipitation is usually quite small in the midnight sector. Although the entire auroral Lα line emission above the geocorona is caused by proton precipitation, less than 10% of the other emissions in the UV region are produced by proton precipitation [*Strickland et al.*, 1983].

The LLA spectra indicated that the T_r of the VK is about 1000 K, which corresponds to an altitude of 165 km based on the MSIS 86 model atmosphere with proper conditions adjusted for the true observation condition [*Hedin*, 1987]. Thus some of the VK emission must come from far above the typical diffuse auroral emission altitude of 120 km. Conversely, the LBH band spectra showed the effect of O_2 SR absorption (Figure 1*b*). Depending on the O density, the altitude of the LBH emission peak can vary by a few kilometers around 115 km for an average 2-keV electron precipitation. The O_2 density also varies by a factor of 3 due to different geophysical conditions, which can change the upper limit altitude of substantial O_2 SR absorption by 10 km around 125 km. Therefore the presence of O_2 SR absorption in the LBH spectra of LLA indicates that a large portion of the LBH emission came from below 135 km. The large difference between the emission altitudes inferred from LBH and VK spectra can be explained if the LLA spectra were the composite of two parts: low-altitude emission (about 110 km, designated as low-altitude emission) and high-altitude emission (about 200 km, designated as high-altitude emission). Figure 4*c* is a composite of the synthetic spectra for T_v = 400 K and 5000 K. The spectrum for T_v = 400 K is modified by SR O_2 absorption as if it had originated at 108 km. No SR O_2 absorption is applied to the 5000 K spectrum. The composite LBH spectrum is a blend of 80% of the synthetic LBH spectrum at 400 K and 20% at 5000 K. This spectrum closely resembles the observed LBH bands in the LLA spectrum in Figure 4*a* between 1600 and 2000 Å. If we assume that the low-altitude spectra have the same characteristics as the typical keV electron diffuse region spectra, then the LLA has spectral characteristics given in Table 2.

The most probable incident particles that produce the high-altitude spectra can be found by reviewing expected atmospheric spectral characteristics from model calculations and laboratory cross-section measurements. In this regard, the estimation of soft electron spectra is fairly reliable because there are many correlative observations, laboratory measurements, and model calculations. However, the estimation of heavy particle spectra should be considered as only approximate because there are far fewer studies and correlative observations.

UV spectra caused by low-energy electrons were investigated by using the updated Strickland model (D. J. Strickland, private communication, 1987). The basic model was explained in *Strickland et al.* [1983] and *Daniell and Strickland* [1986]. The model with the MSIS 86 model atmosphere used here has included updated cross sections for the O I (1356-Å) and N I (1744-Å) lines and the LBH band system. Values are deduced from this calculation for incident electrons of 200 eV characteristic energy with a Maxwellian distribution. According to these calculations, the emission altitude distribution resulting from low-energy electron precipitation peaks near 175 km.

The intensity ratio of the N I (1744-Å) line emission, including the emission from atmospheric N, to the LBH (3–10) band emission due to 200-eV electrons would be about 2 from model calculations. This is far less than the 11 deduced for the high-altitude emission. The intensity ratio of the O I (1356 Å)/LBH (3–10) resulting from 200-eV electrons precipitation from model calculations is 15 to 20, which is also too low to account for the estimated ratio of 55 for the high-altitude emission.

A significant departure of the relative vibrational population of the LBH from the Frank-Condon distribution has been reported for low-energy (less than 20 eV) electron impact on N_2 in labo-

TABLE 2. Spectral Characteristics of High- and Low-Altitude Spectra for the Lower-Latitude Aurora (LLA)

	Low	High
[N I (1744 Å)]/[LBH (3-10)]	1.12	11.0
[N II (2143 Å)]/[LBH (3-10)]	1.29	7.5
[O I (1356 Å)]/[LBH (3-10)]	4.19	55.0
T_r of VK band system	400 K	2000 K
(estimated altitude)	(120 km)	(200 km)
T_v of LBH band system	400 K	5000 K

ratory experiments [*Ajello and Shemansky*, 1985]. The vibronic enhancement by such low-energy primary electrons requires an unrealistic population increase of the secondary electrons below 20 eV. Thus low-energy electrons are unlikely to cause the high-altitude emission.

Most model calculations of the emission produced by heavy particles have been done for the proton aurora in the visible spectral region. A major problem with extending model calculations is the scarcity of laboratory measurements of the emission cross sections. A few proton auroral models [*Rees*, 1982; *Van Zyl et al.*, 1984] calculated the N_2^+ 1 N band, the N_2 2 P band, and the Lα line emission intensities with recently measured cross sections. The only proton auroral model that calculated the UV emissions as well as the visible emissions [*Edgar et al.*, 1973] used the cross sections measured by *Dahlberg et al.* [1967] and extrapolated them using Green's formula. The agreement in intensities of the N_2^+ 1 N and the N_2 2 P band emissions calculated by *Edgar et al.* [1973] and *Van Zyl et al.* [1984] implies that Edgar's calculation appears to be accurate enough to estimate the UV emission intensities. Low-energy proton precipitation, causing emissions at high latitudes, produces a large Lα emission [*Van Zyl et al.*, 1984]. Because of small enhancement of L in the observed LLA spectra, low-energy hydrogen precipitation seems unlikely to have caused the high-altitude emission in the LLA.

Almost no emission cross section has been measured for O impact. The only oxygen and helium precipitation models that calculate some emissions (N_2^+ 1 N and N_2 2 P bands) in the visible region applied the semiempirical formula of *Fleischmann et al.* [1972] to the hydrogen impact cross sections on N_2 to deduce cross sections for oxygen and helium impacts [*Ishimoto et al.*, 1986; *Ishimoto and Torr*, 1987]. If the peak altitude of the N_2^+ 1 N band is close to those of the LBH and VK emissions for O^+ precipitation, then the peak altitude is about 180 km for 10-keV O^+ and 3-keV He^+ precipitation. Oxygen precipitation (up to 12 keV) at 800 km has been measured with energy flux up to 0.4 erg cm s^{-1} sr^{-1} by a satellite [*Shelley et al.*, 1972]; however, observations of helium ion or neutral precipitation have been rare [*Johnson et al.*, 1974]. Therefore we eliminated He^+ precipitation as the cause of the high-altitude emission.

The intensity ratio of the N I (1744 Å)/LBH (3-10) for 1-keV incident protons is about 30 according to *Edgar et al.* [1973]. The ratio for similar velocity O^+ or O impact should be within the same order of magnitude, which is not too far from 11, estimated for the high-altitude emission. No quantitative study has been done on the O I (1356-Å) emission caused by heavy particles. From the analysis of the O I (1304-Å and 1356-Å) emissions in the nightglow near the magnetic equator, the excitation cross sections for the $O(^3S)$ and $O(^5S)$ states, which yield emissions at 1304 and 1356 Å, respectively, were inferred to be greater than 10^{-17} cm^2 [*Abreu et al.*, 1986]. The suggested mechanism was the collision of O atoms in their ground states, producing the $O(^3S)$ and the $O(^5S)$ states. The cross section for this mechanism must have a peak for impact energies of the order of tens of electron volts. Since the energetic oxygen efficiently degrades to this energy and also produces many low-energy atmospheric neutrals (mainly O) through momentum transfer [*Ishimoto et al.*, 1986], a large enhancement of the O I (1356-Å) line emission by oxygen precipitation would be expected around 180 km. Thus O^+ precipitation can account for the derived O I (1356 Å)/LBH (3-10) ratio of 55.

A significant departure of the relative vibrational population of the LBH from the Frank-Condon distribution has been reported for low-energy proton (60 to 1000 eV) impact on N_2 in laboratory experiments [*Dhuicq and Sidis*, 1986]. Slow O^+ or O would also cause an anomalous vibrational population of the LBH band system analogous to the vibrational population change of the N_2^+ 1 N band system by H^+ and other heavy ions/neutrals [*Moore and Doering*, 1969; *Birely*, 1974]. If oxygen atoms cause vibronic excitation, their speed will have to be less than 4×10^7 cm s^{-1}, corresponding to an energy of 11 keV. The maximum incident energy of oxygen may even be higher than 11 keV if energy degradation is included. This energy range is consistent with the O^+ precipitation observed by *Shelley et al.* [1972].

CONCLUSIONS

Spectra from the equatorial part of a diffuse auroral region observed during a large storm ($K_p = 7+$) showed anomalous spectral characteristics different from typical diffuse auroral features. The high T_r of the N_2 VK band system and the evidence of the O_2 SR absorption in the LBH band systems can be explained by two emission sources, one from high altitudes (approximately 200 km) and the other from low altitudes (approximately 120 km). We believe that the low-altitude emissions were caused by electron precipitation associated with diffuse auroras. The high-altitude emission can be attributed to keV ion/neutral hydrogen or oxygen precipitation, on the basis of previous cross-section experiments involving electron and proton collisions with N_2 and electron, proton, and oxygen transport model. The lack of a significant enhancement in Lα emission leads to our conclusion that the high-altitude emission was mainly caused by keV ion/neutral oxygen precipitation. This conclusion is supported by in situ particle observation of heavy ions with appropriate energy flux over the low geomagnetic latitudes during large storms [*Shelley et al.*, 1972].

Acknowledgments. We are grateful to D. J. Strickland for many discussions and his calculations of electron aurora model. This research is supported by Directorate of Chemical and Atmospheric Sciences of the Air Force Office of Scientific Research AFOSR 86-0057 to the Johns Hopkins University Applied Physics Laboratory.

The Editor thanks R. P. Rohrbaugh and B. Van Zyl for their assistance in evaluating this paper.

REFERENCES

Abreu, V. J., R. W. Eastes, J. H. Yee, S. C. Solomon, and S. Chakrabarti, Ultraviolet nightglow production near the magnetic equator by neutral particle precipitation, *J. Geophys. Res.*, *91*, 11,365-11,368, 1986.

Ajello, J. M., and D. E. Shemansky, A reexamination of important N_2 cross sections by electron impact with application to the dayglow: The Lyman-Birge-Hopfield band system and N I (119.99 nm), *J. Geophys. Res.*, *90*, 9845-9861, 1985.

Beiting, E. J., and P. D. Feldman, Ultraviolet spectrum of the aurora (2000-2800 Å), *J. Geophys. Res.*, *84*, 1287-1296, 1979.

Birely, J. H., Formation of N_2^+ $B^2\Pi_u^+$ and N_2C^3 Π_u in collisions of H^+ and H with N_2, *Phys. Rev.*, *10*, 550-561, 1974.

Dahlberg, D. A., D. K. Anderson, and I. E. Dayton, Optical emission produced by proton and hydrogen-atom impact on nitrogen, *Phys. Rev.*, *164*, 20-31, 1967.

Daniell, R. E., Jr., and D. J. Strickland, Dependence of auroral middle UV emissions on the incident electron spectrum and neutral atmosphere, *J. Geophys. Res.*, *91*, 321-327, 1986.

Degen, V., Synthetic spectra for auroral studies: The N_2 Vegard-Kaplan band system, *J. Geophys. Res.*, *87*, 10541-10547, 1982.

Degen, V., Dialup facility for generating auroral and airglow synthetic spectra, *Rep., UAG-R(305)*, Geophys. Inst., Fairbanks, Alaska, April 1986.

Dhuicq, D., and V. Sidis, Vibronic excitations of $N_2(a^1\Pi_g)$ and $CO(A^1\Pi)$ in collisions of H^+ with $N_2(X)$ and $CO(X)$ in the 60-1000 eV energy range, *J. Phys. B*, *19*, 199-212, 1986.

Edgar, B. C., W. T. Miles, and A. E. S. Green, Energy deposition of protons in molecular nitrogen and applications to proton auroral phenomena, *J. Geophys. Res.*, *78*, 6595-6606, 1973.

Fleischmann, H. H., R. C. Dahmel, and S. K. Lee, Direct-transition features in stripping collisions of heavy neutral atoms and ions, *Phys. Rev. A, 5*, 1789–1793, 1972.

Gerard, J.-C., and C. A. Barth, OGO-4 observations of the ultraviolet auroral spectrum, *Planet. Space Sci., 24*, 1059–1063, 1976.

Hardy, D. A., M. S. Gussenhoven, and E. Holdman, A statistical model of auroral electron precipitation, *J. Geophys. Res., 90*, 4229–4248, 1985.

Hedin, A. E., MSIS-86 thermospheric model, *J. Geophys. Res., 92*(A5), 4649–4662, 1987.

Huffman, R. E., F. J. LeBlanc, J. C. Larrabee, and D. E. Paulsen, Satellite vacuum ultraviolet airglow and auroral observations, *J. Geophys. Res., 85*, 2201–2215, 1980.

Ishimoto, M., and M. R. Torr, Energetic He^+ precipitation in a mid-latitude aurora, *J. Geophys. Res., 92*, 3284–3292, 1987.

Ishimoto, M., M. R. Torr, P. G. Richards, and D. G. Torr, The role of energetic O^+ precipitation in a mid-latitude aurora, *J. Geophys. Res., 91*, 5793–5802, 1986.

Ishimoto, M., G. J. Romick, R. E. Huffman, and C.-I. Meng, Auroral electron energy and flux from molecular nitrogen ultraviolet emissions observed by the S3-4 satellite, *J. Geophys. Res., 93*, 9854–9866, 1988.

Johnson, R. G., R. D. Sharp, and E. G. Shelley, The discovery of energetic He^+ ions in the magnetosphere, *J. Geophys. Res., 79*, 3135–3139, 1974.

Loomis, E., The great auroral exhibition of August 28 to September 4, 1859, 8, *Am. J. Sci., 2nd Ser., 32*, 318, 1861.

Moore, J. H., and J. P. Doering, Vibrational excitation in ion-molecule collisions: H^+, H_2^+, He^+, N^+, Ne^+, and electrons with N_2, *Phys. Rev., 177*, 218, 1969.

Rees, M. H., On the interaction of auroral protons with the earth's atmosphere, *Planet. Space Sci., 30*, 463–472, 1982.

Shelley, E. G., R. G. Johnson, and R. D. Sharp, Satellite observation of energy heavy ions during a geomagnetic storm, *J. Geophys. Res., 77*, 6104, 1972.

Strickland, D. J., J. R. Jasperse, and J. A. Whalen, Dependence of auroral FUV emissions on the incident electron spectrum and neutral atmosphere, *J. Geophys. Res., 88*, 8051–8062, 1983.

Tinsley, B. A., Energetic neutral atom precipitation during magnetic storms: Optical emission, ionization, and energy deposition at low and middle latitudes, *J. Geophys. Res., 84*, 1855, 1979.

Tinsley, B. A., R. P. Rohrbaugh, Y. Sahai, and N. R. Teixeira, Energetic oxygen precipitation as a source of vibrationally excited N_2^+ 1N emissions observed at low latitudes, *Geophys. Res. Lett., 9*, 543–546, 1982.

Tinsley, B. A., R. Rohrbaugh, H. Rassoul, Y. Sahai, N. R. Teixeira, and D. Slater, Low-latitude aurorae and storm time current systems, *J. Geophys. Res., 91*, 11,257–11,269, 1986.

Van Zyl, B., M. W. Gealy, and H. Newman, Predictions of photon yields for proton aurorae in an N_2 atmosphere, *J. Geophys. Res., 89*, 1701–1710, 1984.

R. E. Huffman, Air Force Geophysics Laboratory, Hanscom Air Force Base, Bedford, MA 01731.

M. Ishimoto and C.-I. Meng, Applied Physics Laboratory, Johns Hopkins University, Johns Hopkins Road, Laurel, MD 20707.

G. R. Roble, Geophysical Institute, University of Alaska, Fairbanks, AK 99701.

(Received April 29, 1988;
revised September 27, 1988;
accepted October 15, 1988.)

APPENDIX E

A SIMPLE MODEL OF O_2 SCHUMANN-RUNGE ABSORPTION FOR AURORAL LBH BAND EMISSIONS

M. Ishimoto[1], G. R. Romick[2], and C.-I. Meng[1]

[1]The Johns Hopkins University

Applied Physics Laboratory

Laurel, Maryland 20707

[2]Atmospheric Science Division

National Science Foundation

1800 G Street NW

Washington, D. C. 20550

Submitted to Journal of Geophysical Research

January 1989

ABSTRACT

The quantitative estimation of O_2 Schumann-Runge (SR) absorption by the atmosphere in satellite observations of the atmospheric emissions between 1350 and 1650 Å is crucial to the analysis of spectra and energetics. The attenuation of any emission in this wavelength range as detected from nadir-viewing space experiments depends on the emission and O_2 density altitude distributions.

We introduce a simplified approach to determine the O_2 SR absorption. The attenuation of the auroral Lyman-Birge-Hopfield (LBH) band emission is analytically formulated with only O_2 SR cross sections and by using any two observed pure LBH wavelength regions from the satellite. Application of this technique to spectral observation from the S3-4 satellite is illustrated by the deconvolution of the LBH band system from a 30 Å resolution spectrum to reveal clearly some atomic line emissions that are indistinguishable in the original spectrum.

INTRODUCTION

The N_2 Lyman-Birge-Hopfield (LBH) band system is the major molecular band system in the auroral UV emission from 1256 to 2400 Å wavelength, blended with eminent atomic line emissions, such as the OI (1304, 1356, and 1641 Å) and the NI (1411, 1493, and 1744 Å). Spectral analysis of this band system and the line intensities can provide vital information in energetics and also in deducing energy spectra of precipitating electrons as well as atmospheric conditions. The deconvolution of observed auroral UV emission spectra with larger than 5 Å resolution is essential in order to determine intensities of individual bands and lines.

When the N_2 $a^1\Pi_g$ state is excited by direct electron impact on N_2 [Meier et al., 1980], two possible atmospheric effects take place before the LBH emissions reach the satellite, namely, the collisional deactivation by N_2 and the emission absorption by O_2. The collisional deactivation of the $a^1\Pi_g$ state takes place below 95 km [Vallance-Jones, 1974], which is lower than most auroral emission altitudes; therefore, it can be ignored for most auroral LBH events. However, the emission absorption by atmospheric O_2 (Schuman-Runge (SR) continuum) is quite large between 1250 and 1750 Å. Its total absorption rate depends on the altitude distribution of the LBH emission as well as the atmospheric depth of the O_2 between the emission altitude and the observation point. Observations of UV spectra taken at 270 km from the nadir-viewing S3-4 satellite (see Ishimoto et al., 1988 for detailed data processing) clearly demonstrate the presence of SR absorption on the LBH band system (Figure 1a) when compared to both a LBH synthetic spectrum (Figure 1b) [Degen, 1986] and the O_2 SR cross section (Figure 1c) [Hudson, 1971].

The LBH emission transmissivity for a given wavelength λ through the atmosphere at a satellite altitude (z_o) is expressed as

$$T(\lambda) = \frac{1}{N(\lambda)} \int_{z_1}^{z_2} P(\lambda,z)\ \exp[-\rho(z)\sigma(\lambda)]\ dz \qquad (1)$$

where $\sigma(\lambda)$ is the O_2 SR cross section per O_2 molecule [Hudson, 1971]. $P(\lambda,z)$ is the LBH volume emission rate at an altitude of z, bounded between z_1 and z_2. $\rho(z)$ is the total column density of O_2 between z and z_o, expressed as

$$\rho(z) = \int_{z}^{z_o} n(z')\ dz' \qquad (2)$$

where n is O_2 density. $N(\lambda)$, the column volume emission rate without any O_2 SR absorption, is defined as

$$N(\lambda) = \int_{z_1}^{z_2} P(\lambda,z')\ dz'. \qquad (3)$$

Relative intensities of the volume emission rate to the intensity of a wavelength, λ_o, $P(\lambda,z)$, and therefore, $N(\lambda)$ can be deduced from a synthetic spectrum of the LBH band systems such as those by Degen [1986]; i.e.,

$$P(\lambda,z) = C(\lambda) \times P(\lambda_o,z),$$

and

$$N(\lambda) = C(\lambda) \times N(\lambda_o)$$

where $C(\lambda)/C(\lambda_o)$ is a constant value from a synthetic spectrum and λ_o is a standard wavelength, for example 1500 Å. Denoting $P(\lambda_o,z)$ and $N(\lambda_o)$ to be P(z) and N, Equation (1) becomes

$$T(\lambda) = \frac{1}{N} \int_{z_1}^{z_2} P(z) \exp(-\rho(z)\sigma(\lambda)) \, dz \ . \qquad (1)'$$

$\rho(z)$ depends on the atmospheric conditions. P(z) depends on the incident electrons as well as on atmospheric conditions.

Our objective is to find a simple analytic formula of $T(\lambda)$ at any λ from observed LBH emission band intensities at several λ for the deconvolution of the auroral spectra by applying the formula to the synthetic spectrum of the LBH band systems. In this study, we first seek an analytic representation of P(z) by using the electron transport model by Strickland et al., [1983] under a particular atmospheric condition. Second, the impact of different atmospheres on $T(\lambda)$ is investigated by using this $P(\lambda)$. Finally, a simple analytic expression for the transmissivity, derivable from the observation of the LBH band system at two different wavelengths, is obtained and tested by using an observed spectrum.

LBH VOLUME EMISSION RATE

The LBH volume emission rates produced by an electron incident flux of 1 erg $cm^{-2}s^{-1}$ for Maxwellian and Gaussian distributions with several characteristic energies [Strickland et al., 1983, Figure 5] are used as a prototype for the LBH volume emission rate in this study (hereafter referred to as the model). Their atmosphere is reproduced with the MSIS-86 model atmosphere by setting F10.7 = 120, AP = 20 (hereafter referred to as the standard atmosphere). Their Figure 5, whose y coordinate is replaced by the O_2 total column density at 270 km is shown in Figure 2a and 2b. To formulate these families of curves, we define the normalized O_2 total column

density ζ as

$$\zeta(z) = \rho(z)/\rho_o \tag{4}$$

where ρ_o is the O_2 total column density above the volume emission peak altitude. ρ_o is expressed as a function of characteristic energy, E_o, in keV of incident electrons as

$$\rho_o = K_1 \, E_o^{\beta} \tag{5}$$

where K_1 is a constant and β is approximately 1.75 or 2.0 for a Maxwellian or Gaussian distribution, respectively, from Strickland calculation for this particular model atmosphere. By setting the data points of the full model calculation LBH volume emission rate to a curve represented by the following equations for the best fit, we obtain

$$P(\zeta) = K_2 \, \zeta^{\alpha} \exp[-\alpha(\zeta-1)]$$

$$\alpha = 0.9 \quad \text{for } \zeta \leq 1 \quad \text{for Maxwellian distribution}$$

$$0.6 \quad \text{for } \zeta > 1$$

$$\alpha = 1.5 \quad \text{for } \zeta \leq 1 \quad \text{for Gaussian distribution}$$

$$2.0 \quad \text{for } \zeta > 1 \tag{6}$$

where K_2 is the peak volumes emission rate, $P(\zeta=1)$.

To see how well this formula fits the model values, the LBH volume emission rate, $P(z)$, and those LBH emissions that would be observed at the 270-km altitude through the O_2 SR absorption between the emission altitude and 270 km, $T(\lambda_o) \times P(z)$, are shown in Figures 3a and 3b as a function of the altitude for a Maxwellian and for a Gaussian distribution, respectively. We selected the maximum O_2 SR cross section, 1.5×10^{-17} cm^2, for the maximum deviation. The agreement of these curves with the model calculation and from Equation (6) is excellent near the emission peak altitudes, and there is some discrepancy at near-boundary regions, high and low altitude, where the

volume emission rate is about one order of magnitude below the peak.

Figures 4a and 4b illustrate the discrepancy of the transmissivity, $T(\lambda)$, at 270 km as a function of the O_2 SR cross section, between the model calculation and Equation (6). The discrepancy increases as the cross section increases. In general, the equation reproduces the transmissivity of the model calculations for various given characteristic energies of incident electrons, with a maximum error of about 20% for a Maxwellian distribution and only a 4% error for a Gaussian distribution for the average energy of the incident electrons up to 10 keV.

ATMOSPHERIC DENSITIES

According to the MSIS-86 model atmosphere [Hedin, 1986], below the typical auroral emission altitude (100-140 km) where N_2 is the predominant constituent, the N_2 density is insensitive to significant change in the various geophysical conditions. Therefore, the LBH emission altitude distribution for a given incident keV electron energy spectrum is expected to be fairly constant regardless of the particular model atmosphere used for the calculation of the emission rate. On the other hand, the O_2 density and thus the O_2 total column density between a given altitude and an observing satellite at 270 km can differ considerably under varying geophysical conditions as shown in Figure 5. (The standard atmosphere is represented by a solid line.) Thus, the geophysical conditions have a great impact on the transmissivity between a given altitude and the observing platform. The variations of transmissivity for 1-keV Maxwellian and 2-keV Gaussian distributed auroral electrons are calculated as a function of the O_2 SR cross section as shown in Figures 6a and 6b. The difference due to the geophysical

conditions is much greater than that between the model calculation and the Equation (6).

TRANSMISSIVITY

In this section, we will assume that the primary factor for the change of transmissivity for a given particle energy distribution is the atmospheric O_2 density variation. We will focus on the function $P(\zeta)$ to compensate for the O_2 density variations and will attempt to seek a simple analytical expression that can be applied to the actual LBH emission intensity observed from a satellite.

The transmissivity [Equation (1)]can be expressed in terms of ζ by using Equations of (2), (3) and (4):

$$T(\lambda) = \frac{-1}{N} \int_{\zeta_1}^{\zeta_2} \rho_o \, P(\zeta) \exp[-\Sigma(\lambda) \, \zeta] \, \frac{d\zeta}{n(\zeta)} \qquad (1')$$

where

$$\Sigma(\lambda) = \rho_o \, \sigma(\lambda) \qquad (7)$$

is the O_2 optical depth between the volume emission peak and the satellite altitude.

To make the integration algebraically simple and yet retain $P(\zeta)$ close to Equation(6), the volume emission rate is projected in a pseudo atmosphere in which the O_2 density obeys a constant scale height law:

$$n(z) = n_o \exp(-z/H).$$

Then the total column density simply becomes

$$\rho(z) = H \, n(z)$$

where H is an arbitrary constant. Therefore,

$n(z) = (\rho_o/H)\ \zeta(z)$ from Equation (4).

Modifying $P(\zeta)$ of Equation (6) to

$$P(\zeta) = \zeta \exp(-\alpha\zeta) \tag{8}$$

and taking a low enough altitude boundary $\zeta_1 > 100$ and a high enough altitude boundary $\zeta_2 < 0.001$ to include the entire emission altitudes to be integrated, the normalization factor, defined in Equation (3), becomes:

$$N = H/\alpha.$$

The transmissivity in Equation (1) is simplified to

$$T(\lambda) = \alpha \int_{\zeta_2}^{\zeta_1} \exp(-\alpha\zeta)\ \exp(-\Sigma(\lambda)\ \zeta)\ d\zeta. \tag{1"}$$

Integration of Equation (1") results in the transmissivity,

$$T(\lambda) = \frac{\alpha}{\alpha + \Sigma} = \frac{\alpha}{\alpha + \rho_o\sigma(\lambda)} \quad . \tag{9}$$

Equation (9) does not depend on the O_2 scale height, H, explicitly. The O_2 density is a variable of α and ρ_o. α reflects the altitude distribution of the volume emission rate with respect to the O_2 column density, therefore it is implicitly related to H. ρ_o is the O_2 column density above the peak column emission and can be determined by an observable $T(\lambda)$ as

$$\rho_o = \frac{\alpha}{\sigma(\lambda)} \left[\frac{1.}{T(\lambda)} - 1. \right]. \tag{10}$$

Figure 7a compares different calculations of the transmissivity in the standard atmosphere as a function of the optical depth Σ. (Note that higher Σ values correspond to lower altitudes in the O_2 atmosphere.) The O_2 SR cross section used is its maximum value of $1.5 \times 10^{-17} cm^2$ for the purpose of showing the maximum deviation in the different calculations. The solid line in Figure 7a represents the transmissivity expressed by Equation (9) with

α = 1.3 for the best fit to the values from the model calculation. Two simbols (□, o) represent calculated points from the model calculation for the various electron characteristic energies with Maxwellian and Gaussian distributions, respectively. The solid line [Equation (9)] shows an excellent fit to these values. The dotted and broken lines represent the transmissivity obtained from Equation (6) for the incident electrons with the Maxwellian and Gaussian distributions, respectively. The dot-dash line represents the transmissivity if all of the LBH emission comes from the altitude of the peak volume emission from the model calculation. This approximation drastically underestimates the transmissivity at the lager optical depth.

The effect on the transmissivity due to O_2 density change under various geophysical conditions was already demonstrated in Figure 6a and b. Figure 7b demonstrates the transmissivity variations from the model calculations with three atmospheres under the three different geophysical conditions shown in Figure 5. The quiet, moderate, and disturbed levels are coded as L, S, and H, respectively. The solid curve represents the transmissivity from Equation (9) with α = 1.3. Using an O_2 SR cross section of $10^{-17}cm^2$, the solid line shows that the model values agree very well with those obtained from the standard atmosphere, even with a different O_2 SR cross section from the case of Figure 7a. The change of the transmissivity due to different atmospheres is large, particularly for low transmissivities. However, the change has a tendency to slide the values along the solid curve. Figure 7b also shows the variation of Equation (9) with different values of α (dotted lines). The transmissivity under different O_2 densities in the model calculation was bounded by the two dotted lines with α = 0.95 and 1.55.

APPLICATION FOR OBSERVED LBH EMISSION INTENSITIES

In this section, a simple formula for the transmissivity used to modify the LBH synthetic spectra to represent the observed spectra will be derived from Equation (9). This Equation does not include either α or ρ_o. Suppose that I_1 and I_2 are two pure LBH emission intensities at the wavelength of λ_1 and λ_2 measured from a satellite, and that ι_1 and ι_2 are the corresponding intensities where the ratio, e.g., ι_1/ι_2, is known from a synthetic spectrum without SR absorption. Then the transmissivity ratio can be expressed by an observable as

$$\kappa = \frac{T(\lambda_1)}{T(\lambda_2)} = \frac{I_1}{I_2}\,\frac{\iota_2}{\iota_1} \quad . \tag{11}$$

Using Equation (9), the corresponding O_2 total column density above the emission peak is expressed as

$$\rho_o = \frac{\alpha\,(1.-\kappa)}{\kappa\,\sigma(\lambda_1) - \sigma(\lambda_2)} \quad . \tag{12}$$

Substituting (12) into (9), the transmissivity becomes

$$T(\lambda) = \frac{\kappa\sigma(\lambda_1) - \sigma(\lambda_2)}{\sigma(\lambda)(1-\kappa) + \kappa\sigma(\lambda_1) - \sigma(\lambda_2)}, \tag{13}$$

which is independent of α and ρ_o. This simple Equation has two positive characteristics for the estimation of the O_2 SR absorption for satellite-measured LBH emission intensities:

1. The transmissivity is obtained simply from two observables, e.g., LBH emission intensities simultaneously measured at any two wavelengths.

2. The calculation requires no a priori knowledge of the O_2 density altitude distribution and geophysical conditions.

To test this technique on observed spectra, we used an auroral

spectrum taken at 270 km (Figure 1, thick line in Figure 8). The two wavelength regions (1928 Å and 1600 Å) for pure LBH emissions are chosen for I_1 and I_2. The synthetic spectra of the LBH band systems by Degen [1986](thin line) are used to get ι_1 and ι_2. Substituting these values into Equation (13) yields the transmissivity of the LBH band emissions for all wavelengths. The $T(\lambda)$ is applied to the synthetic spectrum (dotted line in Figure 8) to reproduce the synthetic observed spectra (dashed line in Figure 8). The subtraction of this synthetic spectrum from the observed spectrum reveals the atomic line emissions, as should be expected (crosshatched region in Figure 8). This procedure positively demonstrates the usefulness of the simplified estimation of O_2 SR absorption based on the transmissivity Equation (13) from any two LBH observable emissions.

CONCLUSIONS

The transmissivity of the auroral LBH emissions through the SR absorption region can be obtained analytically from any two pure LBH emission wavelengths observed from a satellite, regardless of geophysical and atmospheric conditions. The LBH synthetic spectrum using this transmissivity provides a simple way to separate atomic lines from the observed emissions. In addition, given this transmissivity and the characteristic energy of incident electrons, it allows the determination of the O_2 atmospheric column density and its variability under differing geophysical conditions.

Figure Captions

Figure 1

(a). Diffuse auroral region spectrum (30 Å resolution) taken from nadir-viewing S3-4 satellite at 270 km [Ishimoto et al., 1988].

(b). LBH synthetic spectra without SR absorption (Tr = Tv = 400 K, 30 Å resolution)[Degen, 1986].

(c). O_2 Schumann-Runge absorption cross section [Hudson, 1971].

Figure 2

(a). LBH volume emission rate calculated by an electron transport model for the incident electrons with a Maxwellian distribution for the characteristic energies of 0.5, 1.0, 2.5, and 5.0 keV [Strickland et al., 1983, Figure 5) as a function of O_2 total column density.

(b). LBH volume emission rate calculated by an electron transport model for the incident electrons with a Gaussian distribution for the characteristic energies of 1., 2.0, 3.3, 5.0, 7.5, and 10 keV [Strickland et al., 1983, Figure 5] as a function of O_2 total column density.

Figure 3

(a) The LBH volume emission rate and its observable emission at 270 km through the O_2 SR absorption (σ = 1.5 x 10^{-17} cm^2) from both the model calculation and Equation (6) for a Maxwellian distribution for two different energies.

(b) The LBH volume emission rate and its observable emission at 270 km through the O_2 SR absorption (σ = 1.5 x 10^{-17} cm^2) from both the model calculation and Equation (6) for a Gaussian distribution for two different energies.

Figure 4

(a) Transmissivity of the LBH volume emission rate at 270 km for a Maxwellian distribution of Strickland et al., [1983] (solid line) and for Equation (6) (broken line) for a given characteristic energy of the incident electrons as a function of O_2 SR cross section. Both calculations assumed the standard atmosphere (two lines for 1 keV overlap).

(b). The same as Figure 4a except for a Gaussian distribution (five pairs of lines for 1, 2, 3.3, 5, and 10 keV overlap).

Figure 5

Variation of the O_2 total column density between a given altitude (ordinate) and the observing platform (270 km) due to different geophysical conditions.

Figure 6

(a). Transmissivity as a function of SR cross section calculated from the LBH emission rate for a 1 keV Maxwellian distribution for different atmospheres (see Figure 5).

(b). Transmissivity as a function of SR cross section calculated from the LBH emission rate for a 2 keV Gaussian distribution for different atmospheres.

Figure 7a

Transmissivity as a function of the O_2 optical depth above the emission peak, Σ. □ represents the values from the model calculation for a Maxwellian distribution in the case of the SR cross section, $1.5 \times 10^{-17} cm^2$. o represents those for a Gaussian distribution. The dotted line represents Equation (6) for 1 keV incident electrons with a Maxwellian distribution, and the broken line for a 2 keV Gaussian distribution. The solid line represents

Equation (9) with α = 1.3. The dot-dash line represents the case for all emissions coming from a single altitude.

Figure 7b

The transmissivity variations as a function of the O_2 optical depth above the emission peak, Σ. The values from the model calculations with three atmospheres. The quiet, moderate and disturbed are coded as L, S, and H, respectively. The plot of equation (9) with values for α of 1.3 (solid line), 0.95 and 1.55 (dotted lines) is also shown for comparison. The O_2 SR cross section is set to $10^{-17}cm^2$.

Figure 8

Application of the simplified SR absorption calculation on the LBH band system. A diffuse region auroral spectrum (solid line) is compared to the synthetic LBH spectrum (dotted line) normalized at 1928 Å. The synthetic LBH band system spectrum is modified by applying Equation (13) with α = 1.3 and $\rho_o = 2.2 \times 10^{17}cm^{-3}$ (broken line). The remainder spectrum (shaded area) results from the subtraction of the modified LBH from the observed spectrum and reveals the atomic lines.

REFERENCES

Degen, V., Dialup facility for generating auroral and airglow synthetics spectra, UAG-R(305), Geophysical Institute Report, 1986.

Hedin, A. E., MSIS-86 thermospheric model, J. Geophys. Res., 92, A5, 4649-4662, 1986.

Hudson, R. D., Critical review of ultraviolet photoabsorption cross section for molecules of astrophysical and aeronomic interest, Rev. Geophys. Space Phys., 9, 2, 305-406, 1971.

Ishimoto, M., G. J. Romick, R. H. Huffman, and C.-I. Meng, Auroral electron energy and flux from molecular nitrogen ultraviolet emissions observed by the S3-4 satellite, J. Geophys. Res., 93, A9, 9854-9866, 1988.

Meier, R. R., D. J. Strickland, P. F. Feldman, and E. P. Gentieu, The ultraviolet dayglow 1. Far UV emission of N and N_2, J. Geophys. Res., 85, A5, 2177-2184, 1980.

Strickland D. J., J. R. Jasperse, and J. A. Whalen, Dependence of auroral FUV emissions on the incident electron spectrum and neutral atmosphere. J. Geophys. Res., 88, A10, 8051-8062, 1983.

Vallance-Jones, A., Aurora, D. Reidel, Hingham, Mass, 1974.

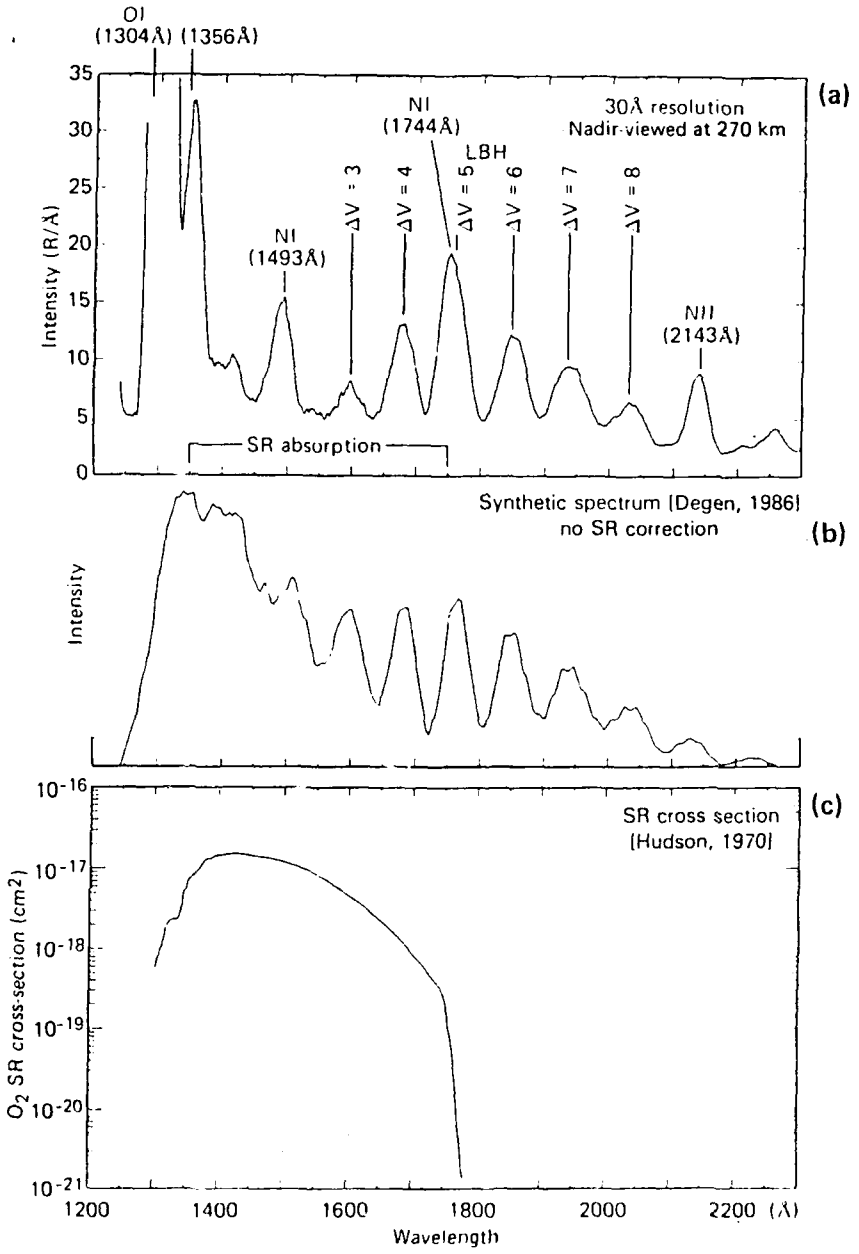
OI
(1304Å) (1356Å)
NI
(1493Å)
ΔV = 3
ΔV = 4
NI
(1744Å)
LBH
ΔV = 5
ΔV = 6
ΔV = 7
ΔV = 8
NII
(2143Å)
30Å resolution
Nadir-viewed at 270 km
(a)
Intensity (R/Å)
SR absorption
Synthetic spectrum (Degen, 1986)
no SR correction
(b)
Intensity
SR cross section
(Hudson, 1970)
(c)
O_2 SR cross-section (cm^2)
Wavelength
(Å)

Fig. 1

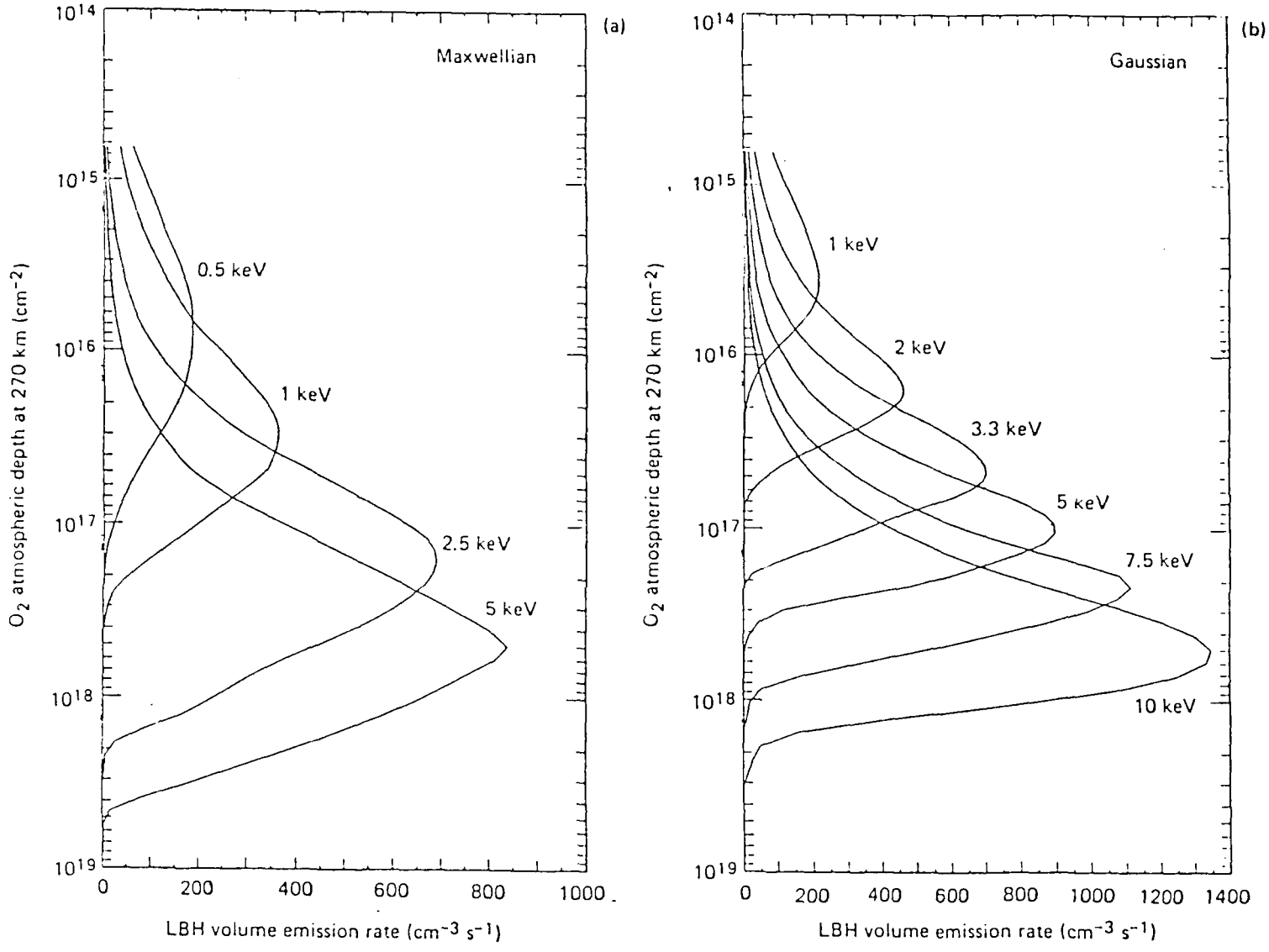
(a)
Maxwellian
0.5 keV
1 keV
2.5 keV
5 keV
10^{14}
10^{15}
10^{16}
10^{17}
10^{18}
10^{19}
O_2 atmospheric depth at 270 km (cm^{-2})
0
200
400
600
800
1000
LBH volume emission rate (cm^{-3} s^{-1})
(b)
Gaussian
1 keV
2 keV
3.3 keV
5 keV
7.5 keV
10 keV
10^{14}
10^{15}
10^{16}
10^{17}
10^{18}
10^{19}
O_2 atmospheric depth at 270 km (cm^{-2})
0
200
400
600
800
1000
1200
1400
LBH volume emission rate (cm^{-3} s^{-1})

Fig. 2

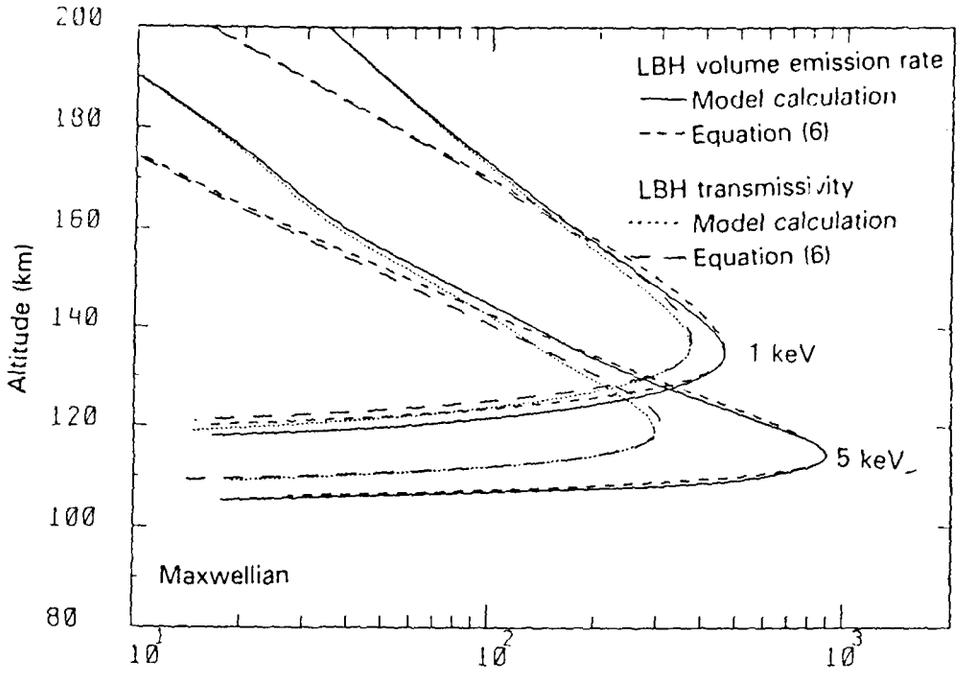
200
180
160
140
120
100
80
Altitude (km)
LBH volume emission rate
Model calculation
Equation (6)
LBH transmissivity
Model calculation
Equation (6)
1 keV
5 keV
Maxwellian
10^1
10^2
10^3
LBH volume emission rate (cm^-3 s^-1)
and observable emission (cm^-3 s^-1)

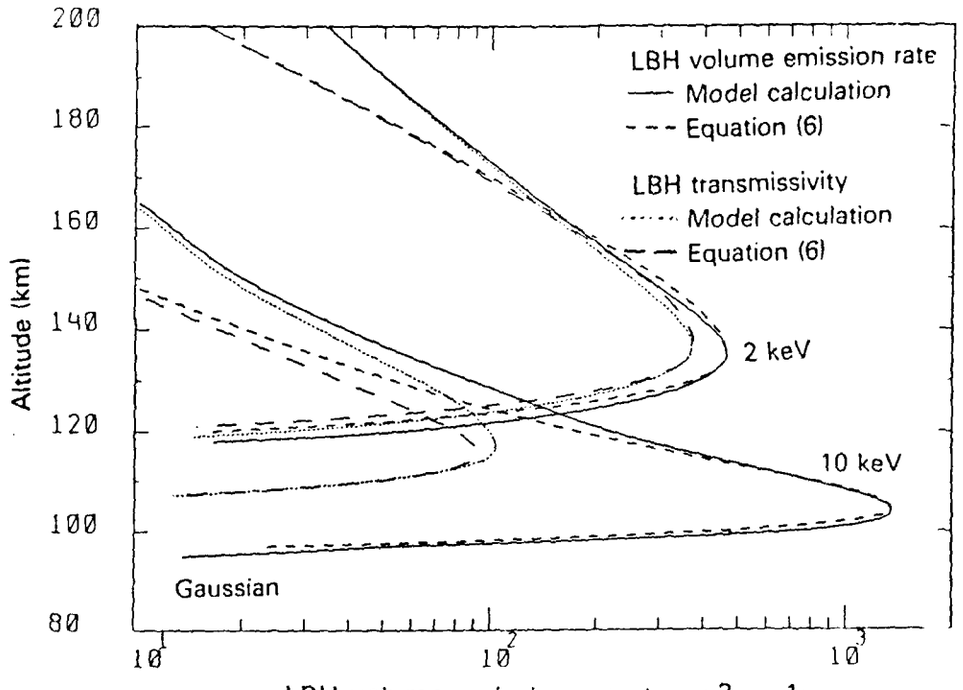
200
180
160
140
120
100
80
Altitude (km)
LBH volume emission rate
Model calculation
Equation (6)
LBH transmissivity
Model calculation
Equation (6)
2 keV
10 keV
Gaussian
10^1
10^2
10^3
LBH volume emission rate (cm^-3 s^-1)
and observable emission (cm^-3 s^-1)

Fig. 3

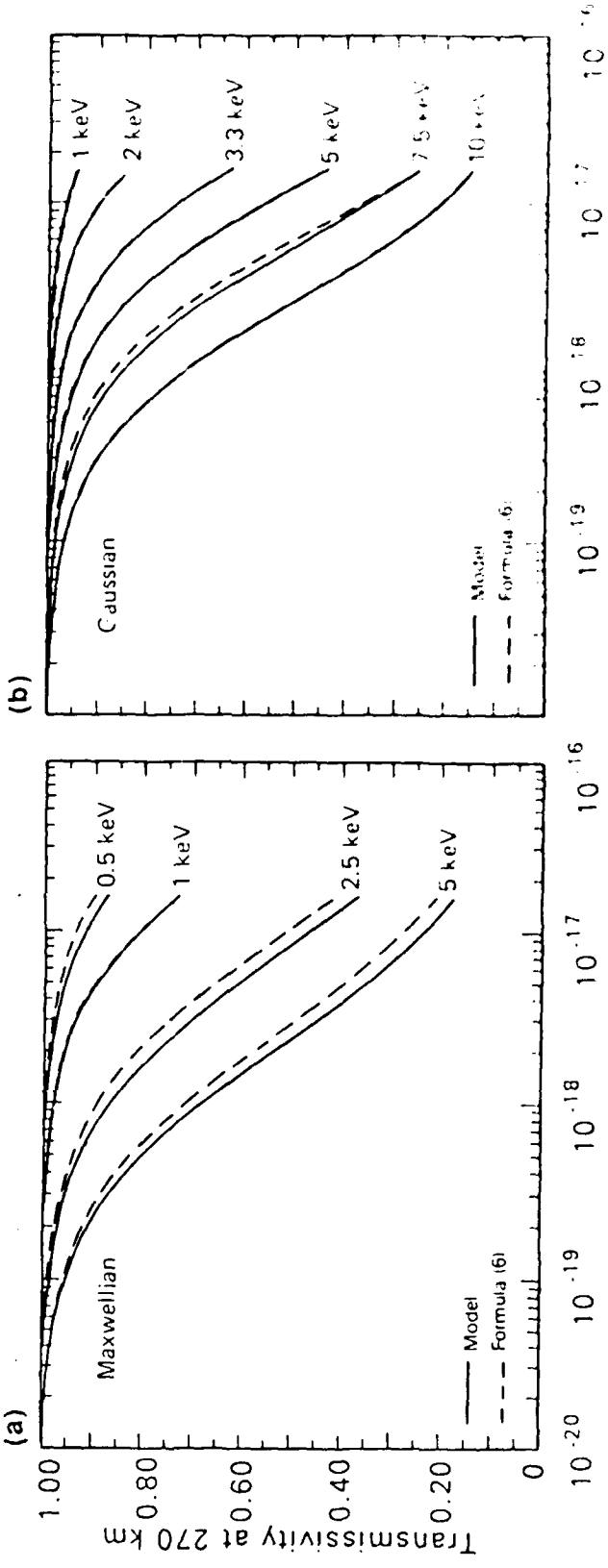
(a)
Maxwellian
0.5 keV
1 keV
2.5 keV
5 keV
Model
Formula (6)
(b)
Gaussian
1 keV
2 keV
3.3 keV
5 keV
Transmissivity at 270 km
1.00
0.80
0.60
0.40
0.20
0
SR cross section (cm²)

Fig. 4

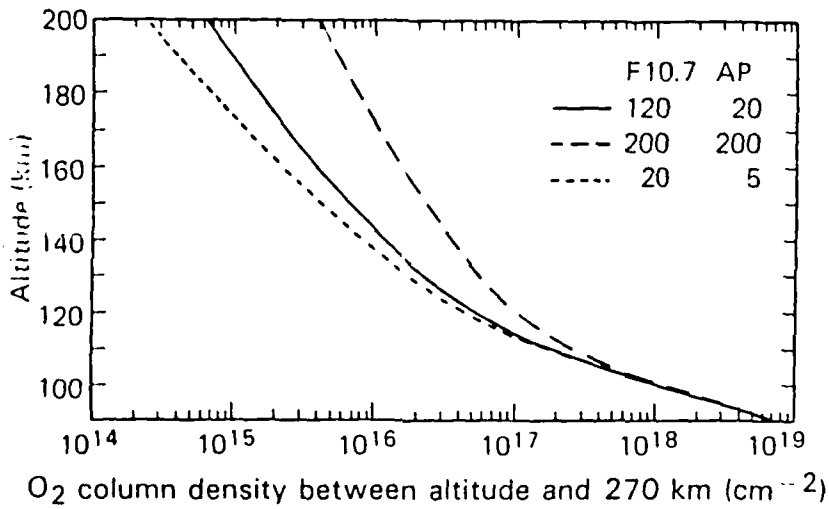
200
180
160
140
120
100
Altitude (km)
F10.7 AP
120 20
200 200
20 5
10^{14}
10^{15}
10^{16}
10^{17}
10^{18}
10^{19}
O_2 column density between altitude and 270 km (cm^{-2})

Fig. 5

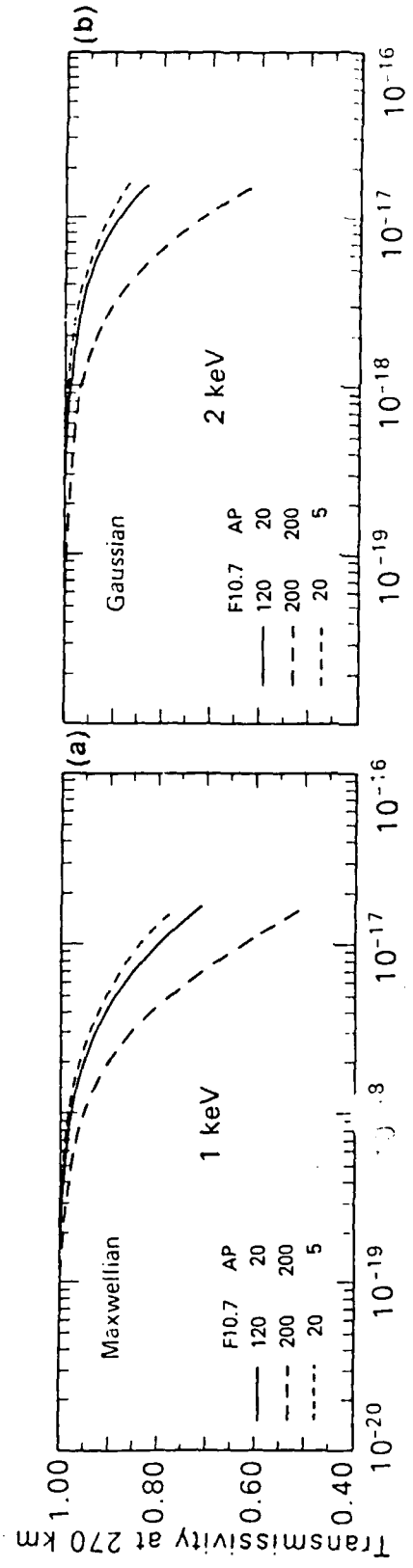
Transmissivity at 270 km
1.00
0.80
0.60
0.40
(a)
Maxwellian
1 keV
F10.7 AP
120 20
200 200
20 5
(b)
Gaussian
2 keV
F10.7 AP
120 20
200 200
20 5
10^{-20}
10^{-19}
10^{-18}
10^{-17}
10^{-16}
SR cross section (cm^2)

Fig. 6

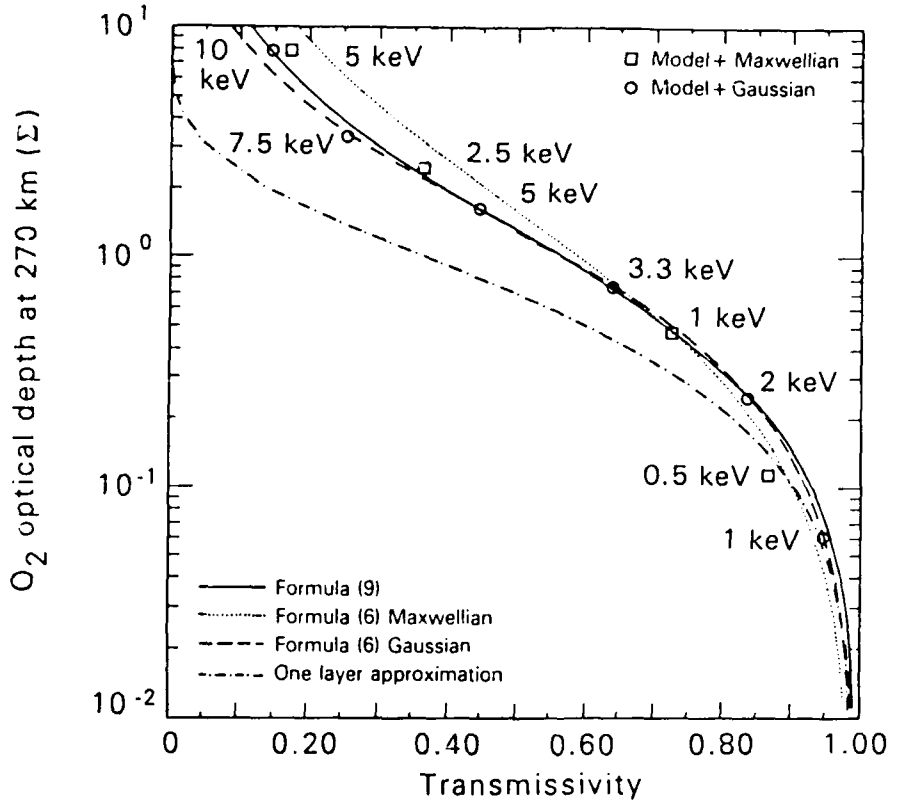
10^1
10^0
10^{-1}
10^{-2}
O_2 optical depth at 270 km (Σ)
10 keV
5 keV
7.5 keV
2.5 keV
5 keV
3.3 keV
1 keV
2 keV
0.5 keV
1 keV
Model + Maxwellian
Model + Gaussian
Formula (9)
Formula (6) Maxwellian
Formula (6) Gaussian
One layer approximation
0
0.20
0.40
0.60
0.80
1.00
Transmissivity

Fig. 7(a)

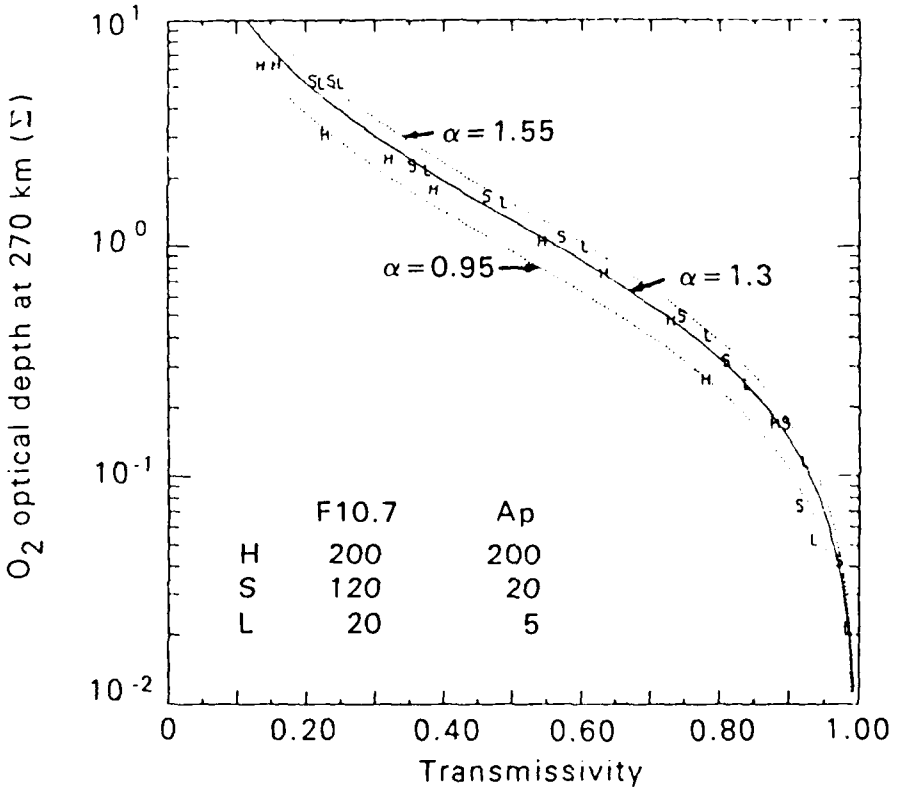
10^1
10^0
10^{-1}
10^{-2}
O_2 optical depth at 270 km (Σ)
$\alpha = 1.55$
$\alpha = 0.95$
$\alpha = 1.3$
F10.7 Ap
H 200 200
S 120 20
L 20 5
0 0.20 0.40 0.60 0.80 1.00
Transmissivity

Fig. 7 (b)

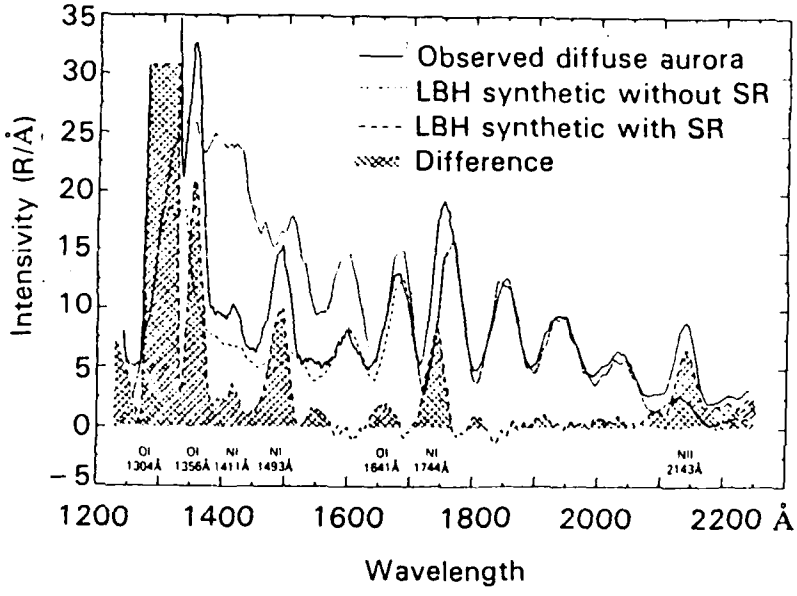
Observed diffuse aurora
LBH synthetic without SR
LBH synthetic with SR
Difference
Intensivity (R/Å)
35
30
25
20
15
10
5
0
−5
OI 1304Å
OI 1356Å
NI 1411Å
NI 1493Å
OI 1641Å
NI 1744Å
NII 2143Å
1200
1400
1600
1800
2000
2200 Å
Wavelength

Fig. 8

APPENDIX F

GEOPHYSICAL RESEARCH LETTERS, VOL. 16, NO. 2, PAGES 143-146, FEBRUARY 1989

DOPPLER SHIFT OF AURORAL LYMAN α OBSERVED FROM A SATELLITE

M. Ishimoto and C. -I. Meng

The Johns Hopkins University Applied Physics Laboratory, Laurel, Maryland

G. R. Romick

Atmospheric Science Division, National Science Foundation, Washington, D.C.

R. E. Huffman

Air Force Geophysics Laboratory, Hanscom Air Force Base, Bedford, Massachusetts

Abstract. The first documentation of Doppler shifted auroral Lyman α emission resulting from incident energetic protons in the auroral regions has been made using nadir VUV satellite spectral observations. The auroral Lyman α emission from high-velocity protons is expected to show a red shifted wavelength displacement based on ground-based observations of Balmer lines. VUV spectra (1100-1900 Å) taken over five sample auroral oval crossings by a nadir-viewing satellite in 1978 consistently show the Lyman α emission displaced toward longer wavelengths with a larger line width. The intensity peaks were shifted up to 4 Å when the geocoronal Lyman α emission profile was subtracted from the Lyman α emission profile observed over the auroral regions. The optical observations infer the auroral proton precipitation with average energies of 34 keV and an energy flux of 0.1 erg $cm^{-1}s^{-1}sr^{-1}$ when interpreted according to available model calculations. These values agree reasonably well with the average values for the characteristics of nightside incident auroral protons based on previous statistical satellite particle precipitation observations.

Introduction

Doppler shifted hydrogen Balmer series emission in the auroral regions was first observed by a ground-based spectrometer and used to infer the energy of precipitating protons [Meinel, 1951]. Subsequent calculations and discussions have been presented by Chamberlain [1961] and Eather [1967]. Figure 1 shows a Doppler shifted and broadened Balmer β line observed in a proton aurora compared to the line observed in the laboratory [Zwick and Shepherd, 1963]. Auroral protons, typically 10-40 keV, precipitate into the atmosphere and lose energy through charge-exchange and charge-stripping cycles with atmospheric constituents. Relatively recent detailed computations of the profile of the hydrogen spectral line emission were performed for ground-based observations in the directions of the magnetic zenith and horizon [Ponomarev, 1976]. The profile showed a good match to the observed Balmer line spectra [Galperin et al., 1976].

The Lyman α emission line (1216 Å) from proton precipitation can be observed only from space. In this study we present the first observations of the Doppler shifted profile of the auroral Lyman α line deduced from a polar orbiting satellite and infer the average energy and energy flux of the auroral protons by comparing the observed Doppler shift and broadening with the available model calculations. The Lyman α Doppler shift of 10-eV hydrogen atoms on Jupiter was recently reported in the American Astronomical Society meeting, Division of Planetary Sciences [Clarke et al., 1988], as pointed out by the reviewer of this paper.

Paper number 89GL00069.
0094-8276/89/89GL-00069$03.00

Observations

The auroral spectral data were obtained by an AFGL UV background experiment flown on the S3-4 satellite in 1978 [Huffman et al., 1980]. On board the satellite, which was in a low-altitude (180-270 km) polar orbit near the noon-midnight meridian plane, was the nadir-viewing 1/4-m, f/5 Ebert-Fastie spectrometer. Fifteen spectra with 8 Å resolution were selected for analysis during periods of strong Lyman emission. All the spectra were taken at a satellite altitude of about 260 km. Table 1 lists the geometrical and geophysical information along with the spectral characteristics from five auroral oval crossings. Figure 2a is an example of the nadir Lyman

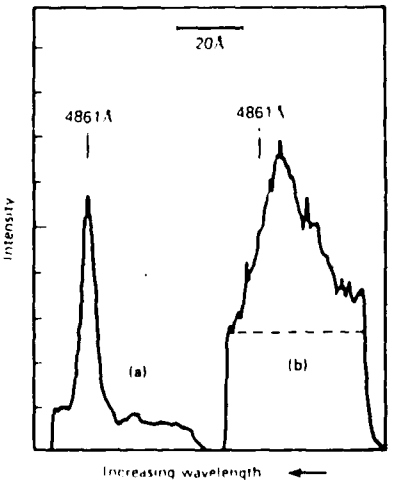

Fig. 1 Examples of hydrogen Balmer β line profiles [from Zwick and Shepherd, 1963]; (a) a hydrogen lamp source, (b) a magnetic zenith profile of a proton aurora.

TABLE 1. Summary of Lα spectra.

Date	h	m	s	Kp	AE	GMLAT	SZA	Intensity (kR) Geo + Aur	Geocorona	Aurora	Spectral profile (Å) Red shift	Geo HWFM	Aur HWFM	Energy (keV)	Energy flux (erg/cm²s)
5/1	7	18	34	6-	600	-67 9	116 2	3 48	1 85	1 63	2 82	8 02	10 92	28	0 49
	7	18	56		600	-67 0	117 6	3 29	1 73	1 56	2 47	8 02	11 78	24	0 42
	7	54	54		500	63 3	95 3	5 76	3 79	1 97	4 44	8 02	9 91	48	0 88
6/5	10	1	36	3+	500	-72 3	115 8	1 94	1 48	0 46	3 35	8 08	12 28	35	0 16
	10	1	58			-72 6	117 1	1 95	1 43	0 52	1 55	8 08	12 07	13	0 09
	10	2	20			-72 5	118 5	1 80	1 43	0 37	4 76	8 08	9 89	52	0 17
	10	3	05			-72 4	119 9	1 85	1 29	0 56	4 40	8 08	12 71	48	0 25
	10	3	27			-72 2	121 3	1 75	1 24	0 51	3 14	8 08	12 78	32	0 17
	10	3	49			-71 8	122 6	1 80	1 15	0 65	4 30	8 08	12 84	47	0 29
6/27	12	57	23	3	550	-61 0	148 1	1 63	0 75	0 88	2 82	7 97	10 34	28	0 27
	12	57	45			-59 7	149 3	1 63	0 74	0 89	2 95	7 97	11 56	30	0 28
7/8	6	4	34	3-	250	-69 7	120 7	1 57	1 13	0 44	2 69	8 02	11 02	27	0 13
	6	4	56			-68 7	122 0	1 67	1 08	0 59	3 35	8 02	11 28	35	0 21
7/14	17	26	38	5+	250	-65 4	114 2	1 35	0 93	0 42	2 46	8 51	10 71	24	0 11
	17	26	50			-63 9	195 4	1 65	0 93	0 72	3 92	8.51	10 39	42	0 29
Averages										0 8	3 3			34	0 3

α line intensity as observed along the entire orbit on May 1, 1978. The geocoronal Lyman α line intensity shows a strong correlation with the solar zenith angle. Figure 2b shows two spectra, one from the proton auroral region and the other from the midlatitude region. The latter is the average of 22 nighttime geocoronal spectra to reduce noise and has the 8 Å half width full maximum (HWFM) line profile. The former has a broader 10 Å HWFM spectral profile with a peak red shifted by 2 Å, indicating that some emission is from high-speed hydrogen moving away from the satellite toward the earth.

Two steps were needed in order to deduce the auroral Lyman α: first, the geocoronal background intensity was estimated by interpolation of the smoothed geocoronal intensities outside the auroral region; second, the geocoronal Lyman α profile with the estimated background intensity was subtracted from the observed Lyman α profile over the proton auroral region as shown in Figures 3a-f. The peak shifts and the HWFM width of the remaining auroral spectra are shown in Table 1; the auroral Lyman α spectrum is broader than that of the geocorona by ~2 Å.

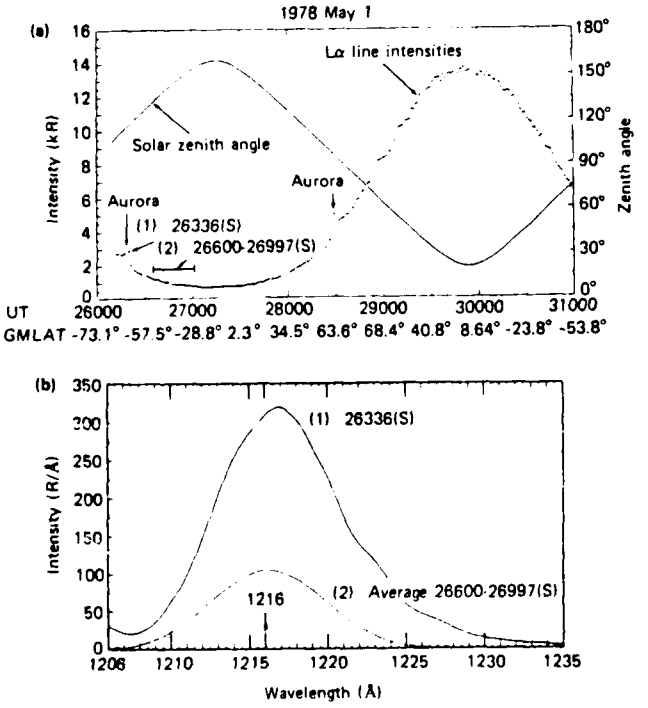

Fig. 2 (a) Observed Lyman α line intensity and solar zenith angle of the S3-4 throughout an orbit. (b) Comparison of the Lyman α profiles taken from auroral and midlatitude regions (the corresponding observation times were indicated in Figure 2a).

Discussion and Conclusions

We used the hydrogen line spectral profiles of auroral protons computed by a Monte Carlo method as our model [Ponomarev, 1976]. The model takes into account the charge-exchange and proton-beam stripping processes in the three dimensional model atmosphere and uses the cross sections of McNeal and Birely [1973]. Figure 4 shows the profile calculated for an isotropic pitch angle distribution as a function of the Doppler velocity in two viewing directions. The centroid of the profile shifts to a more negative Doppler velocity as seen from the ground with increasing energy of the monoenergetic beam. In order to compare this model with our space-based observations, the profiles of Figures 4b and c were transformed for the 1216 Å line and also smeared for 8 Å spectral resolution. Figure 5a shows the increase of both the Doppler shift and the broadening with the increasing energy of the protons as viewed downward from the satellite. In order to reduce the noise level, we averaged six spectra from the same auroral oval pass on July 5 and subtracted the estimated geocoronal Lyman α profile (Figure 5b). Figure 5c illustrates the remaining (i.e., auroral) spectrum and two model spectra calculated for two proton energies. The general shape of the auroral profile matches the calculated 30-keV profile. The observed profile is broader than the 30-keV model profile, as expected, because the energy spectrum of the auroral protons is not a monoenergetic beam and the deduced auroral spectrum is from an average of six spectra. Taking these facts into consideration, the auroral spectrum matches the 30-keV model calculated profile very well.

According to Ponomarev's calculation for isotropic proton precipitation, the spectral peak shift, $\Delta\lambda$, can be related to the proton energy, E_0, by the equation:

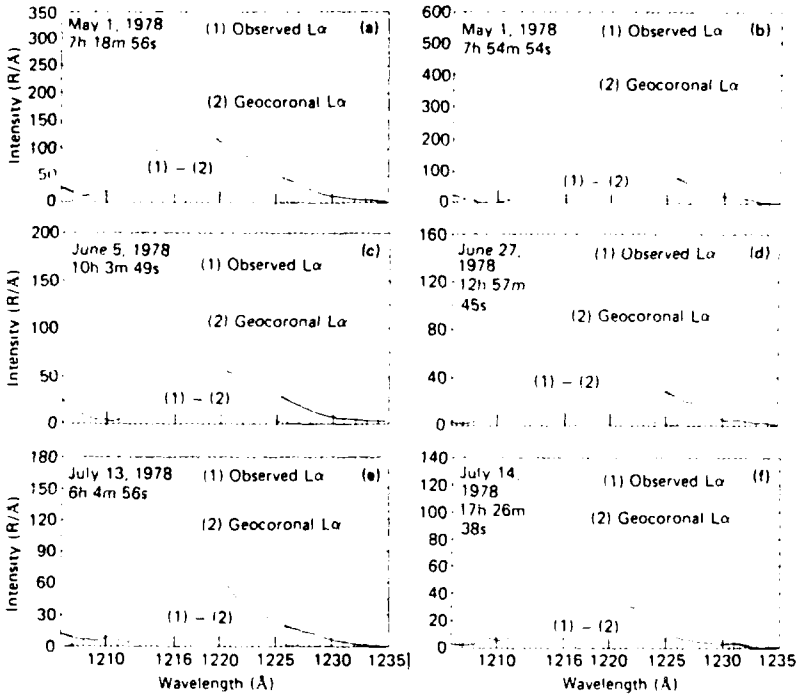

Fig. 3. Examples of Lyman α profiles from an auroral region. The estimated geocoronal Lyman α profile (dotted line) was subtracted from the observed profile to reveal the Lyman α profile from the proton precipitation (designated (1) – (2)).

$$E_0 = 12.321 \times \Delta\lambda - 6.291.$$

Using this equation, the mean energy of auroral protons can be estimated (Table 1). The values are, in general, higher than those from statistical study of ion precipitation measurements reported by Hardy et al. [1988], which are about 20 keV in the midnight region for Kp > 3. However, the DMSP measurement was limited to energies from 30 eV to 30 keV and some spectra were extrapolated to 100 keV to include the high-energy tail of the ion distribution. This extrapolation increased the average energy and the energy flux by less than 30% and 50%, respectively. The Lyman α spectra used here were among the most intense proton emissions in our satellite data set, corresponding to very active periods (up to Kp = 6–). A higher mean energy than the statistical value is expected, because there is no temporal or spatial averaging, which would smooth down the high values. Therefore, the agreement between our inferred and averaged measured proton energy is reasonable.

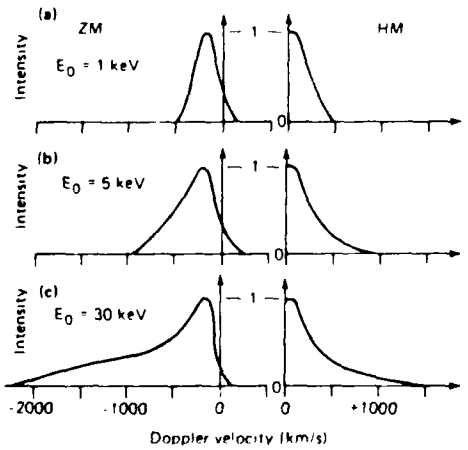

Fig. 4. Hydrogen line profile in the proton aurora as a function of the Doppler velocity computed by the Monte Carlo technique. The geomagnetic zenith (ZM) and horizon (HM) profiles are calculated for an isotropic distribution of the pitch angle for protons of monoenergetic energies of 1, 5, and 30 keV [from Galperin et al. 1976].

For the energy flux estimation, we used the Lyman line emission intensity calculated by Edger et al. [1973] with the emission cross section increased by 22% as suggested by Van Zyl and Newmann [1988]. The estimated energy fluxes are derived using the proton energy inferred from the observed profile (the last column of Table 1). The average value estimated from the observation is ~0.3 erg cm^{-2} s^{-1}. This value would be divided by 3 for the integrated solid angle for comparison with the statistical particle precipitation measurements of 0.1 erg cm^{-2}s^{-1}sr^{-1} reported by Hardy et al. [1988]. Thus, the observed auroral Lyman α profile and emission intensity are consistent with the existing model calculations and ion precipitation measurements. These observations suggest that sensitive high-resolution spectral measurements from a satellite can be used for global imaging of the characteristics of the proton precipitation. However, specific calculations of the resulting Lyman α emission profile expected for different nadir viewing angles, including multiple scattering effects on the emission profile, would be required.

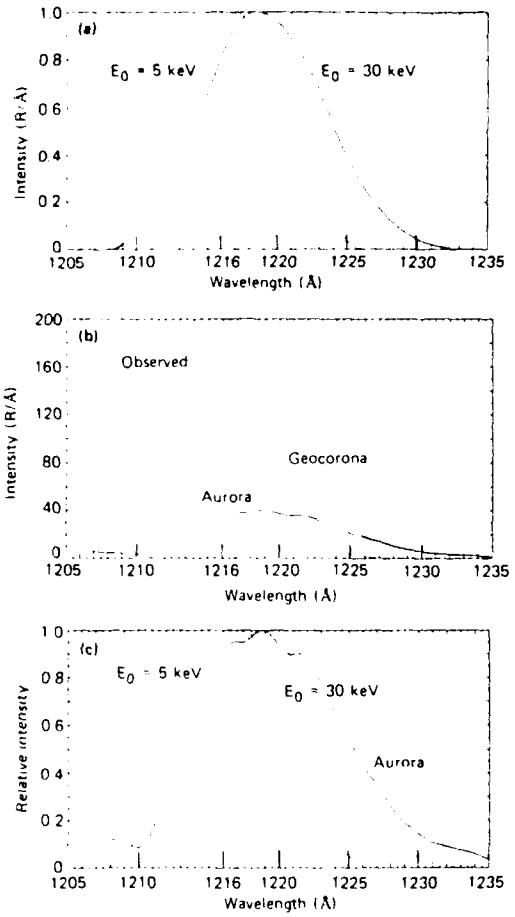

Fig. 5. Comparison of the auroral Lyman α profiles: observed and calculated. (a) Lyman α spectral intensity profile in the proton aurora adapted from model calculations of Ponomarev [1976]. (Figures 4b and 4c are translated from the Doppler velocity to the wavelength.)
(b) Auroral Lyman α spectral intensity profile observed on June 5, 1978. OBSERVED: an average of six consecutive auroral spectra. GEOCORONA: the estimated intensity with a profile of an average of 22 midlatitude spectra from the same orbit. AURORA: OBSERVED − GEOCORONA.
(c) Comparison of observed auroral Lyman α spectral relative intensity profile (AURORA profile in (b)) and model calculation (in (a)).

Acknowledgment. This work is supported by Directorate of Chemical and Atmospheric Sciences grant AFOSR 86-0057 to The Johns Hopkins University Applied Physics Laboratory.

References

Chamberlain, J. W., *Physics of the Aurora and Airglow*, Academic Press, New York, 1961.

Clarke, J. T., J. Trauger, and H. Waite, Doppler shifted H Lyα emission from Jupiter's aurora, *Bulletin of the American Astronomical Society, 20*, 3, 898, 1988.

Eather, R. H., Auroral proton precipitation and hydrogen emissions, *Rev. Geophys., 5*, 207, 1967.

Edger, B. C., W. T. Miles, and A. E. S. Green, Energy deposition of protons in molecular nitrogen and applications to proton auroral phenomena, *J. Geophys. Res., 78*, 28, 6595-6606, 1973.

Galperin, Yu. I., R. A. Kovrazhkin, Yu. N. Ponomarev, J. Crasnier, and J. A. Savaud, Pitch angle distributions of auroral protons, *Ann. Geophys.*, t. 32, fasc. 2, 1976, p. 109-115.

Hardy, D. A., M. S. Gussenhoven, and D. Brautigam, A statistical model of auroral ion precipitation, *J. Geophys. Res., 94*, A1, 370-392, 1989.

Huffman, R. E., F. J. LeBlanc, J. C. Larrabee, and D. E. Paulsen, Satellite vacuum ultraviolet airglow and auroral observations, *J. Geophys. Res., 85*, A5, 2201-2215, 1980.

McNeal, R. J., and J. H. Birely, Laboratory studies of collisions of energetic H^+ and hydrogen with atmospheric constituents, *Rev. Geophys. Space. Phys. 11*, 3, 633-692, 1973.

Meinel, A. B., Doppler shifted auroral hydrogen emission, *Astrophys. J., 113*, 50-54, 1951.

Ponomarev, Yu. N., Partial effect of monoenergetic and multidirectional proton precipitation beams in the upper atmosphere (translated title), Kosmisch, Issled, *14*, No. 1, 1976.

Van Zyl, B., and H. Neuman, Lyman α emission cross sections for low-energy H and H^+ collisions with N_2 and O_2, *J. Geophys. Res., 93*, 12, 1023-1027, 1988.

Zwick, H. H., and G. G. Shepherd, Some observations of hydrogen line profiles in the aurora, *J. Atmos. Terr. Phys., 25*, 604-607, 1963.

R. E. Huffman, Air Force Geophysics Laboratory, Hanscom Air Force Base, Bedford, MA 01731.

M. Ishimoto and C.-I. Meng, The Johns Hopkins University Applied Physics Laboratory, Johns Hopkins Road, Laurel, MD 20707.

G. R. Romick, Atmospheric Science Division, National Science Foundation, Washington, DC 20550.

(Received December 29, 1988;
accepted: January 10, 1989.)